Epistasis decreases with increasing antibiotic pressure but not temperature

Ana-Hermina Ghenu[1,2,3], André Amado[2,3], Isabel Gordo[1], and Claudia Bank[1,2,3]

[1]Instituto Gulbenkian de Ciência, Rua da Quinta Grande 6, Oeiras, 2780-156, Portugal

[2]Institut für Ökologie und Evolution, Universität Bern, Baltzerstrasse 6, CH-3012 Bern, Switzerland

[3]Swiss Institute of Bioinformatics, 1015 Lausanne, Switzerland

August 31, 2022

1 Abstract

Predicting mutational effects is important for the control of antibiotic resistance (ABR). Predictions are difficult when there are strong genotype-by-environment (G×E), gene-by-gene (G×G or epistatic), or gene-by-gene-by-environment (G×G×E) interactions. We quantified G×G×E effects in *Escherichia coli* across environmental gradients. We created intergenic fitness landscapes using gene knock-outs and single nucleotide ABR mutations previously identified to vary in the extent of G×E effects in our environments of interest. Then, we measured competitive fitness across a full combinatorial set of temperature and antibiotic dosage gradients. In this way, we assessed the predictability of 15 fitness landscapes across 12 different, but related, environments. We found higher predictability and less G×G interactions than expected. We detected G×G interactions and rugged fitness landscapes in the absence of antibiotic, but, as antibiotic concentration increased, the fitness effects of ABR genotypes quickly overshadowed those of gene knock-outs and the landscapes became smoother. Despite setting out to promote the role of G×G×E interactions on evolution, our work reiterates that some single mutants, like those conferring resistance or susceptibility to antibiotics, have consistent effects across genotypes. Thus, although epistasis may reduce the predictability of evolution in the absence of antibiotics, evolution may be predictable in the presence of antibiotics.

2 Introduction

Gene-by-gene (G×G) and gene-by-environment (G×E) interactions (and their combination, hereafter termed G×G×E effects) alter expected phenotypes or fitness of individuals and thereby affect the predictability of evolution [1, 2]. Studying their extent and incorporating their effect into evolutionary predictions is difficult because of the complexity of the genotype space and the myriad of environments that could be tested [3]. However, our lack of quantitative knowledge of G×G and G×E effects poses dangers to fields in which genetic and evolutionary models are applied: they could lead to failed genetic rescue of endangered species, or unexpected spread or maintenance of antibiotic resistance (ABR).

At the same time, the existence of G×E interactions is a key assumption in the study of antibiotic resistance evolution, because by definition the original genotype grows well in the antibiotic-free environment and poorly in the antibiotic environment. Conversely, a resistant genotype grows well in the antibiotic environment and is usually assumed to have a low fitness in the antibiotic-free environment, resulting in so-called costs of ABR (reviewed in [4], but see [5]). In addition, G×E interactions with other types of environmental variables have been found to facilitate the evolution of resistant genotypes in the absence of antibiotics [6, 7]. How the G×E relationship between susceptible and resistant genotypes changes across other environmental axes, and how frequently it is modulated by the genetic background (i.e., through G×G effects), is less explored (but see [8–10]).

ABR has been a problem since antibiotics have been clinically used [11], and it was identified by the WHO as a major global threat to health [12]. For this reason, inferring potential resistances, cross-resistances, compensatory mutations, and, ultimately, predicting the evolutionary trajectories of bacterial genomes in the presence of antibiotics is an application of evolutionary biology that is important for the health of humans and the planet [13, 14]. Critically, G×G and G×E effects influencing ABR can complicate the identification of new resistances. For example, with G×G effects, resistance may depend on more than one easily identifiable allele, whereas with G×E effects, laboratory evolution settings may not be informative of the fitness of genotypes in the wild.

Including G×G effects into the study of ABR requires the consideration of many potentially interacting genotypes. Hereby, interactions can be specific between particular mutations due to mechanistic interactions of residues or proteins, for example (reviewed in [15]), or global, where any combination of mutations ultimately shows a pattern of G×G [16, 17]. In contrast to increasing numbers of reports of ubiquitous epistasis [18–20], much existing work to date has considered single ABR genotypes at a time under the assumptions of additive effects (but see [21, 22]). The theoretical concept of a fitness landscape, which maps every possible genotype to its fitness, captures G×G interactions (also termed epistasis) and enables the study of how such

interactions affect evolutionary trajectories (reviewed in [23, 2]). Unless there is a known underlying pattern of interactions, epistasis makes evolution on the fitness landscape less predictable. Moreover, with added G×E interactions the fitness landscape may change across environmental gradients, leading to changes in both single genotypes and epistasis [19, 24] and to different possible evolutionary trajectories [25, 26].

We here take a step towards quantifying G×G×E interactions by studying small fitness landscapes across two environmental gradients and their combination, antibiotic concentration and temperature. In our fitness landscapes, we combine three known resistance mutations in the *rpoB* gene with five gene knock-outs, resulting in 24 genotypes that are screened for competitive fitness in 12 abiotic environments. Unlike previous studies, we study interactions of two different mutation types, single-locus polymorphisms (more specifically, single nucleotide polymorphims, or SNPs) and whole gene deletions. Moreover, by screening the fitness landscapes across a grid of environments, we quantify their change across environmental gradients, which is related to the robustness of fitness predictions under environmental change. Our fitness landscapes feature little epistasis, which decreases at higher antibiotic concentrations. Altogether, we conclude that our fitness landscapes are very predictable across environments.

3 Results

3.1 Choice of genotypes

We selected rifampicin-resistant single-nucleotide mutations that were *a priori* known to differ in their performance between different temperature environments in M9 minimal medium. The ABR mutations modify single amino-acids at the antibiotic target site in the gene RNA polymerase B (*rpoB*). Prior to our study it was unknown how the mutants would preform in different combinations of antibiotic and high temperature environments (i.e., we only knew about the effect of one environmental axis on its own). *RpoB* H526Y was established to have a trade-off between environment types: it confers high rifampicin resistance at $37°C$ but grows poorly as compared to wild-type at higher temperature in the absence of antibiotic [27, 28]. Conversely, *rpoB* S512F was established to have a synergy between environment types: it grows well both at high rifampicin concentrations and at higher temperatures [27]. Finally, *rpoB* I572N is a weak rifampicin resistance mutation that was first identified during evolution to high temperature [6, 29].

We initially tried to select knock-out mutations in a similar way as we had done for *rpoB* mutants: we used data from a large phenotypic screen of *E. coli* (accessed from ecoliwiki.org/tools/chemgen/) to select knock-out mutations that were known to differ in their performance between environment types. However, neither the bacterial colony size s-scores [30] nor the bacterial colony opacity and density s-scores [31] were able to predict the growth effects of Keio collection [32] knock-out mutants in batch culture environments

(data not shown).

Ultimately, we selected knock-out mutations based on their *a priori* functional effects and the presence of segregating knock-out polymorphism in natural populations (accessed from the panX database at pangenome.org; [33]). We selected four knock-outs of functional genes all involved in how the cell interacts with its environment, as follows: *marR* (multiple antibiotic resistance regulator) detects and responds to chemical stressors, and its knock-out is sensitive to heat-shock [34], conferring either resistance [35] or susceptibility [36] to some antibiotics but not rifampicin [30]; *nuoC* and *yidK* are both located on the plasma membrane and involved in transport [37, 38]; and *waaP* impacts outer membrane stability through lipopolysaccharide biosynthesis [39]. The fifth gene, *ybfG*, is a pseudogene and was selected as a control since its knock-out should perform similarly to the wild-type genotype. None of the knock-outs interact directly with *rpoB* or other genes involved in transcription, protein synthesis, or DNA supercoiling. Therefore, any epistasis that will be observed should not be attributable to mechanistic interactions. Figure 1 shows a schematic of the resulting topology of the fitness landscape when combining the ABR and knock-out mutations.

Illumina whole-genome re-sequencing was used to confirm the constructed mutants and identify any *de novo* mutations as compared to the wild-type genotype (table S3). See the supplementary results for details.

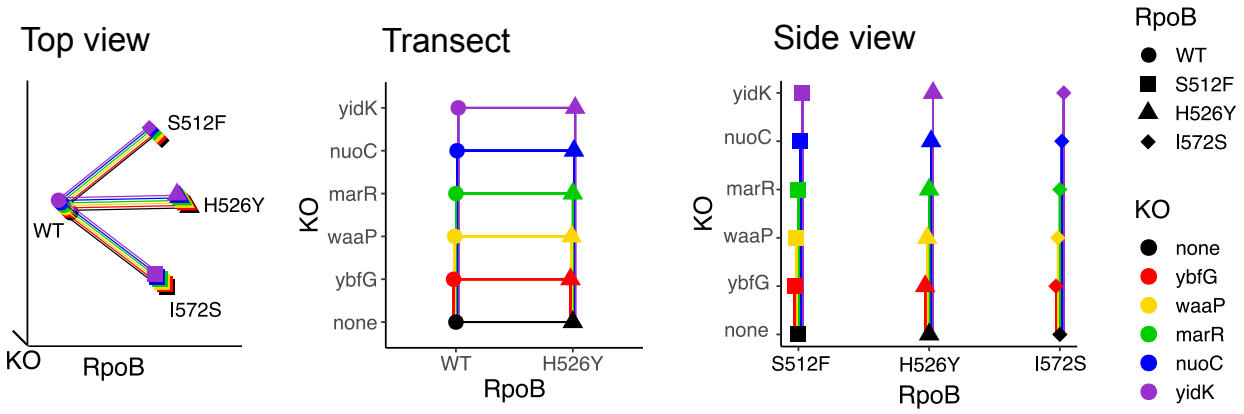

Figure 1: **3-Dimensional schematics depicting the topology of the studied fitness landscapes.** Genotypes are depicted as uniquely coloured shapes with lines connecting genotypes that are one mutational step apart. The shape indicates the *rpoB* point mutation and the colour indicates which gene has been knocked-out (KO); the black circle indicates the wild-type genotype without any mutations on *rpoB* and without any knock-outs. The schematics show the same topology from different perspectives. All mutations are considered to be at unique, di-allelic loci. There are 15 fitness landscapes each composed of the wild-type, a *rpoB* single mutant, a knock-out single mutant, and the resultant double mutant.

3.2 Choice of environments

Since the wild-type and knock-out single mutants are sensitive to rifampicin, the screened antibiotic concentrations were selected based on the wild-type dose-response (figure S14). The screened temperature environments were selected based on their physiological relevance for *E. coli* and its human host: $37°C$ is the temperature of a healthy human host, $40°C$ is the temperature of high fever, and $42°C$ is near the maximum temperature that *E. coli* can withstand. Antibiotic-susceptible genotypes (i.e., genotypes that carry the wild-type allele at the *rpoB* locus) can be considered as 'specialists' of the antibiotic-free environments because their growth deteriorates in the presence of antibiotic, i.e. they show strong G×E interactions. Based on previous results, we expected that the *rpoB* S512F single mutant that grows well both in the presence of antibiotic and at high temperature would exhibit 'generalist' growth in all environments with little G×E interaction.

3.3 Measure of competitive fitness

The GFP-labeled wild-type, single, and double mutants were competed against the same reference genotype, mCherry-labeled *rpoB* H526Y, in all environments by starting at approximately equal ratios and a fixed innoculum size. The competitive index ($\hat{w}$), a proxy for fitness, was estimated after 20 hours of batch culture growth as follows:

$$\hat{w} = ln\left(\frac{D^f_{\text{comp}}/D^f_{\text{ref}}}{D^i_{\text{comp}}/D^i_{\text{ref}}}\right),$$

where D^i represents the initial density and D^f represents the final density as measured by flow cytometry. We found nearly identical $\hat{w}$ estimates when the fluorophores of the reference and competitor genotypes were swapped ($\hat{w}_{\text{GFP}} = \beta * \hat{w}_{\text{mCherry}} + b$; adjusted $R^2 = 0.95$; $\beta = 0.96$, $p < 10^{-15}$; figure S15 and table S4); including the effect of environment in the regression was not significant ($F(11, 127) = 1.27$, $p = 0.25$, table S5 and figure S16), but adding the effect of genotype was significant ($F(11, 127) = 4.00$, $p < 10^{-4}$, figure S17 and table S6) although genotype explains only about 1% more of the variation in the data (adjusted $R^2 = 0.96$ for overall regression) as compared to not including this effect. Therefore we concluded that the fluorescence is a neutral marker.

The mean $\hat{w}$ for all genotypes and environments is shown in figure 2. For all knock-out backgrounds, we compared the competitive fitness of the ABR mutations against the *rpoB* wild-type sequence in the absence of antibiotic to ascertain whether there was a cost of resistance. We observed no consistent cost of resistance across all backgrounds (figure S18) and (in contrast to previous studies [27, 29]) all three ABR mutations

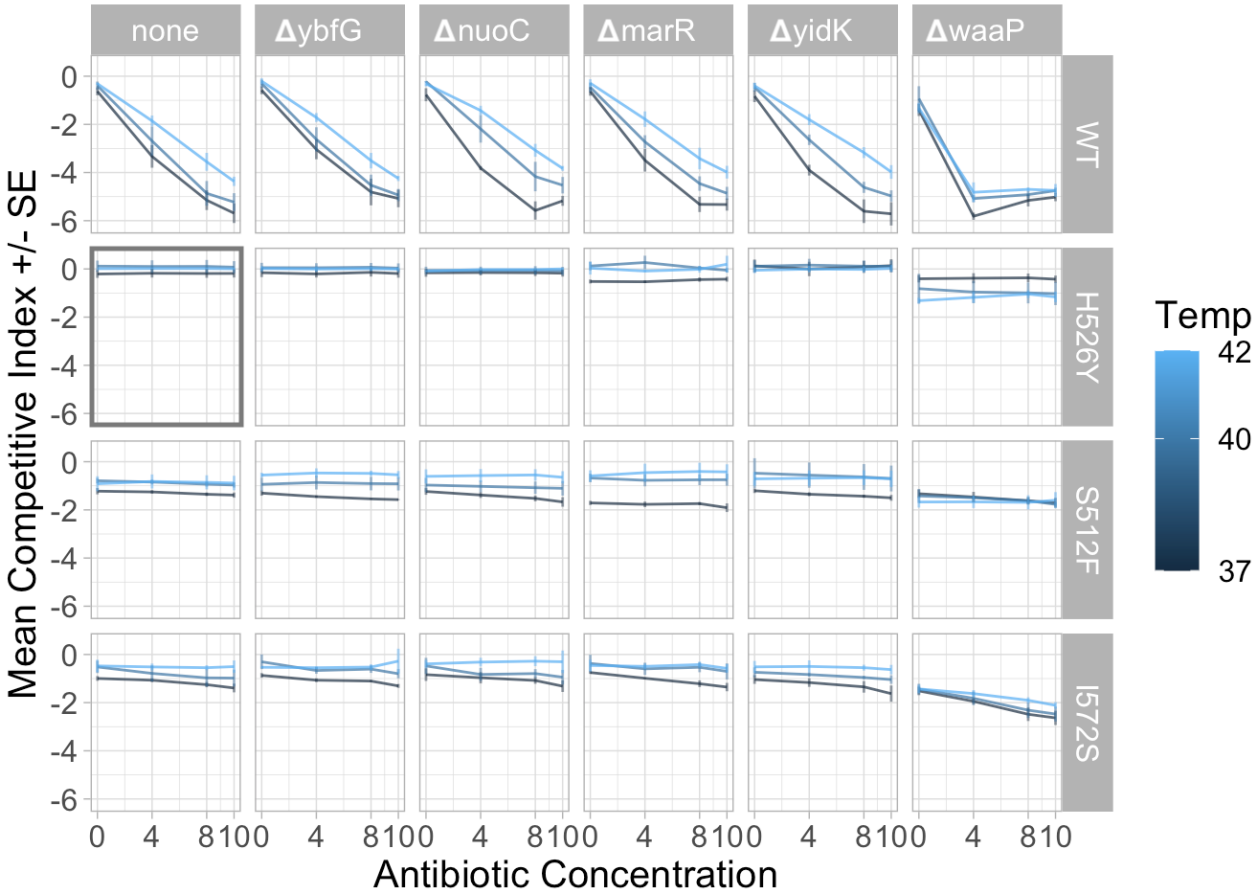

Figure 2: **Estimated competitive index ($\hat{w}$) across all genotypes and environments.** The x-axis shows the four rifampicin antibiotic concentrations environments ($\mu g/mL$) and the y-axis shows the mean estimated competitive index with error-bars for standard errors ($n = 3 - 4$). Shades of blue show the three temperature environments. Knock-out genotypes are shown in each column (with "none" indicating the wild-type like state of having no knock-outs) and *rpoB* antibiotic resistant mutants are shown in each row (with "WT" indicating the susceptible wild-type *rpoB* sequence); therefore the plot on the top left shows the wild-type without any mutations and, similarly, the left column shows all *rpoB* single mutants while the top row shows all knock-out single mutants. Finally, the grey box indicates the *rpoB* H526Y genotype used as the reference for all competitions.

grew similarly to the wild-type at higher temperatures.

3.4 Multiple summary statistics found few G×G interactions

Several measures exist to determine the extent of G×G interactions (also termed epistasis). We first inferred 'classical' pairwise epistasis by using the fitness of the wild-type genotype as a baseline and subtracting the fitness effects of both ABR and knock-out single mutants from the fitness effect of the double mutant (figures S19 & S20 show examples without and with pairwise epistasis, respectively). We estimated pairwise epistasis for each of the 15 sets of double mutations in each of the 12 environments (figure S21). We found significant pairwise epistasis only for the $\Delta waaP$ mutant. The $\Delta waaP$ mutant exhibited positive pair-

wise epistasis on all ABR backgrounds at the low antibiotic concentration of 4μg/mL. This dose-dependent epistasis arises likely because $\Delta waaP$ is susceptible to the antibiotic at lower concentrations and the ABR mutations rescue bacterial growth at this concentration. We detected almost no pairwise interactions of the $\Delta waaP$ mutant at higher antibiotic concentrations, most likely because the relative fitness effect of the $\Delta waaP$ mutation becomes much smaller as compared to the fitness effect of the ABR mutations.

Second, we inferred epistasis over the whole landscape using the gamma statistic [40], which measures the correlation of fitness effects among the different genetic backgrounds where a mutation appears. Mutations that exhibit little G×G interaction have similar effects on different backgrounds; consequently, their effects will be strongly correlated across backgrounds (gamma near one). On the other hand, a weak or negative correlation of the effects of a mutation in different backgrounds (gamma near zero or negative) indicates that a mutation exhibits G×G interactions. Overall, we observed gamma epistasis values near one, which are indicative of very little G×G interaction. Antibiotic concentration was positively correlated with gamma epistasis (figure 3a; $F(1,10) = 52.7$, $p < 10^{-4}$, adjusted $R^2 = 0.825$) regardless of temperature. This means that the amount of G×G interactions decreases as antibiotic concentration increases, and that it was independent of temperature. Focusing solely on the gamma epistasis of ABR mutants or knock-outs, respectively (figure S22), we observed different qualitative but non-significant trends between the mutational classes and between the different temperatures. ABR mutations exhibited the strongest epistasis (i.e., gamma near zero) at the intermediate antibiotic concentration and increasing with temperature. Conversely, knock-out mutations exhibited the strongest epistasis (again, gamma near zero) at the two highest antibiotic concentrations and decreasing with temperature. Independent of the focal mutational class, there was less gamma epistasis at $42°C$ than at $37°C$.

Thirdly, we inferred the presence of sign and reciprocal sign epistasis. Sign epistasis occurs when the beneficial or deleterious effect of a mutation reverses in the presence of another mutation to become deleterious or beneficial, respectively. When two mutations show sign epistasis on each other's background, we infer reciprocal sign epistasis. Importantly, the presence of reciprocal sign epistasis is a prerequisite for multiple peaks in the fitness landscape [41]. In our study, significant reciprocal sign epistasis occurred only in the antibiotic-free environments, but across all temperatures. This trend can be summarized as a negative correlation between antibiotic concentration and the mean fraction of reciprocal sign epistasis (figure 3b; $F(1,10) = 20.3$, $p < 0.005$, adjusted $R^2 = 0.637$). Reciprocal sign epistasis was observed between the weak ABR mutation *rpoB* I572S and most of the knock-out mutations (table S7). Apart from that, the fraction of simple sign epistasis was significant in all environments and showed no trend across environments ($F(1,10) = 2.15$, $p = 0.17$, figure S23).

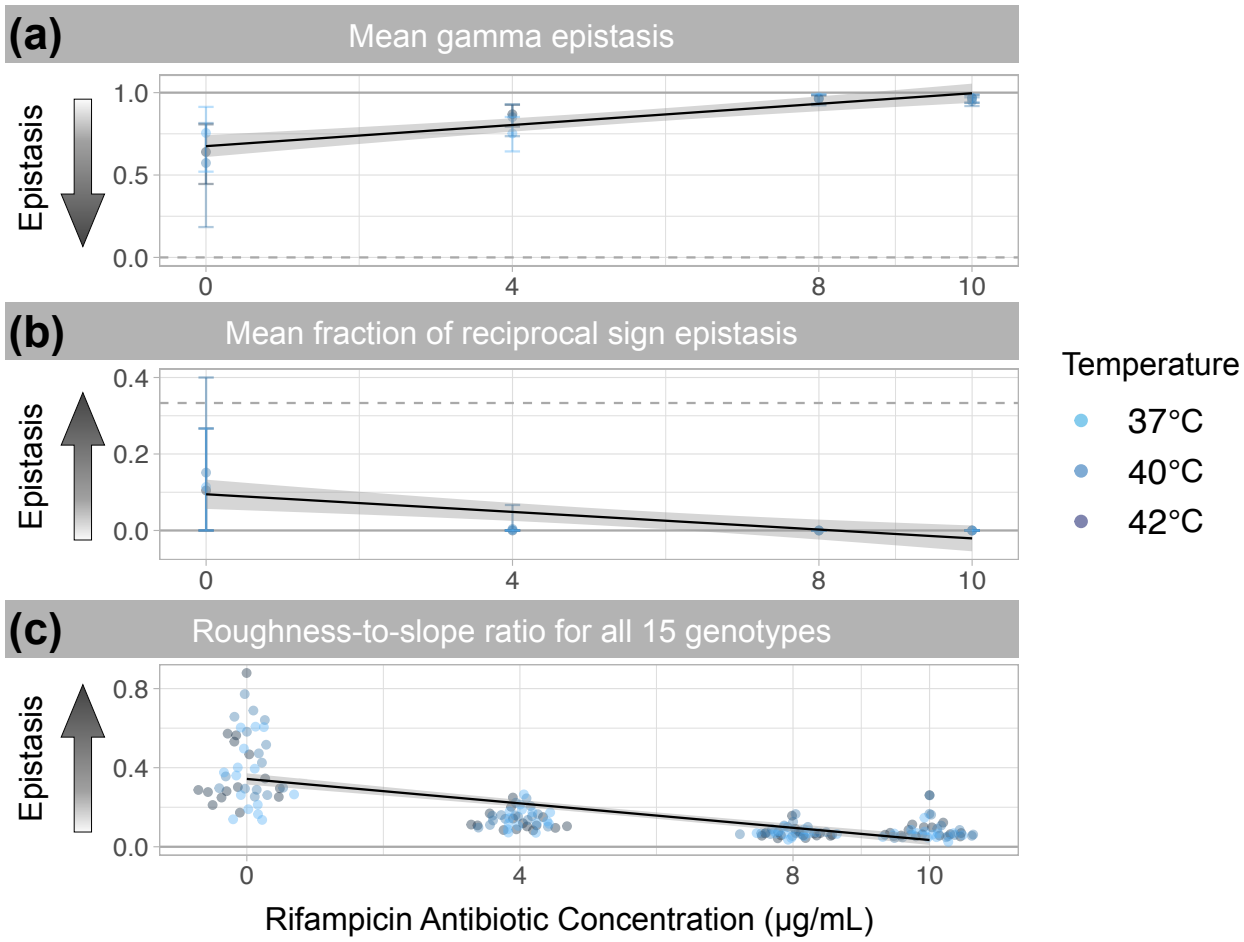

Figure 3: **Antibiotic concentration has a significant negative trend with three measures of epistasis: (a)** the mean gamma epistasis across all loci, **(b)** the mean fraction of loci exhibiting reciprocal sign epistasis, and **(c)** the roughness-to-slope ratios by genotype. For each panel the x-axis shows the rifampicin antibiotic concentration in $\mu g/mL$, the colours show the temperature, and the y-axis shows the value of the epistasis measure. Arrows indicate the direction of stronger epistasis, solid horizontal grey lines show values of no epistasis, and dashed grey lines show the values of the maximum possible epistasis for each metric. The black trend-lines show the significant negative correlations between antibiotic concentration and each epistasis measure, and the grey shaded regions show the 95% confidence interval of the corresponding least-squares estimated linear regression. For panels (a)-(b), the error bars show the 95% parametric bootstrap confidence intervals. For figure clarity, bootstrap confidence intervals are omitted in panel (c) but can be found in figure S24, which shows the roughness-to-slope ratios for individual genotypes and environments. Significance is reported at an $\alpha = 0.01$.

Next, we computed the roughness-to-slope ratio. The roughness-to-slope ratio fits a linear model to the fitness landscape and then quantifies epistasis as the ratio of the residuals to the linear component of the fit. Thus, completely additive landscapes exhibit a roughness-to-slope ratio of zero [41]. In our data, the mean estimated roughness-to-slope ratio was negatively correlated with antibiotic concentration (figure 3c; $F(1, 178) = 206.9$, $p < 10^{-15}$, adjusted $R^2 = 0.535$). Roughness-to-slope ratios were very small for all genotypes in the presence of antibiotic, nevertheless the 95% bootstrap confidence intervals were significantly different from zero for all values.

Finally, we inferred whether the studied fitness landscape exhibited diminishing-returns epistasis. Diminishing-returns epistasis measures whether the effect size of a beneficial mutation decreases as fitness of the genetic background increases, and is one of the most frequently observed patterns of epistasis in fitness landscapes (Bank 2022). We observed that the fitness effects of the knock-out mutations were not correlated with the overall fitness of the background, regardless of the environment (figures 4a & c). In contrast, for most environments, the ABR mutations exhibited a negative correlation with the fitness of the background that the mutation is on, indicating a pattern of diminishing-returns epistasis (figures 4b & c). The observed trend of diminishing returns for the knock-out and ABR mutants did not depend on the low fitness of the $\Delta waaP$ mutants. Indeed, when the $\Delta waaP$ backgrounds were removed from the analysis, the trend became more pronounced as significant diminishing-returns epistasis was observed in all but one of the 12 environments (figure S25).

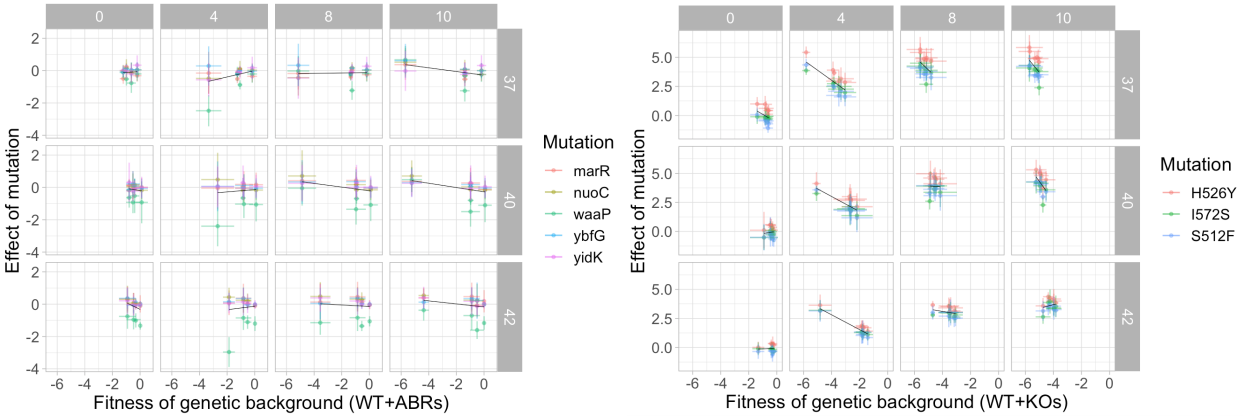

(a) knock-out mutations

(b) ABR *rpoB* mutations

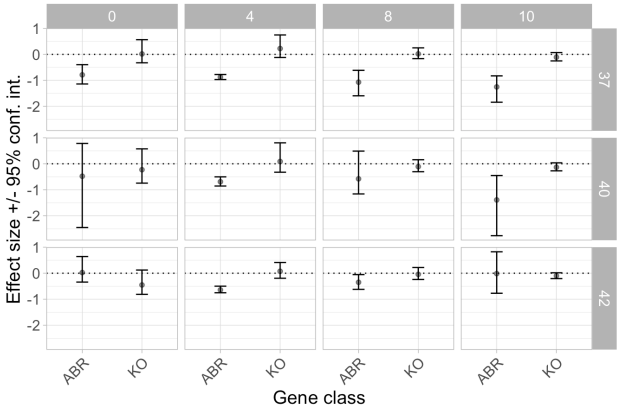

(c) Slopes for the diminishing-returns epistasis of knock-out (KO) and *rpoB* (ABR) mutations.

Figure 4: **Knock-out mutations do not exhibit diminishing-returns epistasis whereas *rpoB* mutations exhibit diminishing-returns epistasis in most environments.** In each panel, the columns show different rifampicin antibiotic concentrations (in units of $\mu g/mL$) and the rows show different temperature environments (in $^{\circ}C$). **(a)** Knock-out mutations do not exhibit diminishing-returns epistasis in any of the environments. The points show mean values and are coloured corresponding to the knock-out mutations. The x-axis shows the fitness $\hat{w}$ of the background (either wild-type or one of the three ABR *rpoB* mutations) and the y-axis shows the effect size of the knock-out mutation on that background. **(b)** ABR *rpoB* mutations exhibit diminishing-returns epistasis in eight of the 12 environments. The x-axis shows the fitness $\hat{w}$ of the background (either wild-type or one of the five knock-out mutations) and the y-axis shows the effect size of the ABR mutation on that background. For panels (a)-(b), the error bars show 95% parametric bootstrap confidence intervals for each value. The black lines show the means of the regressions across all bootstrap samples. **(c)** Quantification of the mean slope effect sizes ($\pm$ 95% confidence intervals) of the diminishing-returns epistasis for the *rpoB* mutations (ABR) and the knock-out mutations (KO). The mean slopes are shown as black trend lines in panels (a) & (b). Confidence intervals are determined from linear regressions of each of the parametric bootstrap samples. The confidence intervals that overlap with zero (dotted line) indicate slopes that are *not* significantly different from zero.

3.5 Competitive fitness is predicted by antibiotic concentration

We used multiple linear regression to study the quantitative effects of antibiotic concentration and temperature environments on the competitive index, $\hat{w}$. We found that the 'null model' regression with $\hat{w}$ as the dependent variable and only additive effects of genotype and environment variables was able to explain a considerable amount of the variation observed in the data (adjusted $R^2 = 0.68$, $F(13, 982) = 162.5$, $p < 10^{-15}$, table S8). Most of the residual variation was attributable to the wild-type *rpoB* genotypes (figure S26). Contrary to resistant genotypes, the antibiotic susceptible genotypes interacted with the rifampicin environments by having higher fitness in the absence of rifampicin but very low fitness at higher rifampicin concentrations.

Next, we quantified the interaction between the *rpoB* antibiotic susceptible and resistant genotypes with the antibiotic concentration by fitting a model with the additive effects and the $G_{rpoB} \times E_{\mathrm{AB}}$ interaction. This model fitted the data better than the additive null model, explaining almost all of the variation (adjusted $R^2 = 0.881$, $F(9, 973) = 186.0$, $p < 10^{-15}$, figure S27). Polynomial contrasts indicated that higher temperature was correlated with increased $\hat{w}$ ($t = 15.0$, $p < 10^{-15}$, figures S28-S29). The fixed effect of antibiotic concentration alone on $\hat{w}$ was not significant (figure S28). Instead, the effect of antibiotic concentration was only significant as an interaction term with the susceptible *rpoB* wild-type genotype or the weak ABR genotype I572S.

Then, we compared the above model with a slightly more complex model that included an additional $G_{rpoB} \times G_{\mathrm{KO}}$ interaction between genotypes (i.e., 'classical' pairwise epistasis between *rpoB* and knock-out mutations). Although this model with G×E and G×G effects was significantly different from the model with only G×E effects ($F(15, 958) = 2.60$, $p < 0.001$, figure S30), none of the additional coefficients were significant (figure S31) and the model predictions were very similar to those of the model with only G×E. Indeed, the amount of variation explained by the more complex model (adjusted $R^2 = 0.883$) showed only a 0.2 percentage-point improvement in the total variation explained as compared to the simpler model with only G×E effects. This finding confirms our previous results of small but statistically significant pairwise epistasis in our data.

Despite our relatively large dataset (n=996), we did not have sufficient data to systematically study higher order interactions without overfitting. For descriptive purposes, we fitted the following more complex possible model without reporting the p-values:

$$\hat{w} \sim \underbrace{G_{rpoB} + G_{\mathrm{KO}} + E_{\mathrm{AB}} + E_{\mathrm{T}}}_{\text{additve effects}} + \underbrace{G_{rpoB} \times E_{\mathrm{AB}} + E_{\mathrm{AB}} \times E_{\mathrm{T}}}_{1^{st}\text{ order interactions}} + \underbrace{G_{rpoB} \times G_{\mathrm{KO}} \times E_{\mathrm{AB}} + G_{rpoB} \times G_{\mathrm{KO}} \times E_{\mathrm{T}}}_{2^{nd}\text{ order interactions}},$$

This model with 157 coefficients (i.e., just over 6 data points per estimated coefficient) resulted in an adjusted $R^2 = 0.916$, a modest improvement as compared to the simpler models with only one or two interactions. Of

the additional interactions, a model without the second-order interaction between epistasis and temperature ($G_{rpoB} \times G_{\mathrm{KO}} \times E_{\mathrm{T}}$) had lower explanatory power (adjusted $R^2 = 0.894$) than models without the second-order interaction between epistasis and antibiotic concentration ($G_{rpoB} \times G_{\mathrm{KO}} \times E_{\mathrm{AB}}$: adjusted $R^2 = 0.906$) or without the first-order interaction between environments ($E_{\mathrm{AB}} \times E_{\mathrm{T}}$: adjusted $R^2 = 0.913$). Thus, there may be higher-order interactions, for example between epistasis and temperature, that our data has insufficient power to reveal statistically.

3.6 Environmental quality is less important for predicting G×G than antibiotic concentration alone

To study the interactions between epistasis and environment (G×G×E) without the problem of over-fitting, we summarized the temperature and antibiotic environments as a single, continuous environmental quality metric that we used to regress the different epistasis measures [42]. We compared three metrics of environmental quality (mean growth of the reference strain, mean growth of all competitor strains, and mean combined growth of reference and competitor strains) and found that the mean growth of all competitor strains in each environment was the best metric of environmental quality (supplementary results 8.7.1). This metric of environmental quality was able to distinguish environments from each other (figure S32) and correctly distinguish specialist from generalist genotypes (figure S33). As expected, the environmental quality metric was correlated with antibiotic concentration (adjusted $R^2 = 0.559$) and somewhat correlated with temperature (adjusted $R^2 = 0.325$).

We computed the correlation of environmental quality with all of the above measures of G×G by fitting the environmental quality metric as a linear predictor of pairwise epistasis (figures S37-S38), gamma epistasis (figure S39), fraction of sign epistasis (figure S40), and the roughness-to-slope ratio (figure S41). Most of the regressions were either not significant to $\alpha = 0.01$ (gamma epistasis for ABR mutations, simple sign epistasis, reciprocal sign epstasis, and pairwise epistasis excluding $\Delta waaP$) or explained very little of the variation in the data (pairwise epistasis including $\Delta waaP$: adjusted $R^2 = 0.036$). For metrics that exhibited a significant effect of environmental quality on G×G (total gamma epistasis, figure S39, and roughness-to-slope ratio, figure S41), antibiotic concentration alone regressed as a dependent variable explained more of the variation in the G×G metric than was explained by environmental quality. Moreover, the results of the regression on environmental quality were broadly in agreement with our above findings that G×G decreases as antibiotic concentration increases and environmental quality deteriorates (i.e., positive correlations were found between the environmental quality metric and the G×G summary statistics). The only exception was the gamma epistasis for knock-out mutations (figure S39), which exhibited the opposite trend as other G×G metrics (i.e., G×G was found to increase as environmental quality deteriorated).

4 Discussion

Whether mutational effects and epistasis vary across environments, and how this matters for evolution, has been debated for decades (reviewed in [43, 2]). Here, we screened small fitness landscapes that were combined of SNPs in genes involved in antibiotic resistance, and selected gene knock-out mutations, at increasing gradients of antibiotic and temperature. We observed relatively little epistasis for four out of the five different measurement types. The benign environments exhibited the most epistasis and the addition of antibiotic resulted in a decrease in epistasis (figure 3). ABR mutations, but not gene knock-outs, exhibited diminishing-returns epistasis in most environments (figure 4). These results suggest that, while epistatic interactions may confound predictions in the absence of antibiotic, the effects of ABR mutations are predictable in the presence of antibiotic.

4.1 Biological significance of our experiment

We studied ABR mutations at the *rpoB* locus because this locus is clinically important and has been shown to exhibit G×G interactions. Amino-acid mutations at the *rpoB* locus (e.g., at site H526 included in our study) are the main, evolutionarily conserved mechanism of rifampicin resistance relevant for many bacterial pathogens [44, 45]. This includes the clinically relevant *Mycobacterium tuberculosis*, against which rifampicin treatment remains an important first-line antibiotic [44]. Previous studies have found that the fitness of *rpoB* mutants depends on the presence of mutations at other mechanistically interacting proteins, like other subunits of the RNA polymerase complex [46] and other protein complexes involved in protein synthesis and DNA stability [21, 47]. This type of 'specific epistasis' is easily explained by the close physical and functional proximity of these proteins to *rpoB*. 'Nonspecific epistasis', however, has been observed between genes and proteins that do not interact directly [15]. *RpoB* is an excellent candidate to investigate nonspecific epistasis as it was already shown to be highly pleiotropic: *rpoB* mutations impact the expression of hundreds of genes and many cell phenotypes [29, 48–50]. This demonstrated functional effect of *rpoB* upon many other genes implies that mutations at other loci could impact the fitness of ABR *rpoB* mutations themselves. Therefore, the quantification of G×G interactions at the *rpoB* locus is important in order to know how the danger of ABR depends on the genetic background.

We combined ABR mutations with gene knock-out mutations because the presence or absence of accessory genes is the most common standing genetic variation in natural populations of *E. coli* [51]. To our knowledge, this is the first study to systematically investigate how G×G interactions between SNPs and gene deletions change across different environments. Given its large population sizes and diverse pangenome composition, the core genes of *E. coli*, like *rpoB*, may have evolved mutational robustness to common polymorphisms like gene gain and loss events. This hypothesis may explain why we observed little pairwise epistasis between

rpoB mutants and gene knock-outs across most environments.

We detected a signal of pairwise epistasis in only one of five gene knock-outs, $\Delta waaP$ (figure S21). We had expected $\Delta marR$ as the most likely knock-out mutation to exhibit pairwise epistasis, given its functional role in responding to chemical stressors and antibiotics [52, 35, 36] as well as its previously observed epistatic interactions with ABR mutations at genes involved in DNA stability [53]. $\Delta marR$ did not display significant pairwise epistasis in any environment, only $\Delta waaP$ did. The $\Delta waaP$ genotype on the susceptible *rpoB* wild-type background was more sensitive to low antibiotic concentration than the wild-type and other knock-out single mutants but this sensitivity was masked in combination with any of the three ABR mutations. Gene deletions of other lipopolysaccharide biosynthesis genes have been shown to exhibit negative pairwise epistasis with ABR mutations [54]. $\Delta waaP$ could make cells more sensitive to rifampicin by increasing the permeability of the outer membrane [55, 56]. Among the four functional genes studied, the *waaP* gene has the highest gene diversity (π_{waaP}=0.034 vs π_{nuoC}=0.015, π_{marR}=0.014, π_{yidK}=0.013) and is most frequently found knocked-out (*waaP* is present in 78.5% of strains as compared to 99.5%, 99.3%, and 90.8% for *nuoC, marR*, and *yidK*, respectively) in natural populations, according to the panX database. Moreover, *waaP* impacts bacterial virulence and, so, is relevant in host-pathogen interactions [57]. *E. coli* strains where *waaP* is absent may be more sensitive to low doses of rifampicin and other antibiotics than *waaP*-carrying genotypes. Our observed pattern of epistasis implies that this sensitivity is masked when the genotype carries a resistance mutation. Thus, the G×G interaction of *waaP* and *rpoB* erases selection against $\Delta waaP$ mutations that would occur at low doses of rifampicin.

4.2 Measurement challenges of G×G interactions

One methodological challenge for detecting G×G interactions in our study was that, in the presence of antibiotics, the fitness effects of the ABR mutants quickly overshadowed those of the knock-outs. In this case, methods that involve a relative comparison of direct fitness effects to epistatic effects are bound to infer less epistasis when there are stronger direct effects. The negative correlation of the roughness-to-slope ratio as a function of antibiotic concentration could be explained by this phenomenon: we observed mostly neutral fitness effects and moderate epistasis in the absence of antibiotic but large beneficial fitness effects and no epistasis in the presence of antibiotic. However, the negative correlation between antibiotic concentration and epistasis was also exhibited by other epistasis summary statistics that are independent of the size of direct fitness effects (i.e., gamma epistasis and the mean fraction of reciprocal sign epistasis, figure 3). Therefore, the observed decrease of epistasis with antibiotic concentration is likely a real biological phenomenon.

Our estimates of gamma epistasis for different gene classes suggest that the fitness landscape as a whole was less epistatic as compared to when only ABR mutations or knock-out mutations were considered. This

could reflect a biological pattern (as supported by the low pairwise epistasis results) where the epistatic interactions between amino-acid mutations and gene knock-outs are smaller than within those mutational classes, perhaps due to evolved mutational robustness for gene knock-outs in *E. coli*. Nevertheless, the different trends observed between the gamma epistasis of the different mutational classes are possibly impacted by the differences in sample size. The gamma statistic relies on averaging over multiple mutational effects, which leads to a dilution of the epistatic signal for larger fitness landscapes. In our study, the total dataset has a larger sample size than subsets of the data, and the knock-out mutational class has a larger sample size than the ABR class. Future work should explore how the gamma epistasis measure can be used more appropriately for comparing epistasis between gene classes and differently sized fitness landscapes, for example by randomly subsampling the data to an equal size for all categories.

4.3 Environmental interactions & their importance

It has long been established that there is a G×E interaction between rifampicin resistance mutations at the *rpoB* locus and temperature [58], among other environmental factors [59, 7, 60]. In a previous experiment, [29] observed that *E. coli* adapted to high temperature evolved rifampicin resistance despite no rifampicin treatment. Therefore, we hypothesized that there would be an E×E interaction between high temperature environments and rifampicin environments, which, if mediated by ABR mutations at the *rpoB* locus, could result in $G_{rpoB} \times E_{AB} \times E_T$ interactions as well. Overall we observed no cost of rifampicin resistance in minimal media, which is consistent with [61] and could be attributed to ABR *rpoB* mutations mimicking the stringent response [46]. There was a modest positive effect of high temperatures on the competitive fitness of all genotypes and a weak E×E interaction between temperature and antibiotic. However, contrary to previous studies that also used batch cultures with glucose and minimal medium [27, 29], the *rpoB* mutations S512F and I572S did not grow better and H526Y did not grow worse than the wild type at higher temperatures. (In fact, H526Y was observed to grow *better* than the wild type at $42°C$.) The discrepancy for I572S could be attributed to G×G×E with the genetic background: [29] found a strong effect of *E. coli* genetic background on the fitness at site I572. On the other hand, the discrepancies for S512F and H526Y could be that, unlike in [27], our batch cultures were not acclimatized to the environment in which the competitions occurred. This underscores the sensitivity of organisms to their environments and the importance of complete reporting of experimental methods.

We used the overall environmental quality as a regressor to quantify the interaction between epistasis and environment, G×G×E. We found that the antibiotic concentration alone was a better regressor of epistasis than the environmental quality, implying that temperature did not have an effect on epistasis. We had expected that the overall environmental quality would be a better regressor because it is highly correlated with

antibiotic concentration while also taking into account the effects of temperature. On the other hand, fitting of linear models with higher-order interactions suggested that temperature exhibited a stronger interaction with $G_{rpoB} \times G_{KO}$ than antibiotic concentration. Unfortunately, we have limited confidence in the linear regression results due to low sample size and the high order of the investigated interactions. However, this apparent contradiction opens up new questions about G×G×E interactions: for example, is it possible that one environmental variable affects direct G×E interactions, whereas the other acts on the G×G×E level? We are not aware of any previous work that has extracted such systematic patterns empirically, inferred their functional underpinnings, or developed models to account for such interaction. Certainly, the consequences of different interaction levels will be important to study in the future to predict potential evolutionary trajectories in varying environments.

4.4 Why is there so little epistasis in these ABR fitness landscapes?

Overall, we found little G×G and G×G×E interactions in our data. This result is in stark contrast to various recent experimental studies, which have presented strong evidence that both fitness effects of single mutations and their epistatic fitness interactions may vary greatly between environments [62, 8, 63] (reviewed in [2]). One reason for this discrepancy may be the choice of mutations for the fitness landscapes. Previous studies focused on SNPs between or within genes that had been found in an adaptive walk [64–66], indirectly inferred strong G×G(×E) by observing that adaptations were unique to the genetic background [20, 67, 10], or measured epistasis as the different effect of ABR mutations across vastly different genetic backgrounds [68, 69]. We here quantified epistatic interactions between ABR SNPs and (non-ABR) gene knock-out mutations that occur in natural populations of *E. coli*. The studied combinations of mutations thus had no immediate relationship except the *rpoB* mutations' previously characterized G×E interaction for fitness under higher temperature or antibiotic. From a quantitative genetic view, our findings are unsurprising; here, epistasis is assumed to be rare or of little importance during evolution [70]. However, multiple studies in systems or molecular biology have shown that epistasis is common (reviewed in [15]). In particular, when two or more beneficial mutations are combined, negative epistasis in the shape of diminishing returns (i.e., where the fitness effect of a mutation is less beneficial when it occurs on a fitter background) has been observed ubiquitously [71, 18, 54, 17], including for *rpoB* mutations conferring ABR to rifampicin [72]. In our study, we observed diminishing-returns epistasis only for the *rpoB* ABR mutations but no diminishing-returns epistasis for the knock-out mutations. Moreover, we did not observe any qualitative environmental trend in the strength of the diminishing-returns epistasis for the ABR mutations, although the mutations shifted from neutral to beneficial as a function of antibiotic. Although there have been studies that derived null expectations of epistasis between random mutations of the same type [73], between mutations characterized

by their fitness effect [74], or between SNPs in a pair of genes in a metabolic pathway [75], we are not aware of any general models or empirical studies that have proposed or quantified a null distribution of epistatic effects between SNPs and different structural mutation types (except the assumption of no epistasis). Therefore, it is not clear whether the low G×G and G×G×E interactions observed in our data are to be expected.

Although we are not aware of general epistatic null models, theoretical and empirical works have proposed a few hypotheses on how much epistasis to expect between mutations that confer ABR. For example, [25] found ubiquitous sign epistasis, in all 30 environments assayed, for a fitness landscape with all possible combinations of four ABR mutations. [21] found that epistasis is rare between combinations of ABR mutations. Our finding that $\sim 20\%$ of randomly selected combinations of mutations exhibit pairwise epistasis is in good quantitative agreement with the results of [21]. One important difference between our work and most previous work on ABR epistasis is that the knock-out mutations we investigated neither interacted directly with *rpoB* (as required for specific epistasis) nor, except $\Delta waaP$, displayed any significant effects on fitness (figure S28). Epistasis expressed by seemingly neutral mutations is termed 'cryptic epistasis', and has been previously observed between mutations that were fixed during an adaptive walk [76, 66]. We have uncovered new instances of cryptic epistasis that depend on environment. Using a theoretical model, [77] related the expected epistasis to the extent of G×E interactions of the involved mutations: they proposed that when there is no cost to the ABR mutations, there should be no epistasis between them. Moreover, a study by [26], considering only ABR mutations with a cost of resistance, predicted using mathematical models, and observed empirically, the strongest epistasis at intermediate antibiotic concentrations. We used intermediate antibiotic concentrations, with 4 $\mu g/mL$ below and 10 $\mu g/mL$ near the minimum inhibitory concentration (MIC) of the wild-type *rpoB* (figure S14), and ABR mutations without a cost of resistance (although a cost had been expected according to previous studies, see above) in combination with non-ABR mutations. Our finding of very little epistasis in the presence of antibiotic is thus most consistent with the prediction of [77].

4.5 ABR fitness landscapes may become smoother in the presence of antibiotic

Our main conclusion is that epistasis decreases with increasing antibiotic concentration. Only in the absence of antibiotic, we observed several instances of reciprocal sign epistasis for all three ABR mutations and at all temperature environments (table S7). The presence of reciprocal sign epistasis implies that the fitness landscape has multiple peaks and that evolution may be less predictable in the absence of antibiotic. Overall, our results are consistent with the conclusion that the underlying fitness landscapes of ABR mutations and gene knock-outs are more rugged in the absence of antibiotic than in the presence of higher concentrations of antibiotic. Extrapolated to the larger sequence space, our results would imply that evolution is more predictable in the presence than in the absence of antibiotic, because ABR mutations have such strong

beneficial effects in the presence of high antibiotic concentrations. Here, the strong effect of the ABR mutations potentially overrides any effects of the genetic background.

5 Data Availability

All flow cytometry raw data, FlowJo analysis files, cell counts, competitive fitness estimates, and the code used to generate the analyses is publicly available at the following Git repository: https://gitlab.com/evoldynamics/epistasis-decreases-with-increasing-antibiotic-pressure. Illumina sequencing data will be deposited to GenBank ASAP (refs to go here).

6 Acknowledgements

We would like to thank the Flow Cytometry Facility of Instituto Gulbenkian de Ciência and the Next Generation Sequencing (NGS) Platform of UBern for their services and assistance. AHG acknowledges funding from FCT PhD funding grant PD/BD/138215/2018. CB acknowledges funding from ERC Starting Grant 804569 (FIT2GO) and SNSF Project Grant 315230_204838/1 (MiCo4Sys). IG and CB acknowledge funding from FCT PREPARE project (JPIAMR/0001/2016-ERA-NET). We are grateful to the members of the Evolutionary Biology group for *E. coli* strains (R. Balbontín & P. Durão), training in microbiology (D. Guleresi), and consultation on methods, and to the members of the Evolutionary Dynamics/Theoretical Ecology and Evolution group for help with preliminary environmental screenings (C. Diwo), genetic engineering (M. Schmitz), consultation on WGS (A. Kapopoulou), and discussions. We thank S. Yeaman, F. Blanquart, and T. Batallion for feedback on results; and the PREPARE consortium for ideas and experimental design.

References

[1] Michael Lässig, Ville Mustonen, and Aleksandra M Walczak. Predicting evolution. *Nature ecology & evolution*, 1(3):1–9, 2017.

[2] Claudia Bank. Epistasis and adaptation on fitness landscapes. *Annual Reviews in Ecology, Evolution, and Systematics*.

[3] JAGM De Visser and Joachim Krug. Empirical fitness landscapes and the predictability of evolution. *Nature Reviews Genetics*, 15(7):480–490, 2014.

[4] Anita H Melnyk, Alex Wong, and Rees Kassen. The fitness costs of antibiotic resistance mutations. *Evolutionary applications*, 8(3):273–283, 2015.

[5] T Lenormand, N Harmand, and R Gallet. Cost of resistance: an unreasonably expensive concept. *Rethinking Ecology*, 3:51–70, 2018.

[6] Olivier Tenaillon, Alejandra Rodríguez-Verdugo, Rebecca L Gaut, Pamela McDonald, Albert F Bennett, Anthony D Long, and Brandon S Gaut. The molecular diversity of adaptive convergence. *Science*, 335(6067):457–461, 2012.

[7] Anna Knöppel, Joakim Näsvall, and Dan I Andersson. Evolution of antibiotic resistance without antibiotic exposure. *Antimicrobial agents and chemotherapy*, 61(11):e01495–17, 2017.

[8] Rafael F Guerrero, Samuel V Scarpino, João V Rodrigues, Daniel L Hartl, and C Brandon Ogbunugafor. Proteostasis environment shapes higher-order epistasis operating on antibiotic resistance. *Genetics*, 212(2):565–575, 2019.

[9] Fernanda Pinheiro, Omar Warsi, Dan I Andersson, and Michael Lässig. Metabolic fitness landscapes predict the evolution of antibiotic resistance. *Nature Ecology & Evolution*, 5(5):677–687, 2021.

[10] Sara Hernando-Amado, Pablo Laborda, José Ramón Valverde, and José Luis Martínez. Mutational background influences *P. aeruginosa* ciprofloxacin resistance evolution but preserves collateral sensitivity robustness. *Proceedings of the National Academy of Sciences*, 119(15):e2109370119, 2022.

[11] Rustam I Aminov. A brief history of the antibiotic era: lessons learned and challenges for the future. *Frontiers in microbiology*, 1:134, 2010.

[12] Christopher JL Murray, Kevin Shunji Ikuta, Fablina Sharara, Lucien Swetschinski, Gisela Robles Aguilar, Authia Gray, Chieh Han, Catherine Bisignano, Puja Rao, Eve Wool, et al. Global burden of bacterial antimicrobial resistance in 2019: a systematic analysis. *The Lancet*, 399(10325):629–655, 2022.

[13] Marta Lukačišinová and Tobias Bollenbach. Toward a quantitative understanding of antibiotic resistance evolution. *Current Opinion in Biotechnology*, 46:90–97, 2017.

[14] Scott A McEwen and Peter J Collignon. Antimicrobial resistance: a one health perspective. *Microbiology spectrum*, 6(2):6–2, 2018.

[15] Júlia Domingo, Pablo Baeza-Centurion, and Ben Lehner. The causes and consequences of genetic interactions (epistasis). *Annual Review of Genomics and Human Genetics*, 20:17.1–17.28, 2019.

[16] Chuan Li and Jianzhi Zhang. Multi-environment fitness landscapes of a trna gene. *Nature ecology & evolution*, 2(6):1025–1032, 2018.

[17] Gautam Reddy and Michael M Desai. Global epistasis emerges from a generic model of a complex trait. *Elife*, 10:e64740, 2021.

[18] L Perfeito, A Sousa, T Bataillon, and I Gordo. Rates of fitness decline and rebound suggest pervasive epistasis. *Evolution*, 68(1):150–162, 2014.

[19] Jasmine Ono, Aleeza C Gerstein, and Sarah P Otto. Widespread genetic incompatibilities between first-step mutations during parallel adaptation of *Saccharomyces cerevisiae* to a common environment. *PLoS biology*, 15(1):e1002591, 2017.

[20] Ákos Nyerges, Bálint Csörgő, Gábor Draskovits, Bálint Kintses, Petra Szili, Györgyi Ferenc, Tamás Révész, Eszter Ari, István Nagy, Balázs Bálint, et al. Directed evolution of multiple genomic loci allows the prediction of antibiotic resistance. *Proceedings of the National Academy of Sciences*, 115(25):E5726–E5735, 2018.

[21] Michael Knopp and Dan I Andersson. Predictable phenotypes of antibiotic resistance mutations. *MBio*, 9(3):e00770–18, 2018.

[22] Portia M Mira, Bjørn Østman, Candace Guzman-Cole, Suzanne Sindi, and Miriam Barlow. Adaptive processes change as multiple functions evolve. *Antimicrobial Agents and Chemotherapy*, 65(4):e01990–20, 2021.

[23] Inês Fragata, Alexandre Blanckaert, Marco António Dias Louro, David A Liberles, and Claudia Bank. Evolution in the light of fitness landscape theory. *Trends in ecology & evolution*, 34(1):69–82, 2019.

[24] Florien A Gorter, Mark GM Aarts, Bas J Zwaan, and J Arjan GM de Visser. Local fitness landscapes predict yeast evolutionary dynamics in directionally changing environments. *Genetics*, 208(1):307–322, 2018.

[25] Portia M Mira, Juan C Meza, Anna Nandipati, and Miriam Barlow. Adaptive landscapes of resistance genes change as antibiotic concentrations change. *Molecular biology and evolution*, 32(10):2707–2715, 2015.

[26] Suman G Das, Susana OL Direito, Bartlomiej Waclaw, Rosalind J Allen, and Joachim Krug. Predictable properties of fitness landscapes induced by adaptational tradeoffs. *Elife*, 9:e55155, 2020.

[27] Sandra Trindade, Ana Sousa, and Isabel Gordo. Antibiotic resistance and stress in the light of Fisher's model. *Evolution*, 66(12):3815–3824, 2012.

[28] Paulo Durão, Sandra Trindade, Ana Sousa, and Isabel Gordo. Multiple resistance at no cost: rifampicin and streptomycin a dangerous liaison in the spread of antibiotic resistance. *Molecular biology and evolution*, 32(10):2675–2680, 2015.

[29] Alejandra Rodríguez-Verdugo, Brandon S Gaut, and Olivier Tenaillon. Evolution of *Escherichia coli* rifampicin resistance in an antibiotic-free environment during thermal stress. *BMC evolutionary biology*, 13:50, 2013.

[30] Robert J Nichols, Saunak Sen, Yoe Jin Choo, Pedro Beltrao, Matylda Zietek, Rachna Chaba, Sueyoung Lee, Krystyna M Kazmierczak, Karis J Lee, Angela Wong, et al. Phenotypic landscape of a bacterial cell. *Cell*, 144(1):143–156, 2011.

[31] George Kritikos, Manuel Banzhaf, Lucia Herrera-Dominguez, Alexandra Koumoutsi, Morgane Wartel, Matylda Zietek, and Athanasios Typas. A tool named Iris for versatile high-throughput phenotyping in microorganisms. *Nature microbiology*, 2(5):17014, 2017.

[32] Tomoya Baba, Takeshi Ara, Miki Hasegawa, Yuki Takai, Yoshiko Okumura, Miki Baba, Kirill A Datsenko, Masaru Tomita, Barry L Wanner, and Hirotada Mori. Construction of *Escherichia coli* K-12 in-frame, single-gene knockout mutants: the Keio collection. *Molecular systems biology*, 2:2006.0008, 2006.

[33] Wei Ding, Franz Baumdicker, and Richard A Neher. panX: pan-genome analysis and exploration. *Nucleic acids research*, 46(1):e5, 2018.

[34] Anita Krisko, Tea Copic, Toni Gabaldón, Ben Lehner, and Fran Supek. Inferring gene function from evolutionary change in signatures of translation efficiency. *Genome biology*, 15:R44, 2014.

[35] Lisa Praski Alzrigat, Douglas L Huseby, Gerrit Brandis, and Diarmaid Hughes. Resistance/fitness trade-off is a barrier to the evolution of MarR inactivation mutants in *Escherichia coli*. *Journal of Antimicrobial Chemotherapy*, 76(1):77–83, 2021.

[36] Esmeralda Z Reyes-Fernández and Shimon Schuldiner. Acidification of cytoplasm in *Escherichia coli* provides a strategy to cope with stress and facilitates development of antibiotic resistance. *Scientific reports*, 10(1):1–13, 2020.

[37] Thorsten Friedrich. The NADH:ubiquinone oxidoreductase (complex I) from *Escherichia coli*. *Biochimica et Biophysica Acta (BBA)-Bioenergetics*, 1364(2):134–146, 1998.

[38] Daniel O Daley, Mikaela Rapp, Erik Granseth, Karin Melén, David Drew, and Gunnar Von Heijne. Global topology analysis of the *Escherichia coli* inner membrane proteome. *Science*, 308(5726):1321–1323, 2005.

[39] Jeremy A Yethon and Chris Whitfield. Purification and characterization of waaP from *Escherichia coli*, a lipopolysaccharide kinase essential for outer membrane stability. *Journal of Biological Chemistry*, 276(8):5498–5504, 2001.

[40] Luca Ferretti, Benjamin Schmiegelt, Daniel Weinreich, Atsushi Yamauchi, Yutaka Kobayashi, Fumio Tajima, and Guillaume Achaz. Measuring epistasis in fitness landscapes: The correlation of fitness effects of mutations. *Journal of Theoretical Biology*, 396:132–143, 2016.

[41] Ivan G Szendro, Martijn F Schenk, Jasper Franke, Joachim Krug, and J Arjan GM De Visser. Quantitative analyses of empirical fitness landscapes. *Journal of Statistical Mechanics: Theory and Experiment*, 2013:P01005, 2013.

[42] Marcos Malosetti, Jean-Marcel Ribaut, and Fred A van Eeuwijk. The statistical analysis of multi-environment data: modeling genotype-by-environment interaction and its genetic basis. *Frontiers in physiology*, 4:44, 2013.

[43] Michael C Whitlock, Patrick C Phillips, Francisco B-G Moore, and Stephen J Tonsor. Multiple fitness peaks and epistasis. *Annual review of ecology and systematics*, 26:601–629, 1995.

[44] Beth P Goldstein. Resistance to rifampicin: a review. *The Journal of antibiotics*, 67(9):625–630, 2014.

[45] Laura Cutugno, Jennifer Mc Cafferty, Jan Pané-Farré, Conor O'Byrne, and Aoife Boyd. *rpoB* mutations conferring rifampicin-resistance affect growth, stress response and motility in *Vibrio vulnificus*. *Microbiology*, 166(12):1160, 2020.

[46] Anastasia Koch, Valerie Mizrahi, and Digby F Warner. The impact of drug resistance on *Mycobacterium tuberculosis* physiology: what can we learn from rifampicin? *Emerging microbes & infections*, 3(1):1–11, 2014.

[47] Roberto Balbontín, Nelson Frazão, and Isabel Gordo. DNA breaks-mediated fitness cost reveals RNase HI as a new target for selectively eliminating antibiotic-resistant bacteria. *Molecular biology and evolution*, 38(8):3220–3234, 2021.

[48] Shaun M Hug and Brandon S Gaut. The phenotypic signature of adaptation to thermal stress in *Escherichia coli*. *BMC evolutionary biology*, 15(1):177, 2015.

[49] Franziska Pietsch, Jessica M Bergman, Gerrit Brandis, Linda L Marcusson, Anna Zorzet, Douglas L Huseby, and Diarmaid Hughes. Ciprofloxacin selects for RNA polymerase mutations with pleiotropic antibiotic resistance effects. *Journal of Antimicrobial Chemotherapy*, 72(1):75–84, 2016.

[50] Alejandra Rodríguez-Verdugo, Olivier Tenaillon, and Brandon S Gaut. First-step mutations during adaptation restore the expression of hundreds of genes. *Molecular biology and evolution*, 33(1):25–39, 2016.

[51] Marie Touchon, Claire Hoede, Olivier Tenaillon, Valérie Barbe, Simon Baeriswyl, Philippe Bidet, Edouard Bingen, Stéphane Bonacorsi, Christiane Bouchier, Odile Bouvet, et al. Organised genome dynamics in the *Escherichia coli* species results in highly diverse adaptive paths. *PLoS genetics*, 5(1):e1000344, 2009.

[52] Dinesh K Deochand and Anne Grove. MarR family transcription factors: dynamic variations on a common scaffold. *Critical reviews in biochemistry and molecular biology*, 52(6):595–613, 2017.

[53] Linda L Marcusson, Niels Frimodt-Møller, and Diarmaid Hughes. Interplay in the selection of fluoroquinolone resistance and bacterial fitness. *PLoS pathogens*, 5(8):e1000541, 2009.

[54] Marta Lukačišinová, Booshini Fernando, and Tobias Bollenbach. Highly parallel lab evolution reveals that epistasis can curb the evolution of antibiotic resistance. *Nature communications*, 11(1):1–14, 2020.

[55] Zhou Wang, Jianli Wang, Ge Ren, Ye Li, and Xiaoyuan Wang. Influence of core oligosaccharide of lipopolysaccharide to outer membrane behavior of *Escherichia coli*. *Marine drugs*, 13(6):3325–3339, 2015.

[56] Ge Xu, Hangchi Liu, Xudong Jia, Xiaomin Wang, and Peng Xu. Mechanisms and detection methods of *Mycobacterium tuberculosis* rifampicin resistance: The phenomenon of drug resistance is complex. *Tuberculosis*, 128:102083, 2021.

[57] Jeremy A Yethon, John S Gunn, Robert K Ernst, Samuel I Miller, Line Laroche, Danielle Malo, and Chris Whitfield. *Salmonella enterica* serovar typhimurium *waaP* mutants show increased susceptibility to polymyxin and loss of virulence in vivo. *Infection and immunity*, 68(8):4485–4491, 2000.

[58] Ding Jun Jin and Carol A Gross. Characterization of the pleiotropic phenotypes of rifampin-resistant *rpoB* mutants of *Escherichia coli*. *Journal of bacteriology*, 171(9):5229–5231, 1989.

[59] AR Hall. Genotype-by-environment interactions due to antibiotic resistance and adaptation in *Escherichia coli*. *Journal of Evolutionary Biology*, 26(8):1655–1664, 2013.

[60] Violeta Zorraquino, Minseung Kim, Navneet Rai, and Ilias Tagkopoulos. The genetic and transcriptional basis of short and long term adaptation across multiple stresses in *Escherichia coli*. *Molecular Biology and Evolution*, 34(3):707–717, 2017.

[61] Wenfang Lin, Jie Zeng, Kun Wan, Lu Lv, Lizheng Guo, Xi Li, and Xin Yu. Reduction of the fitness cost of antibiotic resistance caused by chromosomal mutations under poor nutrient conditions. *Environment international*, 120:63–71, 2018.

[62] Kenneth M Flynn, Tim F Cooper, Francisco BG Moore, and Vaughn S Cooper. The environment affects epistatic interactions to alter the topology of an empirical fitness landscape. *PLoS genetics*, 9(4):e1003426, 2013.

[63] Julia M Flynn, Ammeret Rossouw, Pamela Cote-Hammarlof, Ines Fragata, David Mavor, Carl Hollins III, Claudia Bank, and Daniel NA Bolon. Comprehensive fitness maps of Hsp90 show widespread environmental dependence. *Elife*, 9:e53810, 2020.

[64] Anne E Hall, Kedar Karkare, Vaughn S Cooper, Claudia Bank, Tim F Cooper, and Francisco B-G Moore. Environment changes epistasis to alter trade-offs along alternative evolutionary paths. *Evolution*, 73(10):2094–2105, 2019.

[65] Tyler N Starr, Julia M Flynn, Parul Mishra, Daniel NA Bolon, and Joseph W Thornton. Pervasive contingency and entrenchment in a billion years of Hsp90 evolution. *Proceedings of the National Academy of Sciences*, 115(17):4453–4458, 2018.

[66] Yeonwoo Park, Brian PH Metzger, and Joseph W Thornton. Epistatic drift causes gradual decay of predictability in protein evolution. *Science*, 376(6595):823–830, 2022.

[67] Marloes Hoeksema, Martijs J Jonker, Stanley Brul, and Benno H Ter Kuile. Effects of a previously selected antibiotic resistance on mutations acquired during development of a second resistance in *Escherichia coli*. *BMC genomics*, 20(1):1–14, 2019.

[68] Thomas Vogwill, Mila Kojadinovic, and RC MacLean. Epistasis between antibiotic resistance mutations and genetic background shape the fitness effect of resistance across species of *Pseudomonas*. *Proceedings of the Royal Society B: Biological Sciences*, 283(1830):20160151, 2016.

[69] Gábor Apjok, Gábor Boross, Ákos Nyerges, Gergely Fekete, Viktória Lázár, Balázs Papp, Csaba Pál, and Bálint Csörgő. Limited evolutionary conservation of the phenotypic effects of antibiotic resistance mutations. *Molecular biology and evolution*, 36(8):1601–1611, 2019.

[70] Michael Lynch and Bruce Walsh. *Genetics and analysis of quantitative traits*, volume 1. Sinauer, Sunderland, MA, 1998.

[71] Aisha I Khan, Duy M Dinh, Dominique Schneider, Richard E Lenski, and Tim F Cooper. Negative epistasis between beneficial mutations in an evolving bacterial population. *Science*, 332(6034):1193–1196, 2011.

[72] RC MacLean, GG Perron, and Andy Gardner. Diminishing returns from beneficial mutations and pervasive epistasis shape the fitness landscape for rifampicin resistance in *Pseudomonas aeruginosa*. *Genetics*, 186(4):1345–1354, 2010.

[73] Guillaume Martin, Santiago F Elena, and Thomas Lenormand. Distributions of epistasis in microbes fit predictions from a fitness landscape model. *Nature genetics*, 39(4):555–560, 2007.

[74] Guillaume Martin and Thomas Lenormand. The fitness effect of mutations across environments: Fisher's geometrical model with multiple optima. *Evolution*, 69(6):1433–1447, 2015.

[75] Harry Kemble, Catherine Eisenhauer, Alejandro Couce, Audrey Chapron, Mélanie Magnan, Gregory Gautier, Hervé Le Nagard, Philippe Nghe, and Olivier Tenaillon. Flux, toxicity, and expression costs generate complex genetic interactions in a metabolic pathway. *Science Advances*, 6(23):eabb2236, 2020.

[76] Mark Lunzer, G Brian Golding, and Antony M Dean. Pervasive cryptic epistasis in molecular evolution. *PLoS genetics*, 6(10):e1001162, 2010.

[77] Jan Engelstädter. Fitness landscapes emerging from pharmacodynamic functions in the evolution of multidrug resistance. *Journal of evolutionary biology*, 27(5):840–853, 2014.

[78] Sandra Trindade, Ana Sousa, Karina Bivar Xavier, Francisco Dionisio, Miguel Godinho Ferreira, and Isabel Gordo. Positive epistasis drives the acquisition of multidrug resistance. *PLoS genetics*, 5(7):e1000578, 2009.

[79] Lynn C Thomason, Nina Costantino, and Donald L Court. *E. coli* genome manipulation by P1 transduction. *Current protocols in molecular biology*, 79:1.17.1–1.17.8, 2007.

[80] Kirill A Datsenko and Barry L Wanner. One-step inactivation of chromosomal genes in *Escherichia coli* K-12 using PCR products. *Proceedings of the National Academy of Sciences*, 97(12):6640–6645, 2000.

7 Supplementary

Contents

8 Supplementary results **25**
- 8.1 Sample confirmation by whole genome re-sequencing . . . 25
- 8.2 Antibiotic dose response curves of the wild-type genotype . . . 52
- 8.3 Ascertaining flow cytometry estimates of competitive fitness . . . 53
- 8.4 Cost of resistance . . . 56
- 8.5 GxG summary statistics . . . 57
  - 8.5.1 'Classical' pairwise epistasis . . . 57
  - 8.5.2 Gamma epistasis . . . 60
  - 8.5.3 Fraction of sign epistasis . . . 61
  - 8.5.4 Roughness-to-slope ratio . . . 63
  - 8.5.5 Diminishing-returns epistasis . . . 64
- 8.6 Multiple regression for competitive fitness . . . 65
- 8.7 Finlay-Wilkinson regression on overall environmental quality . . . 71
  - 8.7.1 Selecting the metric of environmental quality . . . 71
  - 8.7.2 Finlay-Wilkinson environmental quality regression for GxG summary statistics . . . 77

9 Materials & Methods **82**
- 9.1 Constructing and confirming the genotypes . . . 82
  - 9.1.1 Obtaining the ABR Mutations . . . 82
  - 9.1.2 Genetic engineering . . . 82
  - 9.1.3 Whole genome sequencing and analysis . . . 87
- 9.2 Estimating the competitive fitnesses . . . 92
  - 9.2.1 Cell growth protocol . . . 92
  - 9.2.2 Flow cytometry protocol . . . 92
  - 9.2.3 Estimating competitive index . . . 94
- 9.3 Analyses . . . 94

8 Supplementary results

8.1 Sample confirmation by whole genome re-sequencing

The genotypes were verified by Illumina whole-genome sequencing to just over 115-fold read-depth on average and consistent coverage throughout the reference genome/sequences (see tables S1-S2 and representative figures S1-S9, S11). Sequencing results suggested that the double-mutant *rpoB* S512F Δ*ybfG* (AHG100) was contaminated by the preceding double-mutant sample from our library, *rpoB* S512F Δ*waaP* (AHG098; evidence shown in figures S7, S9d, S10), at a near 50% population frequency based on the relative read depth of the new junction evidences (figure S12). PCR of the potentially contaminated *rpoB* S512F Δ*ybfG* $-80°C$ stock culture and the DNA extraction sent for sequencing failed to amplify the contaminating Δ*waaP* construct (figure S13). Therefore we assume that the contamination happened during sequencing and results from *rpoB* S512F Δ*ybfG* are included in all analyses. The complete list of mutations identified by whole-genome re-sequencing as compared to the wild-type genotype (sample AHG015) is given in table S3. Three genotypes (the double-mutant *rpoB* I572S Δ*nuoC*, the single-mutant *rpoB* S512F, and the single-mutant Δ*yidK*) had mutations in coding sequence regions as compared to the wild-type.

Of the 25 genotypes, three were found to have *de novo* mutations that may impact our results. The anticipated effects of these *de novo* mutations are as follows: *I.* The double-mutant *rpoB* I572S Δ*nuoC* had two non-conservative mutations, N135K in the phage superinfection exclusion protein *sieB* and D263Y in the respiratory enzyme *glpD*. We anticipate that the first mutation would not have any functional effects in our study as phages are dormant in the MG1655 strain. Similarly, we anticipate little functional effects from the second mutation since the gene is involved in glycerol metabolism and glycerol is absent from our experimental media. *II.* The single-mutant *rpoB* S512F had a very conservative amino-acid mutation (A32G) in a gene of unknown function (*yaeC*); we anticipate little functional effects for this mutation. *III.* Finally, the single-mutant Δ*yidK* had an in-frame 9 bp mobile element insertion in a putative endonuclease involved in DNA recombination and Type VI secretion (*yhhZ*). We cannot anticipate what the effect of this mutation would be in our experiment.

It is unlikely that the *de novo* mutations of the aforementioned three genotypes impact the main results of our experiment. If these *de novo* mutations had significant effects on the fitnesses of the genotypes they are found on, we might expect to detect this as pairwise epistasis because each *de novo* mutation occurred on a different background. However, none of the genotypes above was found to have a different pattern of pairwise epistasis as compared to other backgrounds.

Table S1: Summary of Illumina sequencing quality for all 25 genotypes used in competitions. (Engineered mutations are listed in table S12.)

Sample	**Total reads**	**Percent $\geqq$ Q30 bases**	**Mean quality score**
AHG015	2 386 555	94.8%	36.1
AHG052	2 548 429	94.2%	36.0
AHG058	2 776 656	94.8%	36.1
AHG060	1 909 742	94.1%	36.0
AHG064	1 936 480	94.4%	36.0
AHG066	2 261 715	94.7%	36.0
AHG068	2 468 947	95.0%	36.1
AHG070	2 422 297	94.7%	36.0
AHG072	2 282 396	94.8%	36.0
AHG074	2 210 693	93.9%	35.9
AHG076	2 689 166	95.0%	36.1
AHG078	2 495 375	95.0%	36.1
AHG079	2 325 135	94.9%	36.1
AHG080	2 632 699	95.1%	36.1
AHG082	2 441 375	94.5%	36.0
AHG088	2 500 358	94.3%	36.0
AHG090	2 294 050	94.9%	36.1
AHG092	2 473 343	95.0%	36.1
AHG094	2 558 647	94.8%	36.1
AHG096	2 690 571	95.0%	36.1
AHG098	2 291 453	94.7%	36.0
AHG100	2 606 356	94.7%	36.0
AHG102	3 107 144	91.8%	35.5
AHG104	2 162 073	94.6%	36.0
AHG106	2 458 521	94.6%	36.0

Table S2: Summary of breseq sequence mapping quality for all 25 genotypes used in competitions. Total reads used is less than total reads sequenced from table S1 since an average read depth limit of 120x was set, as recommended in the breseq manual. Mean read depth is the average across all reference sequences (*not* weighted by reference sequence length). Engineered mutations are listed in table S12.

Sample	**Total reads used**	**Mean read length**	**% reads mapped**	**Mean read depth**
AHG015	3 700 125	150.6 bases	97.8%	117.2
AHG052	3 702 686	150.6 bases	97.6%	120.0
AHG058	3 702 707	150.6 bases	98.2%	119.7
AHG060	3 702 714	150.6 bases	98.2%	111.7
AHG064	3 702 704	150.6 bases	97.9%	116.1
AHG066	3 702 744	150.6 bases	98.1%	113.9
AHG068	3 702 740	150.6 bases	98.3%	117.2
AHG070	3 702 725	150.6 bases	98.1%	116.2
AHG072	3 702 732	150.6 bases	97.8%	115.3
AHG074	3 702 768	150.6 bases	97.5%	115.7
AHG076	3 702 698	150.6 bases	97.8%	116.9
AHG078	3 702 667	150.6 bases	97.9%	113.6
AHG079	3 704 544	150.6 bases	98.1%	122.5
AHG080	3 702 716	150.6 bases	98.1%	116.4
AHG082	3 702 707	150.6 bases	97.9%	119.4
AHG088	3 702 678	150.6 bases	97.8%	113.9
AHG090	3 702 737	150.6 bases	97.6%	116.5
AHG092	3 702 711	150.6 bases	98.0%	114.6
AHG094	3 702 620	150.6 bases	94.8%	115.5
AHG096	3 702 724	150.6 bases	97.9%	116.0
AHG098	3 702 699	150.6 bases	97.3%	112.5
AHG100	3 702 690	150.6 bases	97.8%	121.3
AHG102	3 702 620	150.6 bases	97.0%	117.2
AHG104	3 702 751	150.6 bases	98.2%	117.0
AHG106	3 702 704	150.6 bases	97.9%	112.4

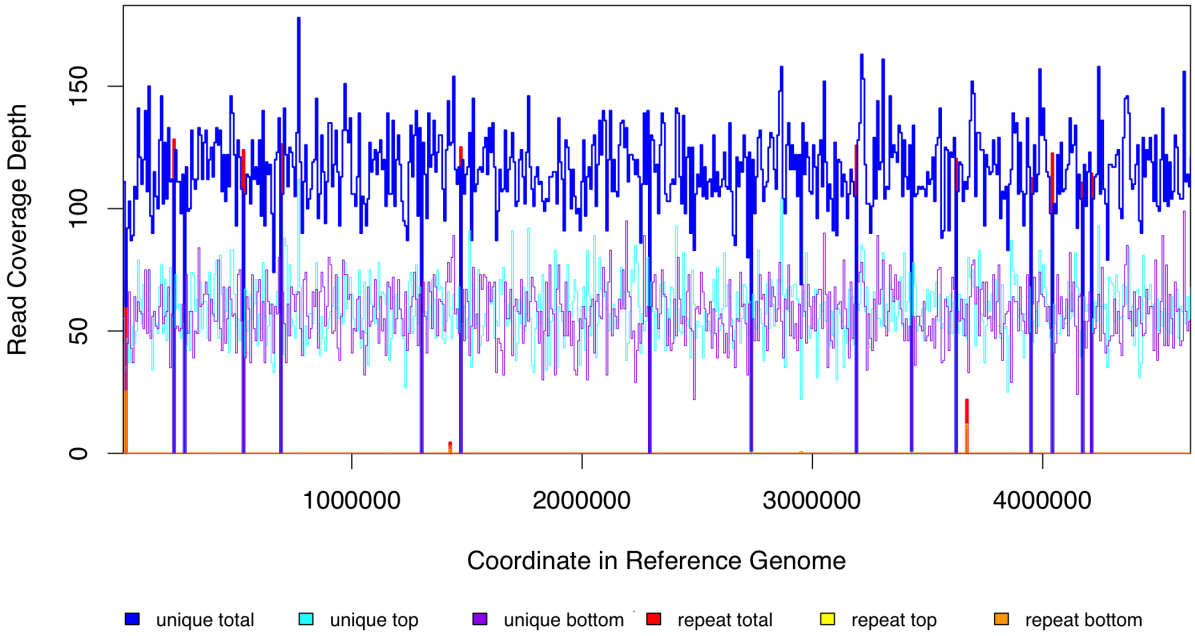

(a) Reference sequence: NC000913.

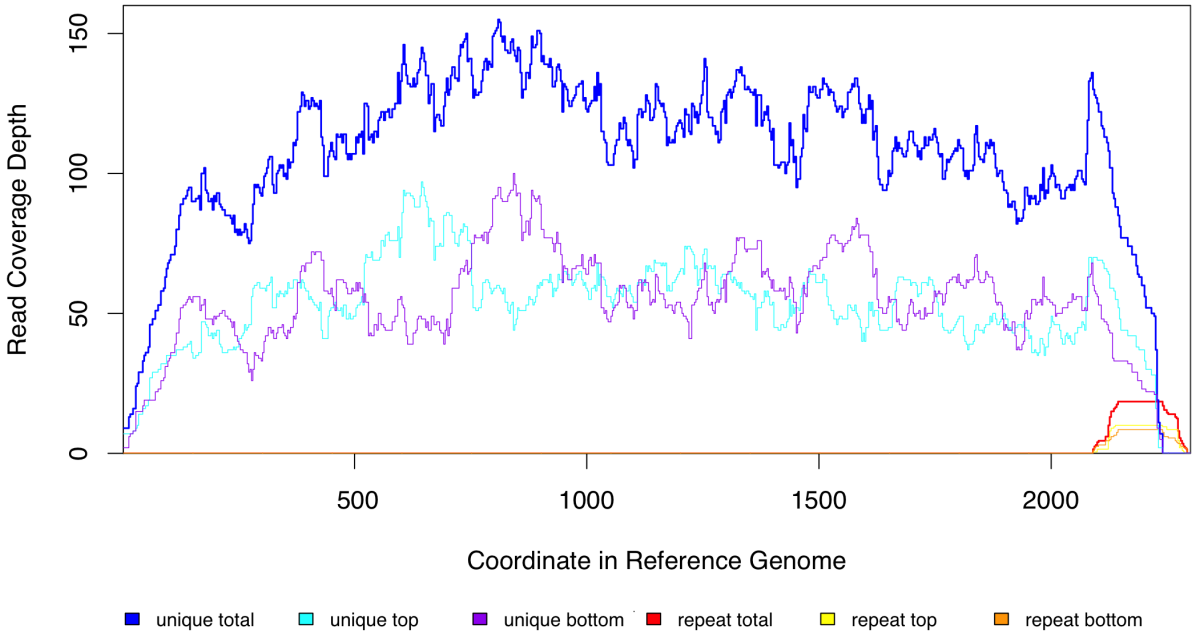

(b) Reference sequence: sfGFP.

Figure S1: Breseq read coverage plots of all reference genomes used for wild-type sample (AHG015). a) 'NC000913' is the MG1655 reference sequence from GenBank (NC_000913.3) and b) the sequence for the sfGFP construct is included in the supplementary methods.

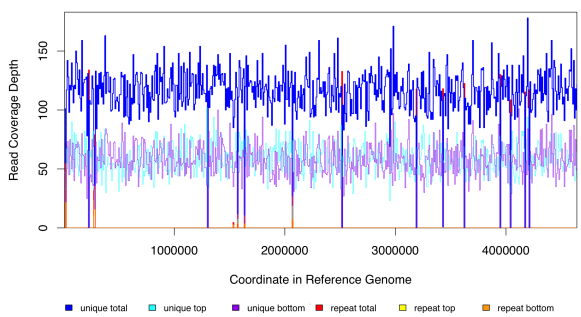

(a) Reference sequence: NC000913.

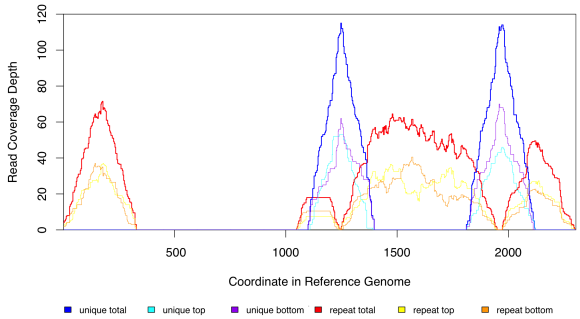

(b) Reference sequence: sfGFP.

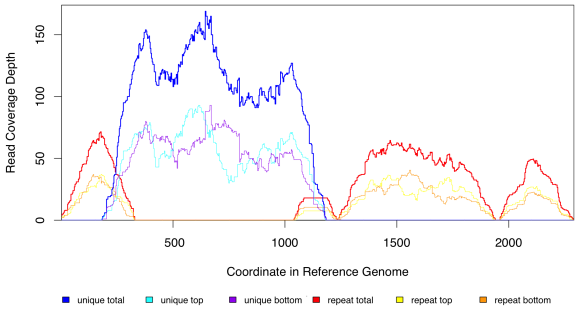

(c) Reference sequence: mCherry.

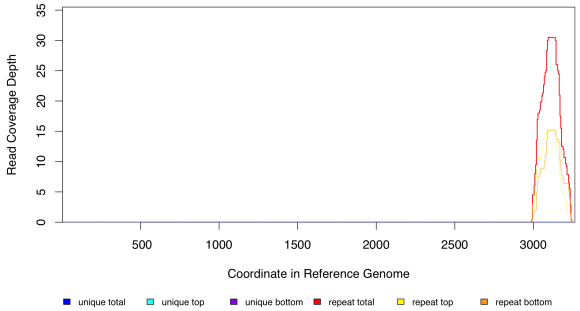

(d) Reference sequence: AY048743.

Figure S2: Breseq read coverage plots of all reference genomes used for the *rpoB* H526Y sample that was used as the common, mCherry-labeled reference in all competitions (AHG079). a) 'NC000913' is the MG1655 reference sequence from GenBank (NC_000913.3). b) There are no unique reads mapped to the sfGFP coding sequence on the construct because sample AHG079 has c) the mCherry construct instead (both reference sequences are included in the supplementary methods). d) AY048743 is the pDK4 plasmid sequence from GenBank (AY048743.1). Unique reads do not map to this sequence because there is no engineered gene knock-out (nor kanamyacin cassette) present.

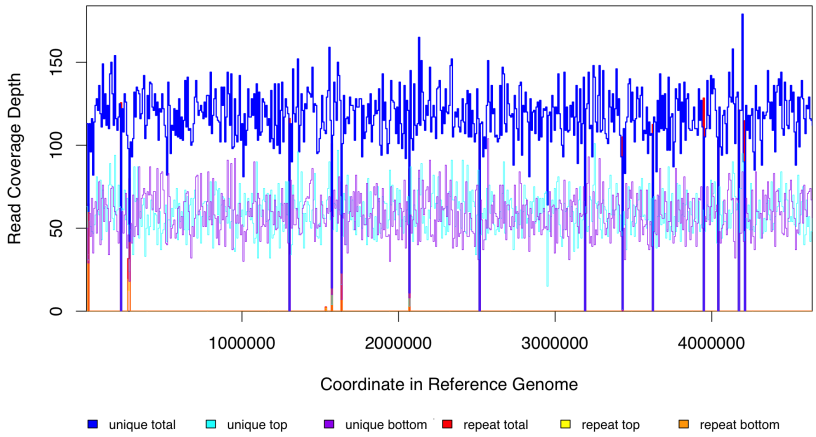

(a) Reference sequence: NC000913.

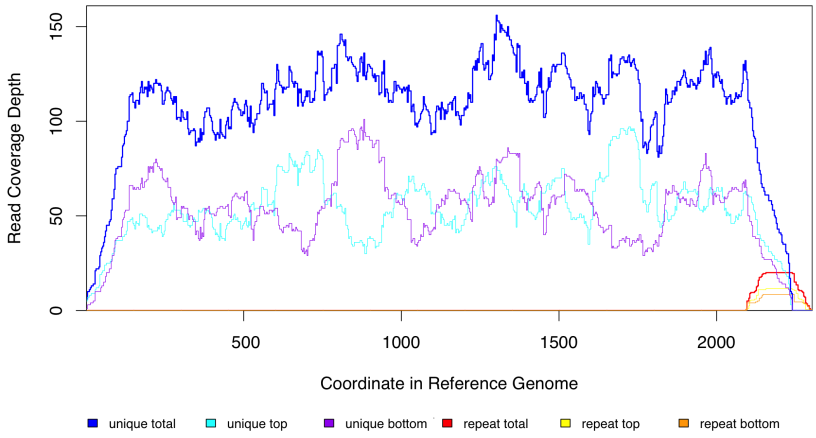

(b) Reference sequence: sfGFP.

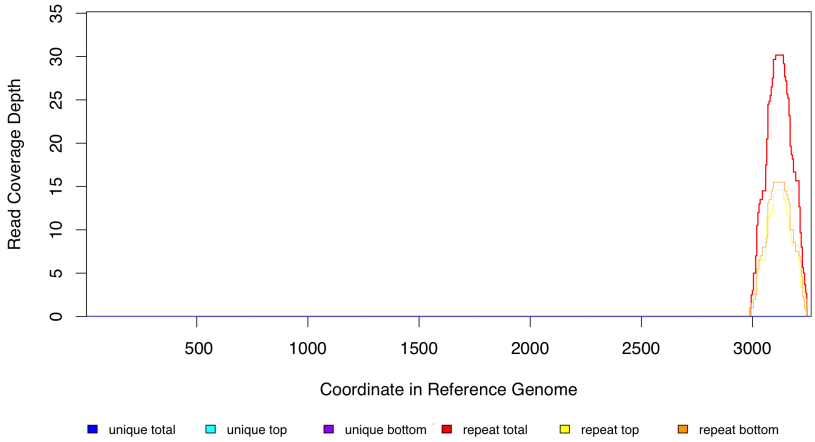

(c) Reference sequence: AY048743.

Figure S3: Breseq read coverage plots of all reference genomes used for sample AHG068. a) 'NC000913' is the MG1655 reference sequence from GenBank (NC_000913.3). b) The sequence for the sfGFP construct is included in the supplementary methods. c) AY048743 is the pDK4 plasmid sequence from GenBank (AY048743.1). Unique reads do not map to this sequence because there is no engineered gene knock-out (nor kanamyacin cassette) present.

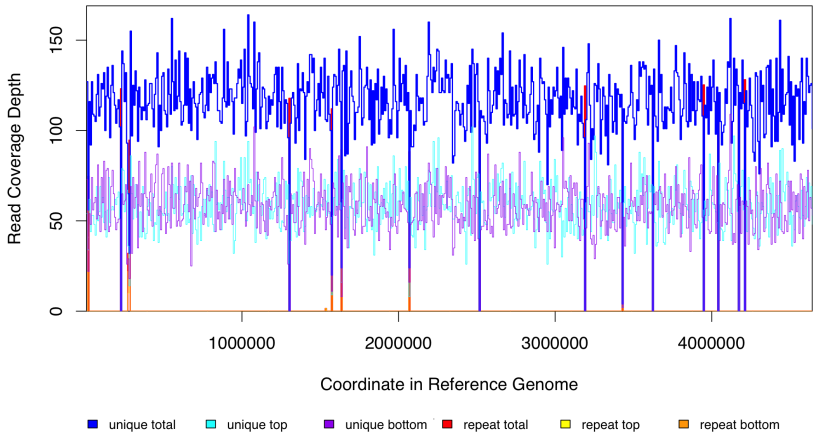

(a) Reference sequence: NC000913.

(b) Reference sequence: sfGFP.

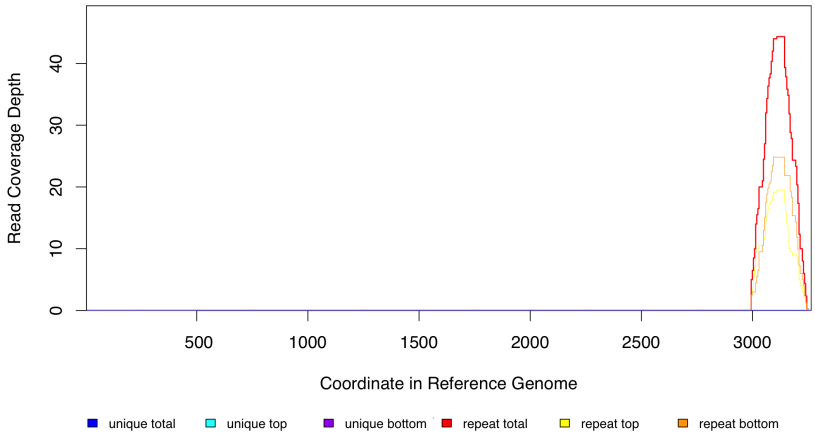

(c) Reference sequence: AY048743.

Figure S4: Breseq read coverage plots of all reference genomes used for sample AHG080. a) 'NC000913' is the MG1655 reference sequence from GenBank (NC_000913.3). b) The sequence for the sfGFP construct is included in the supplementary methods. c) AY048743 is the pDK4 plasmid sequence from GenBank (AY048743.1). Unique reads do not map to this sequence because there is no engineered gene knock-out (nor kanamyacin cassette) present.

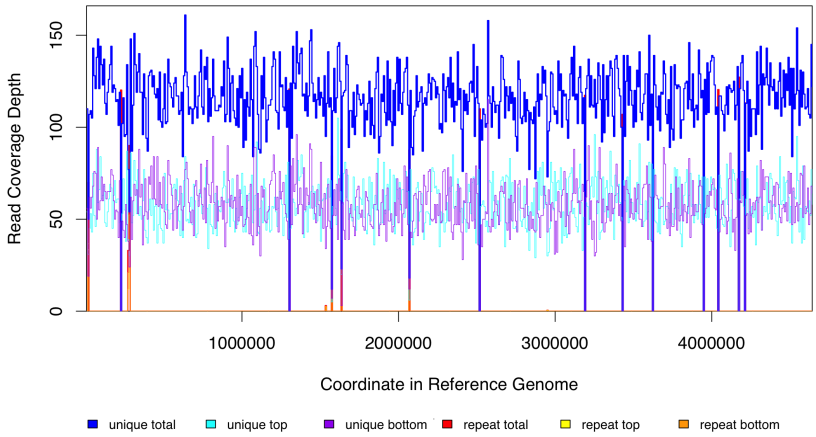

(a) Reference sequence: NC000913.

(b) Reference sequence: sfGFP.

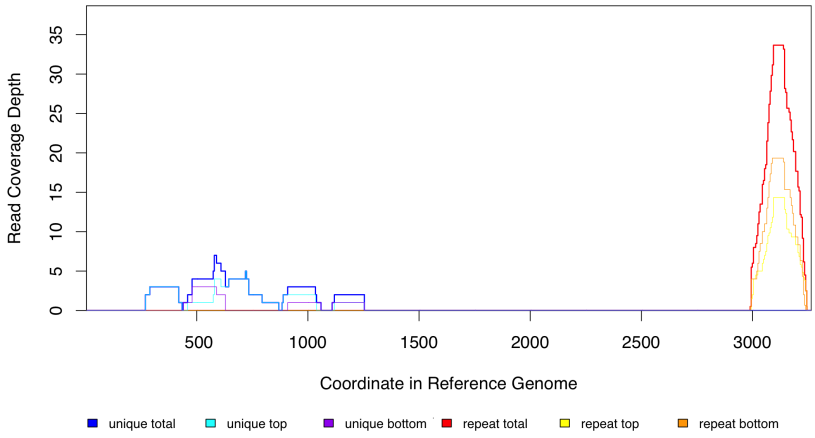

(c) Reference sequence: AY048743.

Figure S5: Breseq read coverage plots of all reference genomes used for sample AHG082. a) 'NC000913' is the MG1655 reference sequence from GenBank (NC_000913.3). b) The sequence for the sfGFP construct is included in the supplementary methods. c) AY048743 is the pDK4 plasmid sequence from GenBank (AY048743.1). Unique reads do not map to this sequence because there is no engineered gene knock-out (nor kanamyacin cassette) present.

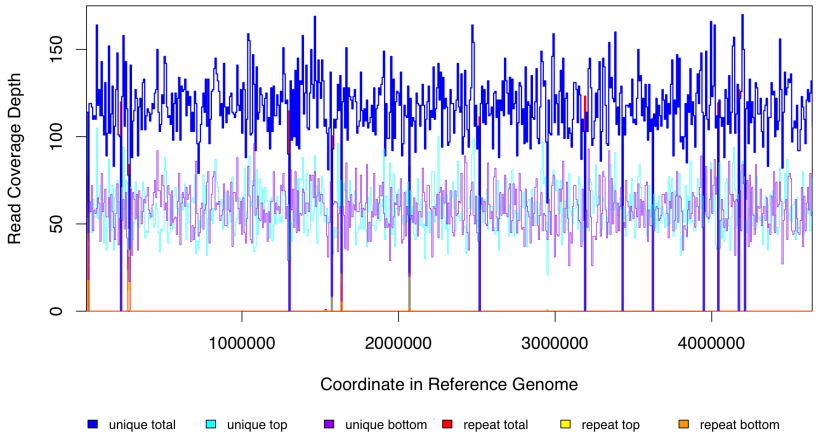

(a) Reference sequence: NC000913.

(b) Reference sequence: sfGFP.

(c) Reference sequence: AY048743.

Figure S6: Breseq read coverage plots of all reference genomes used for sample AHG052. This sample is represenative of all coverage plots. a) 'NC000913' is the MG1655 reference sequence from GenBank (NC_000913.3). b) The sequence for the sfGFP construct is included in the supplementary methods. c) AY048743 is the pDK4 plasmid sequence from GenBank (AY048743.1). Reads map to this sequence because there is an engineered gene knock-out created by swapping the gene of interest with a kanamyacin cassette.

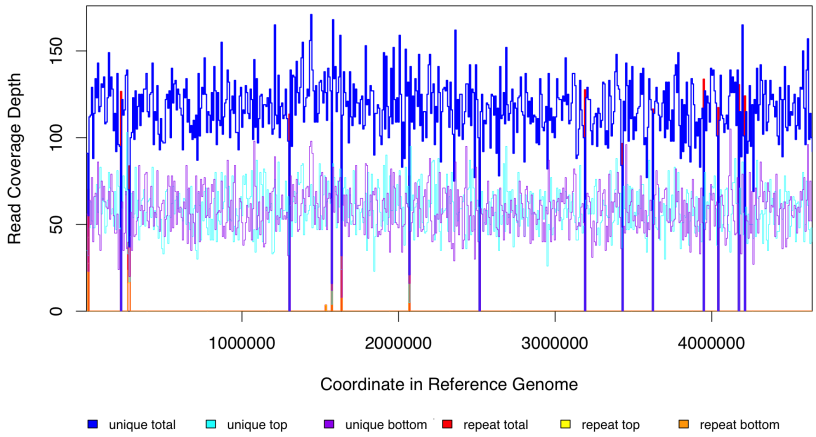

(a) Reference sequence: NC000913.

(b) Reference sequence: sfGFP.

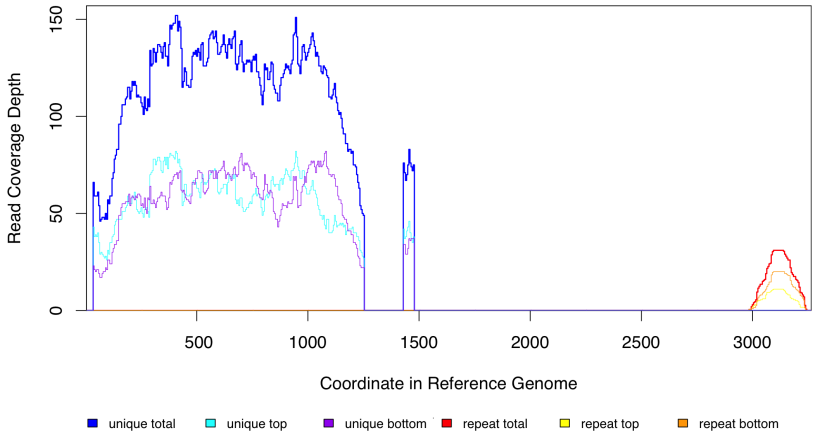

(c) Reference sequence: AY048743.

Figure S7: Breseq read coverage plots of all reference genomes used for sample AHG100. This sample is represenative of all coverage plots. a) 'NC000913' is the MG1655 reference sequence from GenBank (NC_000913.3). b) The sequence for the sfGFP construct is included in the supplementary methods. c) AY048743 is the pDK4 plasmid sequence from GenBank (AY048743.1). Reads map to this sequence because there is an engineered gene knock-out created by swapping the gene of interest with a kanamyacin cassette.

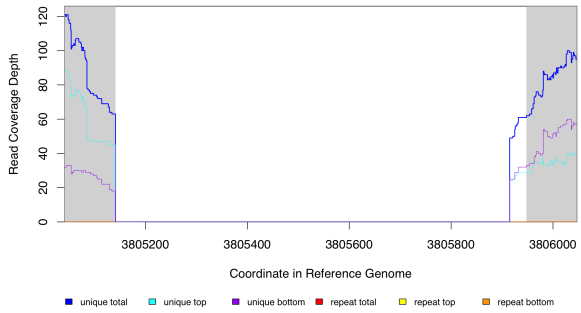

(a) Sample: AHG052.

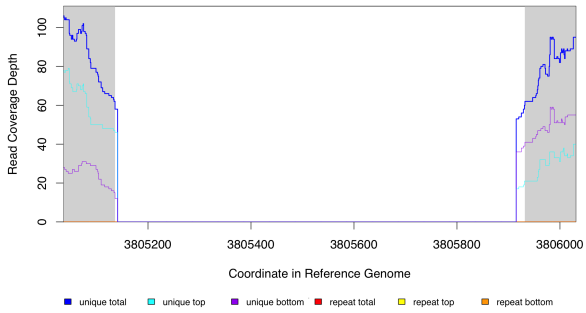

(b) Sample: AHG078.

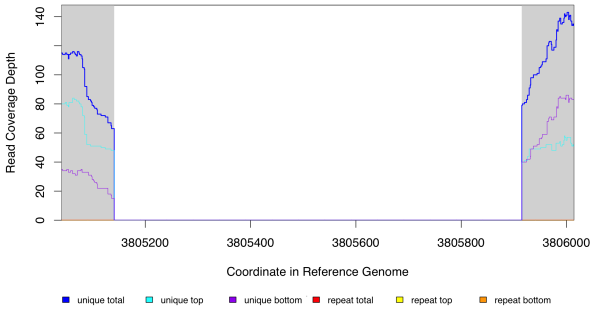

(c) Sample: AHG088.

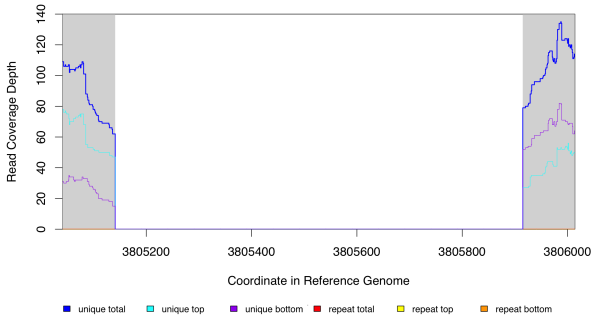

(d) Sample: AHG098.

Figure S8: Breseq read coverage plots for the region of the NC_000913.3 reference sequence around the gene *waaP* for the four samples engineered to have a knock-out at this gene: a) AHG052, b)AHG078, c) AHG088, and d) AHG098. The white background on the plot shows the region detected by breseq as having a reduced read coverage as compared to the regions with grey background.. No reads map to the *waaP* coding sequence because a knock-out has been engineered at this region by replacing the gene coding sequence with a kanamyacin cassette. Only samples with Δ*waaP* are included as representative since the coverage plots at the knock-out sites for the other genes and samples are similar.

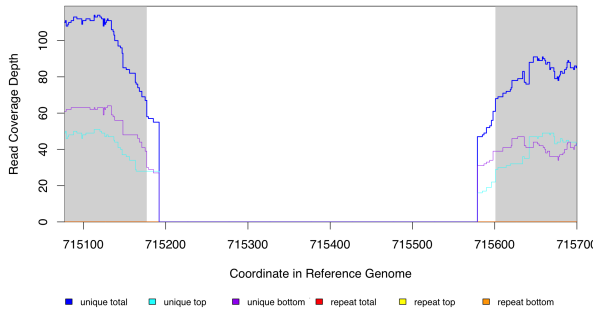

(a) Sample: AHG058.

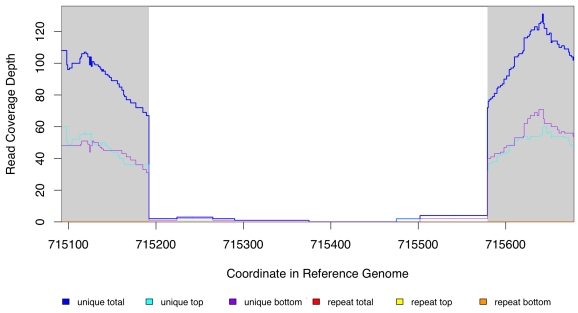

(b) Sample: AHG070.

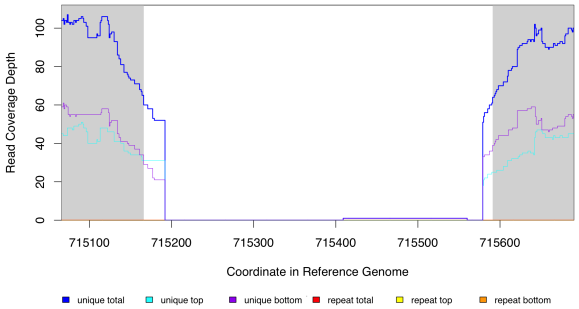

(c) Sample: AHG090.

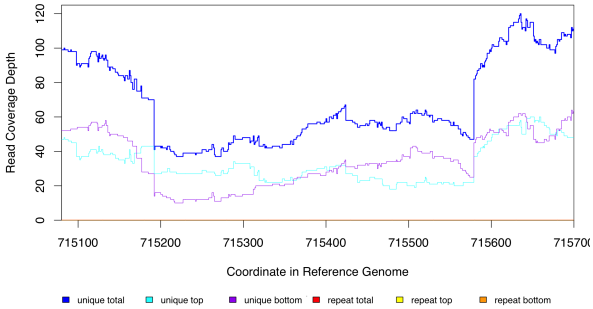

(d) Sample: AHG100.

Figure S9: Breseq read coverage plots for the region of the NC_000913.3 reference sequence around the pseudogene *ybfG* for the four samples engineered to have a knock-out at this locus: a) AHG058, b)AHG070, c) AHG090, and d) AHG100. In a-c), no reads map to the *ybfG* putative coding sequence because a knock-out has been engineered at this region by replacing the pseudogene sequence with a kanamyacin cassette. However, for d) there has likely been contamination by sample AHG098 (Δ*waaP*, *rpoB* S512F) into sample AHG100 (Δ*ybfG*, *rpoB* S512F) and so reads are mapping to the region around *ybfG* (see also read coverage plot in figure S10 and read junction evidence in figure S12). The white background on the plots for panels a-c) shows the region detected by breseq as having a reduced read coverage as compared to the regions with grey background. Panel d) was created manually at the *ybfG* locus using the breseq BAM2COV command and so there is no background shading to the plot.

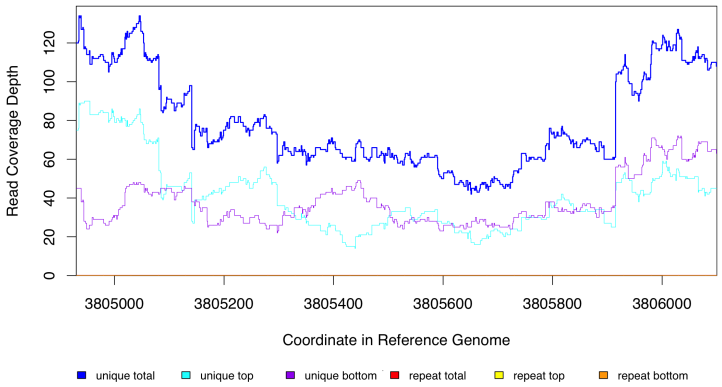

Figure S10: Breseq read coverage plots for the region of the NC_000913.3 reference sequence around the gene *waaP* (3805140 - 3805915) for the AHG100 samples that is **not** engineered to have a knock-out at this site. There has likely been contamination by sample AHG098 (Δ*waaP*, *rpoB* S512F) into sample AHG100 (Δ*ybfG*, *rpoB* S512F) and so there is decreased read coverage at the *waaP* locus as a result (see also read coverage plot in figure S9d and read junction evidence in figure S12).

(a) New junction evidence upstream of the *waaP* gene for sample AHG052. (Figure continues on next page.)

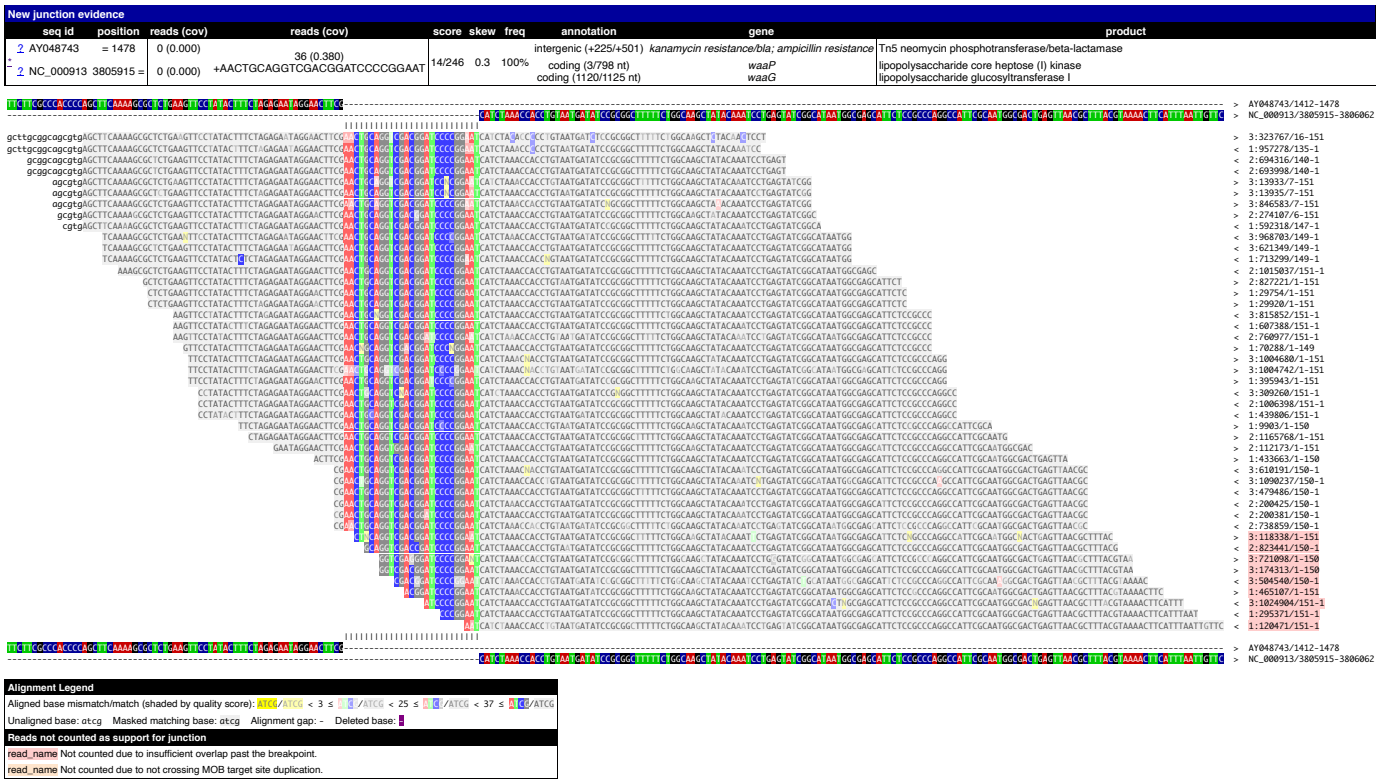

(b) New junction evidence downstream of the *waaP* gene for sample AHG052. (Figure continued from previous page.)

Figure S11: Breseq new junction evidence supporting the insertion of the kanamyacin cassette from the pKD4 plasmid (AY048743.1) at the region of the NC_000913.3 reference sequence around the *waaP* gene for sample AHG052. Panel a), which is on the previous page, shows evidence in support of a new junction at position 3 805 150 of the NC_000913.3 reference sequence (upstream of the *waaP* gene). Panel b) shows evidence of a second junction around position 3 805 915 (downstream of the *waaP* gene). These positions correspond well with the lack of read coverage for this sample at this region shown in figure S8a. Only the new junction evidence from AHG052 is shown as a representative since new junction evidence for other samples and knocked-out genes look similar. All plots are from Breseq.

(a) New junction evidence upstream of the *ybfG* pseudogene for sample AHG100. (Figure continues on next page.)

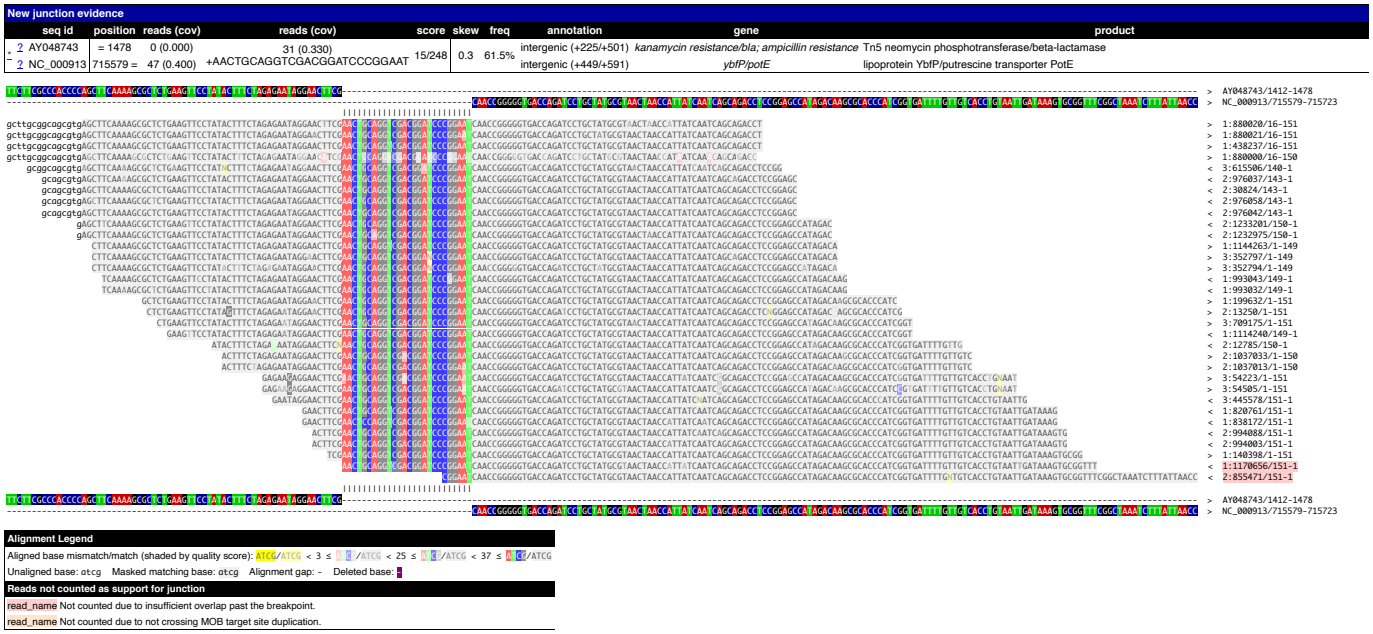

(b) New junction evidence downstream of the *ybfG* pseudogene for sample AHG100. (Figure continued from previous page and continues on next page.)

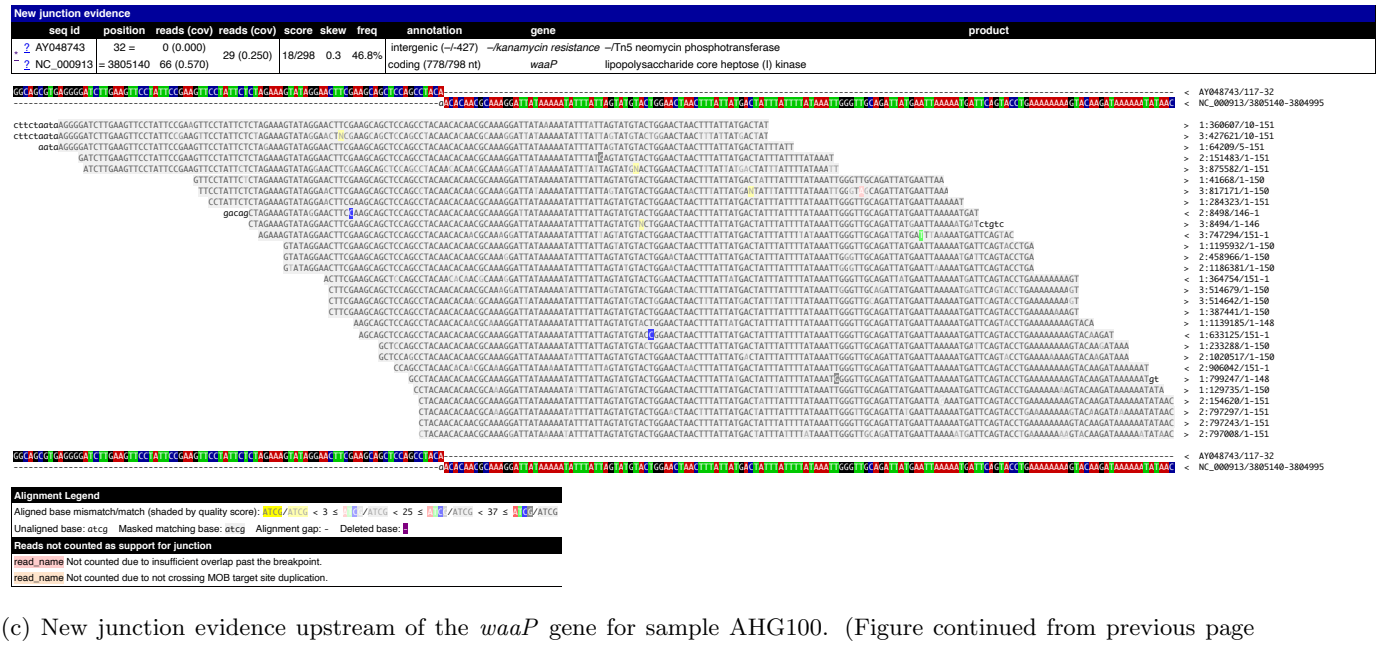

(c) New junction evidence upstream of the *waaP* gene for sample AHG100. (Figure continued from previous page and continues on next page.)

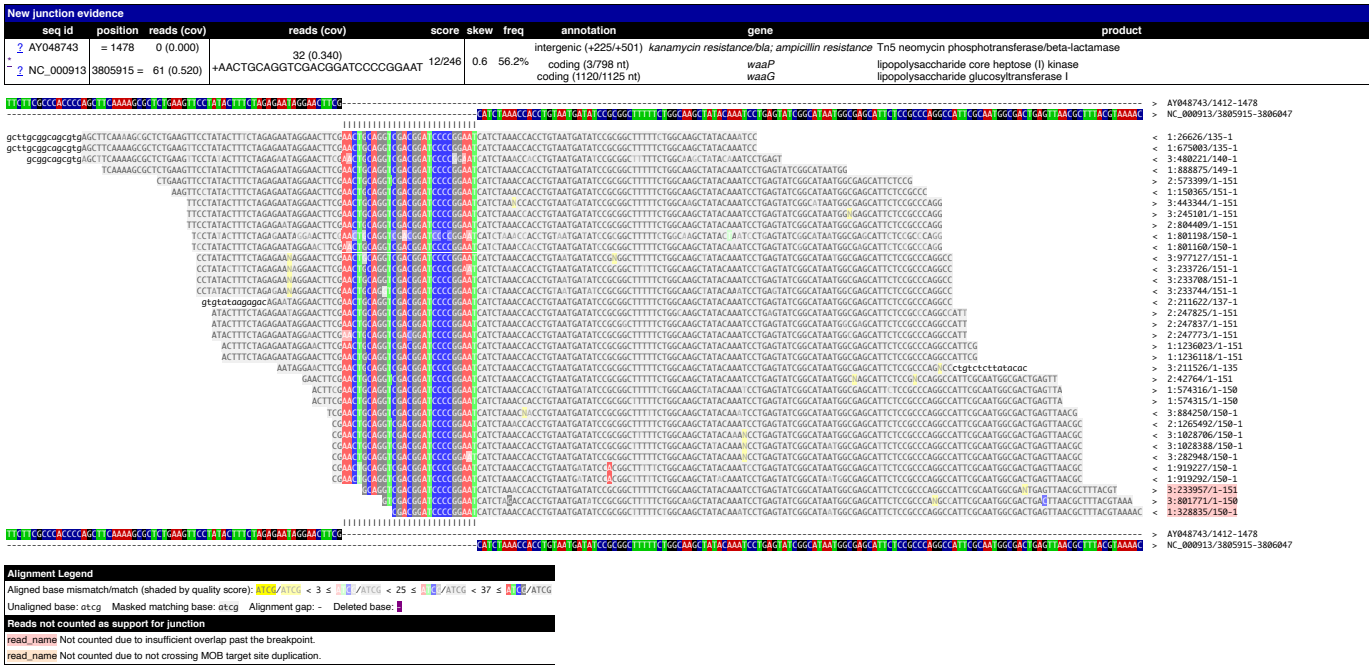

(d) New junction evidence downstream of the *waaP* gene for sample AHG100. (Figure continued from previous page.)

Figure S12: Breseq new junction evidence supporting the hypothesis of likely contamination by sample AHG098 (Δ*waaP*, *rpoB* S512F) into sample AHG100 (Δ*ybfG*, *rpoB* S512F); see also read coverage plots in figures S9d and S10. The new junction evidence for sample AHG100 shows existence of insertion of the kanamyacin cassette from the pKD4 plasmid (AY048743.1) at two different loci of the NC_000913.3 reference sequence. Panels a-b) show the new junctions around the *ybfG* pseudogene and panels c-d) show the new junctions around the *waaP* gene. All plots are from Breseq.

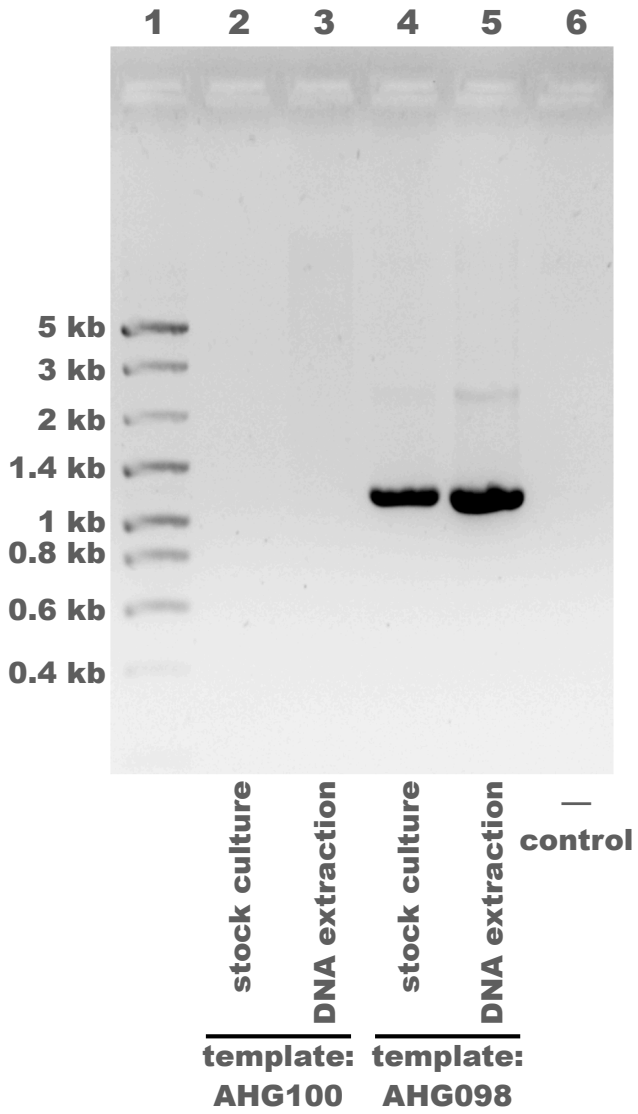

Figure S13: **PCR suggests that contamination of sample AHG100 (*rpoB* S512F Δ*ybfG*) occurred after creation of the stock culture and after DNA extraction, perhaps during DNA sequencing.** PCR was done using a Δ*waaP*-specific primer (waaP_76747_For in table S13) and the Datsenko-Wanner K1 primer specific to the inserted kanamyacin cassette. Therefore amplification is expected only when the Δ*waaP* knock-out DNA sequence is present in the PCR template. The test sample, AHG100: *rpoB* S512F Δ*ybfG*, was used as a PCR template in lanes 2-3; lanes 4-5 show the positive control with AHG098: *rpoB* S512F Δ*waaP* and lane 6 shows the negative control without any PCR template. No amplification is observed for the test sample AHG100, this suggests that the sample was not contaminated prior to being sent for DNA sequencing. The frozen stock cultures (lanes 2, 4) and the DNA extractions that were sent for sequencing (lanes 3, 5) were used as PCR templates for both samples. For the stock cultures, 1mL of LB was inoculated directly with frozen stock, incubated for 1.5 hours at $37°C$, then $1\mu L$ was added to the PCR reaction. A $25\mu L$ total PCR reaction volume was used with DreamTaq DNA polymerase, annealing temperature of $55°C$, and 2 minute elongation time. Gel electrophoresis was done in 1% agarose. Lane 1 shows the NZYDNA Ladder VIII, with band sizes labeled at left.

Table S3: Complete list of mutations as identified by breseq for each of the 25 genotypes. (Engineered mutations listed in table S12.) Rows coloured in gray highlight mutations identified by breseq that correspond with the genetic constructs created for this study. Rows coloured in blue highlight non-synonymous nucleotide substitutions that were not engineered and differ from the wild-type strain (AHG015). All other types of mutations (synonymous nucleotide substitutions, intergenic nucleotide substitutions, small indels, and mobile element insertions) that were not engineered and mutations present on the wild-type strain are listed on white background. Sample AHG079 is labeled with "(Ref.)" to highlight that this was the reference genotype used in competitions.

Sample	Mutation	Gene name	Gene product	Annotation	Reference	Position
AHG015 (WT)	large deletion	insB9, insA9, [crl]	insB9, insA9, [crl]	Δ776 bp	MG1655 (NC_000913.3)	257908-258676
AHG015 (WT)	small indel	ybjO	putative inner membrane protein	+33 bp coding (413-445/489 nt)	MG1655 (NC_000913.3)	898401
AHG015 (WT)	intergenic mobile element insertion	bamD/raiA	outer membrane protein assembly factor BamD/ribosome-associated inhibitor A	IS1 (+) +8 bp	MG1655 (NC_000913.3)	2737118-2737125
AHG015 (WT)	small indel	rrlA	23S ribosomal RNA	Δ1 bp noncoding (207/2905 nt)	MG1655 (NC_000913.3)	4037725
AHG015 (WT)	small indel	gltP/yjcO	glutamate / aspartate : H(+) symporter GltP/Sel1 repeat-containing protein YjcO	+GC intergenic (+587/+55)	MG1655 (NC_000913.3)	4296381
AHG015 (WT)	SNP intergenic	sfGFP/cat	Superfolder GFP fluorophore / type A chloramphenicol O-acetyltransferase	T→C intergenic (+204/-99)	sfGFP construct (sequence)	1248
AHG015 (WT)	small indel	cat	type A chloramphenicol O-acetyltransferase	+A coding (609/639 nt)	sfGFP construct (sequence)	1955
AHG015 (WT)	small indel	cat	type A chloramphenicol O-acetyltransferase	+T coding (621/639 nt)	sfGFP construct (sequence)	1967
AHG058	SNP synonymous	nptII	Tn5 neomycin phosphotransferase	S104S (A311G)	pKD4 plasmid (AY048743.1)	770

Continued on next page

Table S3 – continued from previous page

Sample	Mutation	Gene name	Gene product	Annotation	Reference	Position
AHG058	gene knock-out	ybfP/potE	lipoprotein YbfP/putrescine transporter PotE	Missing coverage (figure S9a) & new junction evidence	MG1655 (NC_000913.3)	715177-715600
AHG060	gene knock-out	marR	DNA-binding transcriptional repressor MarR	Missing coverage & new junction evidence	MG1655 (NC_000913.3)	1618307-1618725
AHG064	mobile element insertion	yhhZ	putative endonuclease YhhZ	IS1 (+) +9 bp coding (666-674/1179 nt)	MG1655 (NC_000913.3)	3582495-3582503
AHG064	gene knock-out	yidK	putative transporter YidK	Missing coverage & new junction evidence	MG1655 (NC_000913.3)	3858389-3860101
AHG066	SNP synonymous	nptII	Tn5 neomycin phosphotransferase	V83V (T248C)	pKD4 plasmid (AY048743.1)	707
AHG066	gene knock-out	nuoC	NADH:quinone oxidoreductase subunit CD	Missing coverage & new junction evidence	MG1655 (NC_000913.3)	2401267-2403045
AHG066	SNP synonymous	kgtP	α keto-glutarate: H(+) symporter	V350V (C1049A)	MG1655 (NC_000913.3)	2723888
AHG052	gene knock-out	waaP/waaG	lipopolysaccharide core heptose (I) kinase / lipopolysaccharide glucosyltransferase I	Missing coverage (figure S8a) & new junction evidence (figure S11)	MG1655 (NC_000913.3)	3805141-3805947
AHG052	SNP intergenic	–/nptII	–/Tn5 neomycin phosphotransferase	C→T intergenic (–/-223)	pKD4 plasmid (AY048743.1)	236
AHG052	SNP intergenic	–/nptII	–/Tn5 neomycin phosphotransferase	A→T intergenic (–/-88)	pKD4 plasmid (AY048743.1)	371
AHG079 (Ref.)	large deletion	ntpII	kanamycin resistance,bla;	Δ3267 bp (no reads mapped to pKD4 plasmid, figure S2d)	pKD4 plasmid (AY048743.1)	1-3267
AHG079 (Ref.)	small indel	ybjO	putative inner membrane protein	+33 bp pseudogene (412/456 nt)	MG1655 (NC_000913.3)	897624

Continued on next page

Table S3 – continued from previous page

Sample	Mutation	Gene name	Gene product	Annotation	Reference	Position
AHG079 (Ref.)	SNP non-synonymous	*rpoB*	RNA polymerase subunit beta	H526Y (C1575T)	MG1655 (NC_000913.3)	4182786
AHG079 (Ref.)	large deletion	sfGFP	Superfolder GFP fluorophore	Missing coverage evidence, figure S2b	sfGFP construct (sequence)	1-1227
AHG079 (Ref.)	gene insertion	mCherry	mCherry fluorophore	Reads mapped to mCherry CDS, figure S2c	mCherry construct (sequence)	325-1035
AHG080	large deletion	ntpII	kanamycin resistance,bla;	Δ3267 bp (no reads mapped to pKD4 plasmid, figure S4c)	pKD4 plasmid (AY048743.1)	1-3267
AHG080	SNP non-synonymous	*rpoB*	RNA polymerase subunit beta	H526Y (C1575T)	MG1655 (NC_000913.3)	4182786
AHG090	SNP synonymous	nptII	Tn5 neomycin phosphotransferase	S104S (A311G)	pKD4 plasmid (AY048743.1)	770
AHG090	gene knock-out	ybfP/potE	lipoprotein YbfP/putrescine transporter PotE	Missing coverage (figure S9c) & new junction evidence	MG1655 (NC_000913.3)	715166-715590
AHG090	SNP non-synonymous	*rpoB*	RNA polymerase subunit beta	H526Y (C1575T)	MG1655 (NC_000913.3)	4182786
AHG092	gene knock-out	marR	DNA-binding transcriptional repressor MarR	Missing coverage & new junction evidence	MG1655 (NC_000913.3)	1618315-1618725
AHG092	SNP non-synonymous	*rpoB*	RNA polymerase subunit beta	H526Y (C1575T)	MG1655 (NC_000913.3)	4182786
AHG094	gene knock-out	yidK	putative transporter YidK	Missing coverage & new junction evidence	MG1655 (NC_000913.3)	3858389-3860089
AHG094	SNP non-synonymous	*rpoB*	RNA polymerase subunit beta	H526Y (C1575T)	MG1655 (NC_000913.3)	4182786
AHG096	SNP synonymous	nptII	Tn5 neomycin phosphotransferase	V83V (T248C)	pKD4 plasmid (AY048743.1)	707

Continued on next page

Table S3 – continued from previous page

Sample	Mutation	Gene name	Gene product	Annotation	Reference	Position
AHG096	gene knock-out	nuoC	NADH:quinone oxidoreductase subunit CD	Missing coverage & new junction evidence	MG1655 (NC_000913.3)	2401261-2403045
AHG096	SNP non-synonymous	*rpoB*	RNA polymerase subunit beta	H526Y (C1575T)	MG1655 (NC_000913.3)	4182786
AHG088	SNP intergenic	–/nptII	–/Tn5 neomycin phosphotrans-ferase	C→T intergenic (–/-223)	pKD4 plasmid (AY048743.1)	236
AHG088	SNP intergenic	–/nptII	–/Tn5 neomycin phosphotrans-ferase	A→T intergenic (–/-88)	pKD4 plasmid (AY048743.1)	371
AHG088	gene knock-out	waaP	lipopolysaccharide core heptose (I) kinase	Missing coverage (figure S8c) & new junction evidence	MG1655 (NC_000913.3)	3805141-3805914
AHG088	SNP non-synonymous	*rpoB*	RNA polymerase subunit beta	H526Y (C1575T)	MG1655 (NC_000913.3)	4182786
AHG082	large deletion	ntpII	kanamycin resis-tance,bla;	Δ3267 bp (no reads mapped to pKD4 plas-mid, figure S5c)	pKD4 plasmid (AY048743.1)	1-3267
AHG082	SNP non-synonymous	yeaC	DUF1315 domain-containing pro-tein YeaC	A32G (G94C)	MG1655 (NC_000913.3)	1861071
AHG082	SNP synonymous	zinT	metal-binding protein ZinT	S23S (G68A)	MG1655 (NC_000913.3)	2040634
AHG082	SNP intergenic	insH6/yoeA	CP4-44 prophage; IS5 transposase and trans-activator/CP4-44 prophage; TonB-dependent recep-tor plug domain-containing pro-tein YoeA	T→C intergenic (-1316/-34)	MG1655 (NC_000913.3)	2067792
AHG082	SNP non-synonymous	*rpoB*	RNA polymerase subunit beta	S512F (C1534T)	MG1655 (NC_000913.3)	4182745
AHG100	SNP synonymous	zinT	metal-binding protein ZinT	S23S (G68A)	MG1655 (NC_000913.3)	2040634

Continued on next page

Table S3 – continued from previous page

Sample	Mutation	Gene name	Gene product	Annotation	Reference	Position
AHG100	SNP intergenic	insH6/yoeA	CP4-44 prophage; IS5 transposase and trans-activator/CP4-44 prophage; TonB-dependent receptor plug domain-containing protein YoeA	T→C intergenic (-1316/-34)	MG1655 (NC_000913.3)	2067792
AHG100	SNP non-synonymous	*rpoB*	RNA polymerase subunit beta	S512F (C1534T)	MG1655 (NC_000913.3)	4182745
AHG102	gene knock-out	marR	DNA-binding transcriptional repressor MarR	Missing coverage & new junction evidence	MG1655 (NC_000913.3)	1618308-1618725
AHG102	SNP synonymous	zinT	metal-binding protein ZinT	S23S (G68A)	MG1655 (NC_000913.3)	2040634
AHG102	SNP intergenic	insH6/yoeA	CP4-44 prophage; IS5 transposase and trans-activator/CP4-44 prophage; TonB-dependent receptor plug domain-containing protein YoeA	T→C intergenic (-1316/-34)	MG1655 (NC_000913.3)	2067792
AHG102	SNP non-synonymous	*rpoB*	RNA polymerase subunit beta	S512F (C1534T)	MG1655 (NC_000913.3)	4182745
AHG104	SNP synonymous	zinT	metal-binding protein ZinT	S23S (G68A)	MG1655 (NC_000913.3)	2040634
AHG104	SNP intergenic	insH6/yoeA	CP4-44 prophage; IS5 transposase and trans-activator/CP4-44 prophage; TonB-dependent receptor plug domain-containing protein YoeA	T→C intergenic (-1316/-34)	MG1655 (NC_000913.3)	2067792
AHG104	gene knock-out	yidK	putative transporter YidK	Missing coverage & new junction evidence	MG1655 (NC_000913.3)	3858381-3860080

Continued on next page

Table S3 – continued from previous page

Sample	Mutation	Gene name	Gene product	Annotation	Reference	Position
AHG104	SNP non-synonymous	*rpoB*	RNA polymerase subunit beta	S512F (C1534T)	MG1655 (NC_000913.3)	4182745
AHG106	SNP synonymous	nptII	Tn5 neomycin phosphotransferase	V83V (T248C)	pKD4 plasmid (AY048743.1)	707
AHG106	SNP synonymous	zinT	metal-binding protein ZinT	S23S (G68A)	MG1655 (NC_000913.3)	2040634
AHG106	SNP intergenic	insH6/yoeA	CP4-44 prophage; IS5 transposase and transactivator/CP4-44 prophage; TonB-dependent receptor plug domain-containing protein YoeA	T→C intergenic (-1316/-34)	MG1655 (NC_000913.3)	2067792
AHG106	gene knock-out	nuoC	NADH:quinone oxidoreductase subunit CD	Missing coverage & new junction evidence	MG1655 (NC_000913.3)	2401267-2403045
AHG106	SNP non-synonymous	*rpoB*	RNA polymerase subunit beta	S512F (C1534T)	MG1655 (NC_000913.3)	4182745
AHG098	SNP intergenic	–/nptII	–/Tn5 neomycin phosphotransferase	C→T intergenic (–/-223)	pKD4 plasmid (AY048743.1)	236
AHG098	SNP intergenic	–/nptII	–/Tn5 neomycin phosphotransferase	A→T intergenic (–/-88)	pKD4 plasmid (AY048743.1)	371
AHG098	SNP synonymous	zinT	metal-binding protein ZinT	S23S (G68A)	MG1655 (NC_000913.3)	2040634
AHG098	SNP intergenic	insH6/yoeA	CP4-44 prophage; IS5 transposase and transactivator/CP4-44 prophage; TonB-dependent receptor plug domain-containing protein YoeA	T→C intergenic (-1316/-34)	MG1655 (NC_000913.3)	2067792
AHG098	SNP synonymous	gcvP	glycine decarboxylase	L822L (C2465T)	MG1655 (NC_000913.3)	3046543

Continued on next page

Table S3 – continued from previous page

Sample	Mutation	Gene name	Gene product	Annotation	Reference	Position
AHG098	gene knock-out	waaP	lipopolysaccharide core heptose (I) kinase	Missing coverage (figure S8d) & new junction evidence	MG1655 (NC_000913.3)	3805141-3805914
AHG098	SNP non-synonymous	*rpoB*	RNA polymerase subunit beta	S512F (C1534T)	MG1655 (NC_000913.3)	4182745
AHG098	SNP synonymous	nrfA	cytochrome c552 nitrite reductase	A440A (C1319A)	MG1655 (NC_000913.3)	4289049
AHG068	large deletion	ntpII	kanamycin resistance,bla;	Δ3267 bp (no reads mapped to pKD4 plasmid, figure S3c)	pKD4 plasmid (AY048743.1)	1-3267
AHG068	SNP synonymous	ascB	6-phospho-beta-glucosidase AscB	K366K (G1097A)	MG1655 (NC_000913.3)	2842054
AHG068	SNP non-synonymous	*rpoB*	RNA polymerase subunit beta	I572S (T1714G)	MG1655 (NC_000913.3)	4182925
AHG070	SNP synonymous	nptII	Tn5 neomycin phosphotransferase	S104S (A311G)	pKD4 plasmid (AY048743.1)	770
AHG070	gene knock-out	ybfP/potE	lipoprotein YbfP/putrescine transporter PotE	Missing coverage (figure S9c) & new junction evidence	MG1655 (NC_000913.3)	715192-715578
AHG070	SNP non-synonymous	*rpoB*	RNA polymerase subunit beta	I572S (T1714G)	MG1655 (NC_000913.3)	4182925
AHG072	gene knock-out	marR	DNA-binding transcriptional repressor MarR	Missing coverage & new junction evidence	MG1655 (NC_000913.3)	1618315-1618725
AHG072	SNP non-synonymous	*rpoB*	RNA polymerase subunit beta	I572S (T1714G)	MG1655 (NC_000913.3)	4182925
AHG074	gene knock-out	yidK	putative transporter YidK	Missing coverage & new junction evidence	MG1655 (NC_000913.3)	3858382-3860079
AHG074	SNP non-synonymous	*rpoB*	RNA polymerase subunit beta	I572S (T1714G)	MG1655 (NC_000913.3)	4182925
AHG076	SNP synonymous	nptII	Tn5 neomycin phosphotransferase	V83V (T248C)	pKD4 plasmid (AY048743.1)	707

Continued on next page

Table S3 – continued from previous page

Sample	Mutation	Gene name	Gene product	Annotation	Reference	Position
AHG076	SNP non-synonymous	sieB	Rac prophage; phage superinfection exclusion protein	N135K (C404A)	MG1655 (NC_000913.3)	1418266
AHG076	gene knock-out	nuoC	NADH:quinone oxidoreductase subunit CD	Missing coverage & new junction evidence	MG1655 (NC_000913.3)	2401265-2403045
AHG076	SNP non-synonymous	glpD	aerobic glycerol 3-phosphate dehydrogenase	D263Y (G786T)	MG1655 (NC_000913.3)	3562766
AHG076	SNP non-synonymous	*rpoB*	RNA polymerase subunit beta	I572S (T1714G)	MG1655 (NC_000913.3)	4182925
AHG078	SNP intergenic	–/nptII	–/Tn5 neomycin phosphotransferase	C→T intergenic (–/-223)	pKD4 plasmid (AY048743.1)	236
AHG078	SNP intergenic	–/nptII	–/Tn5 neomycin phosphotransferase	A→T intergenic (–/-88)	pKD4 plasmid (AY048743.1)	371
AHG078	gene knock-out	waaP/waaG	lipopolysaccharide core heptose (I) kinase / lipopolysaccharide glucosyltransferase I	Missing coverage (figure S8b) & new junction evidence	MG1655 (NC_000913.3)	3805136-3805931
AHG078	SNP non-synonymous	*rpoB*	RNA polymerase subunit beta	I572S (T1714G)	MG1655 (NC_000913.3)	4182925

8.2 Antibiotic dose response curves of the wild-type genotype

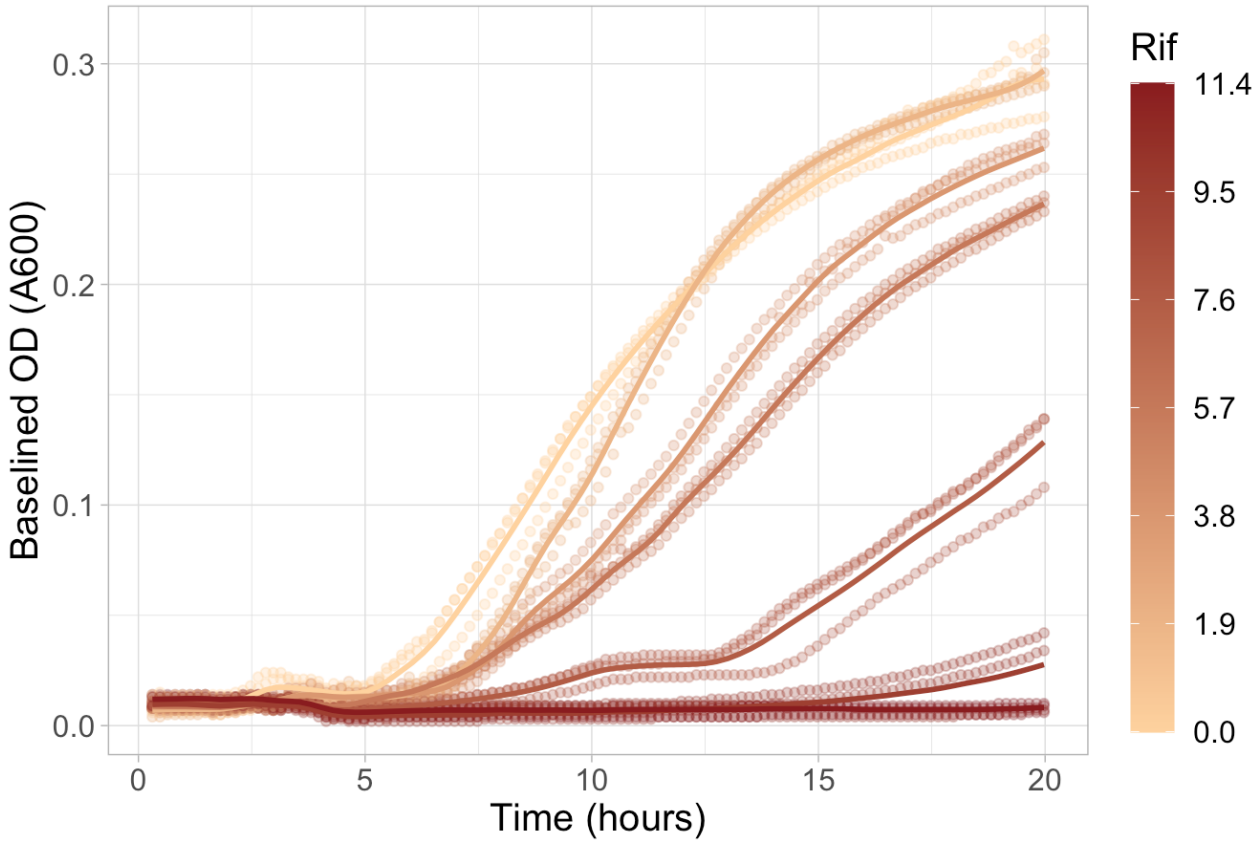

Figure S14: Dose response curves of the antibiotic-susceptible, wild-type genotype (sample AHG015) to different rifampicin concentrations. The y-axis shows the time in hours, the x-axis shows the baseline-subtracted optical density (OD) at 600nm, and the colours indicate different rifampicin concentrations with the legend on the right in units of $\mu g/mL$. Each line shows the average of three growth curve replicates (loess smoothing was used to interpolate) and points show the individual replicates. Baselining was done by subtracting the smallest observed OD value (including blank wells) at each time point.

8.3 Ascertaining flow cytometry estimates of competitive fitness

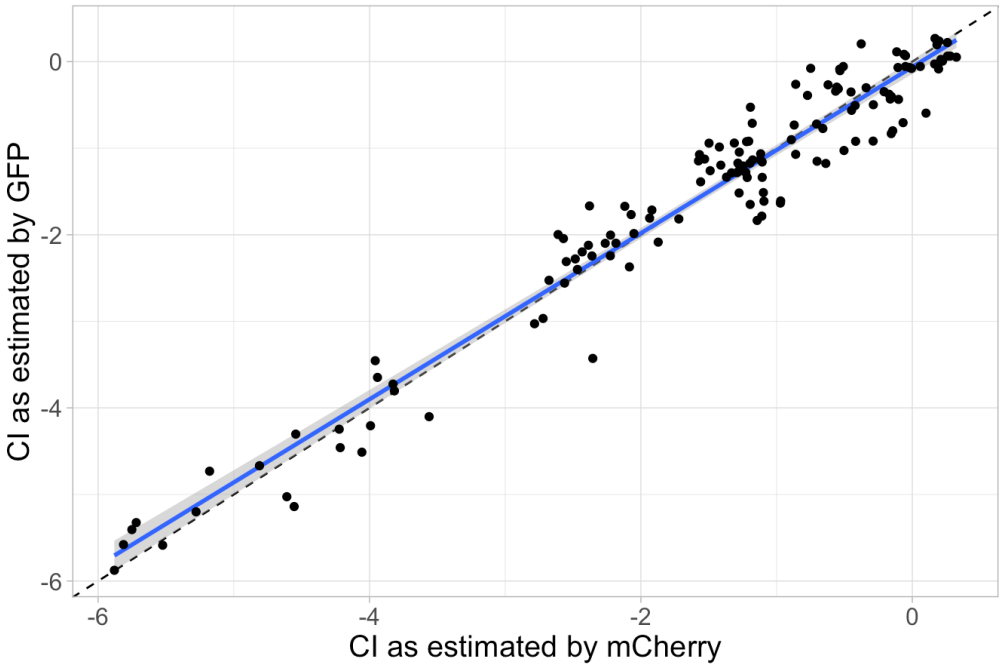

Figure S15: **Nearly identical $\hat{w}$ estimates were found when the fluorophores of the reference and competitor genotypes were swapped.** The competitive index ($\hat{w}$) as estimated by using mCherry-labeled competitor genotypes and a GFP-labeled reference genotype (shown in x-axis) corresponds well with the same metric estimated by using GFP-labeled competitor genotypes and an mCherry-labeled reference genotype (shown in y-axis). Data corresponds to a sample of genotypes representing all knock-outs and *rpoB* mutants as assayed once in all environments. The dashed, black line shows $y = x$. The blue line shows the mean and the blue shaded region shows the 95% confidence interval of the mean for the least-squares estimated linear regression. The coefficients of this regression are given in table S4; the overall regression is statistically significant and explains most of the variation in the response variable (adjusted $R^2 = 0.949$, $F(1, 138) = 2586$, $p < 10^{-15}$).

Table S4: Least-squares estimated coefficients of the linear regression shown in figure S15.

Coefficient	**Estimate**	**Standard Error**	**t statistic**	**p-value**
Intercept (b)	-0.0619	0.0410	-1.51	0.133
CI as estimated by mCherry (β)	0.960	0.0189	50.8	$< 10^{-15}$

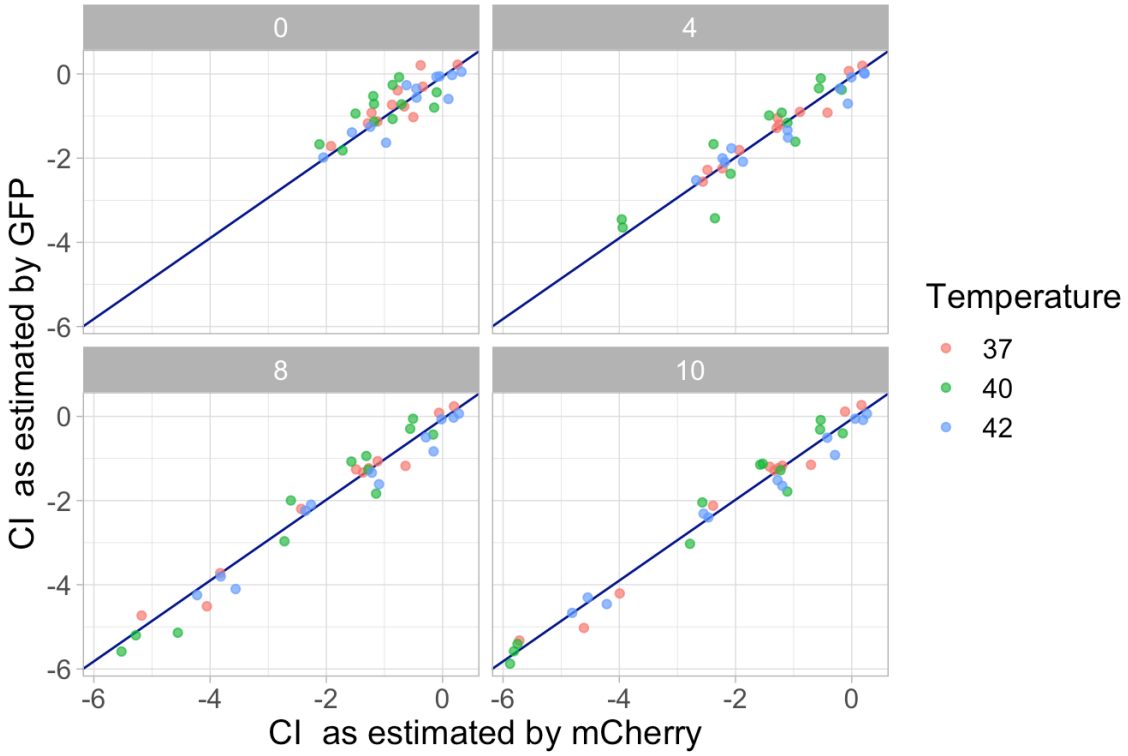

Figure S16: The plot shows environment-specific effects of swapping fluorophores. The same data is plotted as in figure S15 but here panels show the different antibiotic concentrations and points are coloured by temperature. The blue line shows the simple linear regression on CI as estimated by mCherry, and whose coefficient estimates are given in table S4. As shown in table S5, the effect of environment is not significant.

Table S5: Results of ANOVA show that the environment-specific effect of swapping fluorophores is not statistically significant.

Source of Variation	**SS**	**df**	**MS**	**F statistic**	**p-value**
CI as estimated by mCherry	300	1	300	2641	$< 10^{-15}$
Environment	1.59	11	0.14	1.27	0.25
Residuals	14.4	127	0.11		

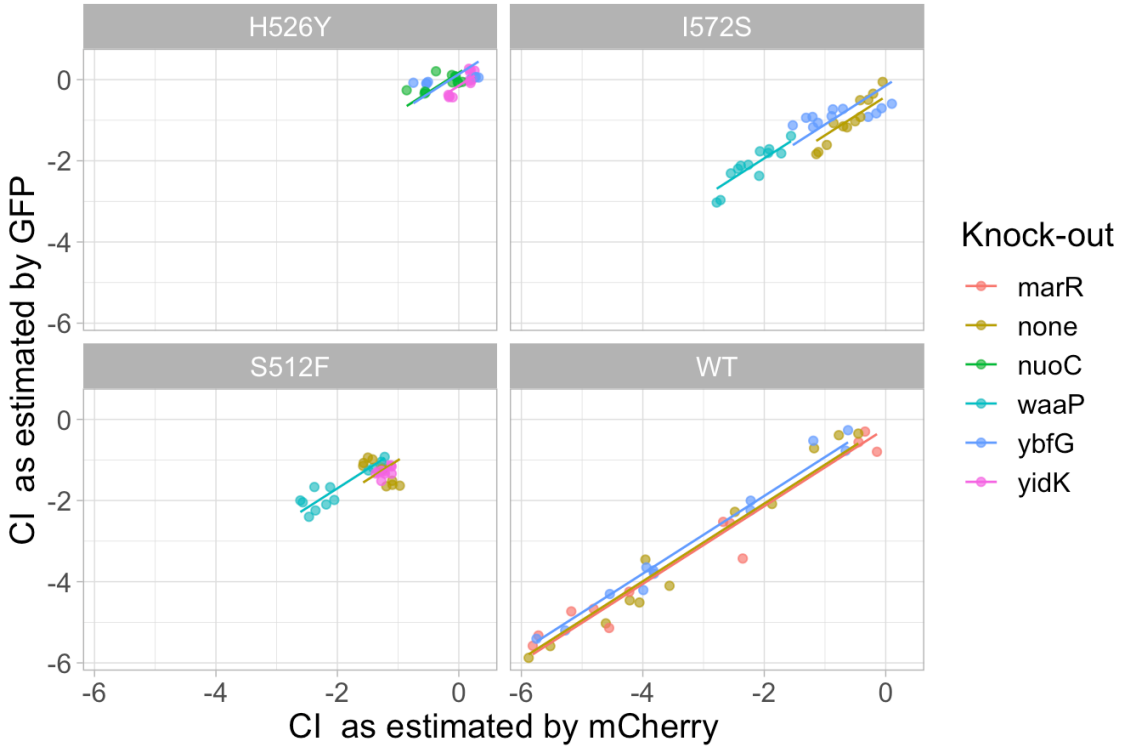

Figure S17: The plot shows genotype-specific effects of swapping fluorophores. The same data is plotted as in figure S15 but here panels show the different *rpoB* substitutions and points are coloured by genotype. Lines show the multiple regression on genotype as detailed in table S6. This effect is statistically significant; however it explains only about 1% more of the variation in the data (adjusted $R^2 = 0.9588$ for overall regression) as compared to not including this effect.

Table S6: Results of ANOVA show that the genotype-specific effect of swapping fluorophores is statistically significant but small.

Source of Variation	**SS**	**df**	**MS**	**F statistic**	**p-value**
CI as estimated by mCherry	300	1	300	3204	$< 10^{-15}$
Genotype	4.12	11	0.37	4.00	$< 10^{-4}$
Residuals	11.9	127	0.09		

8.4 Cost of resistance

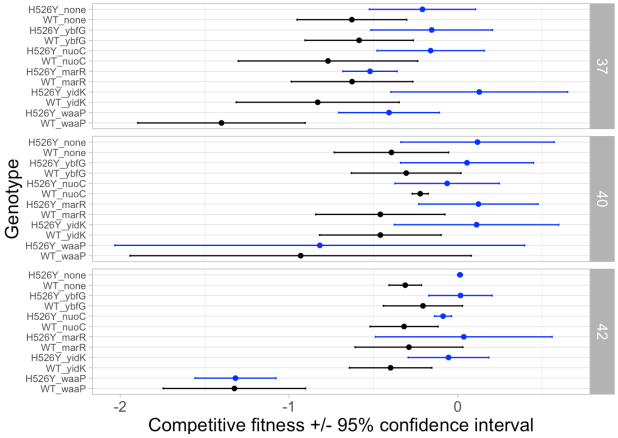

(a) ABR *rpoB* H526Y shown in blue.

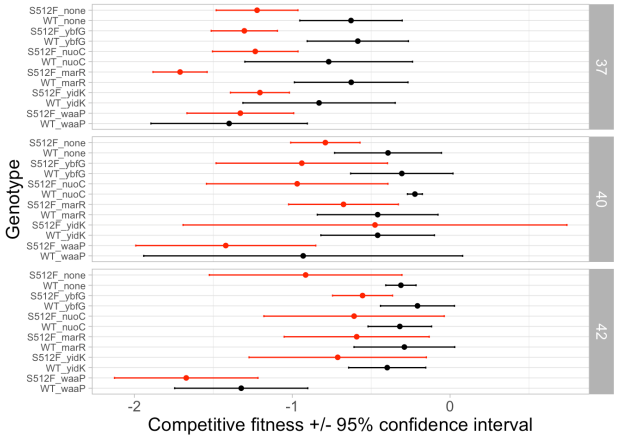

(b) ABR *rpoB* S512F shown in red.

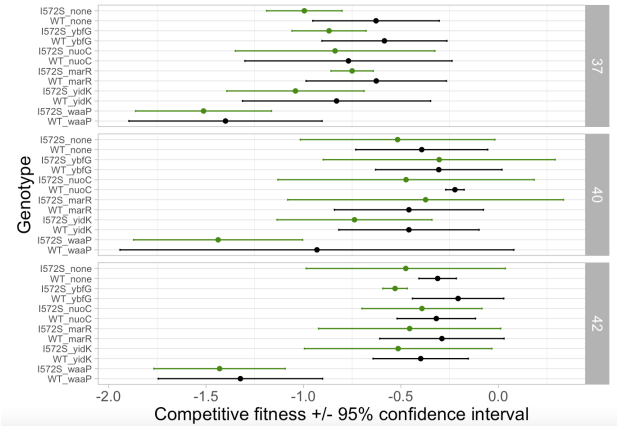

(c) ABR *rpoB* I572S shown in green.

Figure S18: Competitive fitness for ABR mutations in the absence of antibiotic ($0\mu g/mL$ rifampicin) indicates the cost of resistance. Each panel shows a different ABR *rpoB* mutation (colours) as compared to the wild-type *rpoB* (black). The x-axis indicates the competitive index, with points showing mean values and error bars showing the 95% confidence interval on the mean values. The y-axis shows the genotype, with first the *rpoB* mutation then the knock-out (e.g., "H526Y_nuoC" indicates the H526Y mutation at *rpoB* on the $\Delta nuoc$ background); "WT" refers to the wild-type *rpoB* sequence and "none" indicates that there is no knock-out. In each panel, the facets show the three different temperature environments. **(a)** Contrary to previous studies [27, 28], the H526Y mutation has no significant fitness cost – in fact, it exhibits a significantly higher fitness than wild-type at $42°C$ and has a fitness advantage on the $\Delta waaP$ background at $37°C$. **(b)** The S512F mutation has no significant fitness cost on most backgrounds except two at $37°C$ ($\Delta ybfG$ and $\Delta marR$, but not on the wild-type *rpoB* background) and one ($\Delta nuoC$) at $40°C$. This is contrary to previous studies that have found S512F to have a higher fitness than wild-type at $40°C$ [27]. **(c)** The I572S mutation has no significant fitness costs, except on the $\Delta ybfG$ background at $42°C$.

8.5 GxG summary statistics

8.5.1 'Classical' pairwise epistasis

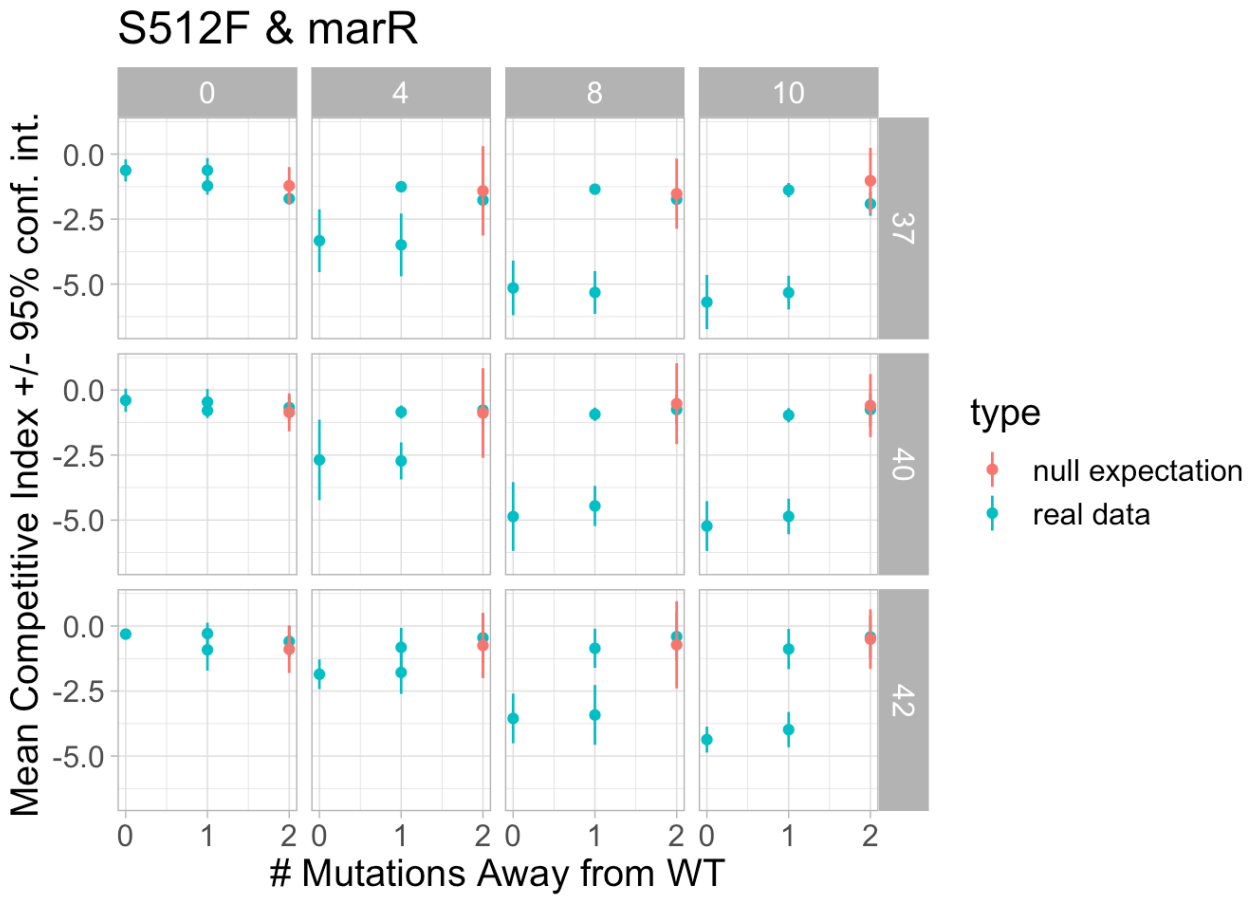

Figure S19: An illustration of how pairwise epistasis was calculated, in this case for the combination of the S512F *rpoB* ABR and the Δ*marR* knock-out mutations. The plot shows the observed mean competitive index ($\pm$ the 95% confidence interval as determined from parametric boostrapping) in blue on the y-axis as a dependent-variable of the number of mutations away from wild-type (x-axis) in each of the 12 environments. Different antibiotic concentrations are shown in each column and different temperatures are shown on each row. The red points show the mean competitive index expected under the null hypothesis of no epistasis. In this example there are no instances where the epistasis is significantly different from zero as shown by the consistent overlap between the 95% confidence interval error bars and the points indicating mean values. Figure S21 summarizes the pairwise epistasis estimates for all genotypes combinations in all environments.

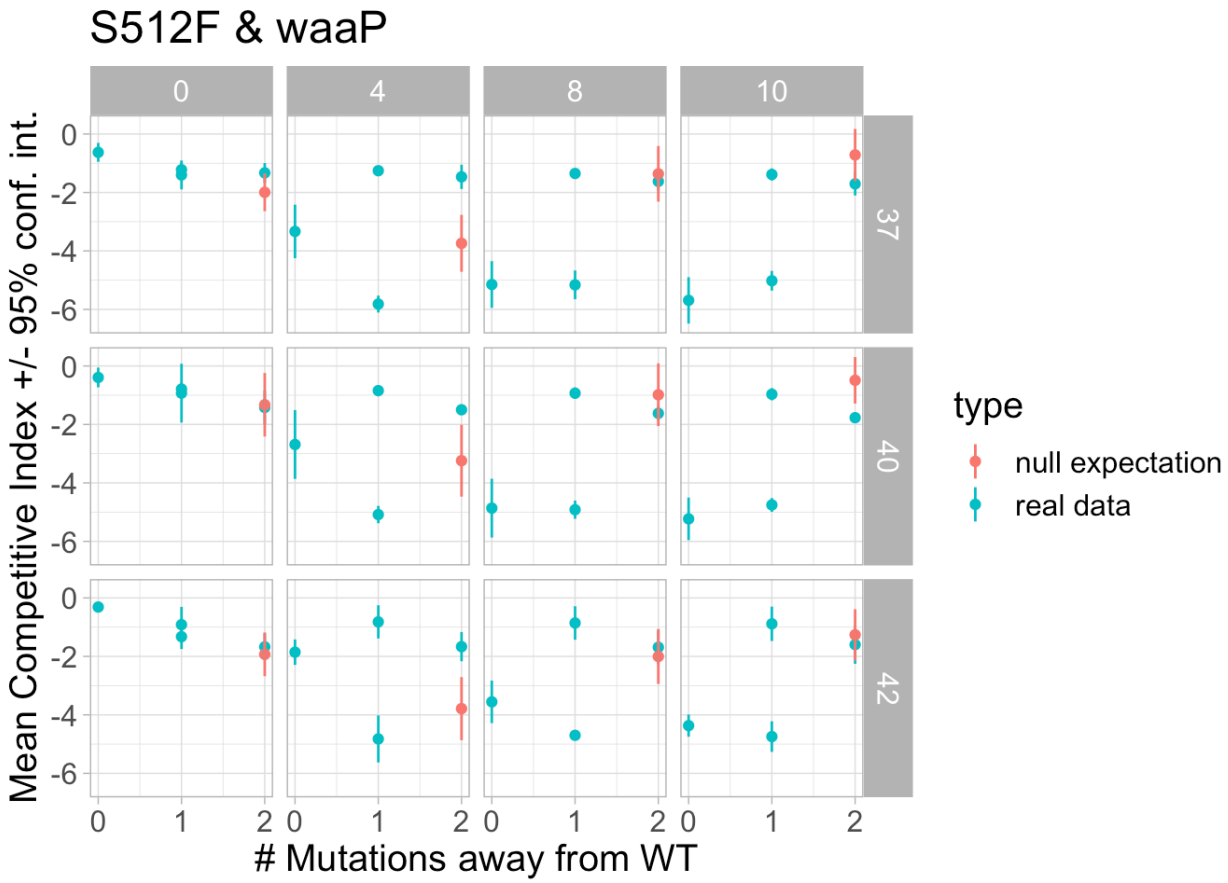

Figure S20: An example of significant pairwise epistasis, in this case for the combination of the S512F *rpoB* ABR and the Δ*waaP* knock-out mutations. The data is plotted in the same style as described in figure S19. Positive epistasis is apparent in all of the temperature environments with 4μg/mL rifampicin, as seen by the larger fitness values of the real data (blue points) as compared to the null expectation of no epistasis (red points). No overlap between the 95% confidence intervals and the mean indicates that the effect is statistically significant. The equivalent plots for Δ*waaP* in combination with the other ABR mutants, H526Y and I572S, show a similar trend of positive epistasis at 4μg/mL rifampicin, as summarized in figure S21. The $40°C$ and 10μg/mL environment displays significant negative pairwise epistasis.

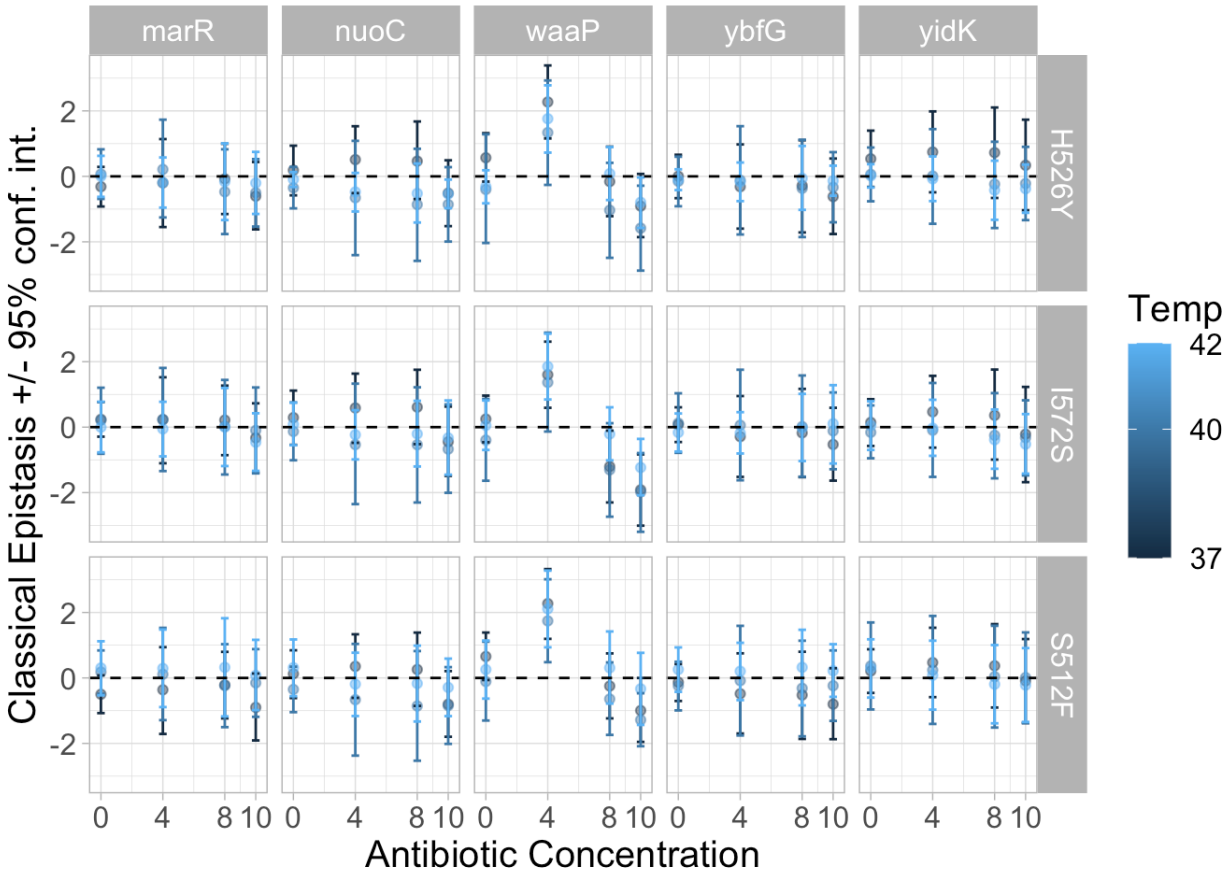

Figure S21: **Estimated pairwise epistasis across all genotypes and environments.** The plots are laid out in the same manner as figure 2 except that the y-axis here shows the mean estimated 'classical' pairwise epistasis and error bars show the 95% confidence interval as determined from parametric bootstrapping.

8.5.2 Gamma epistasis

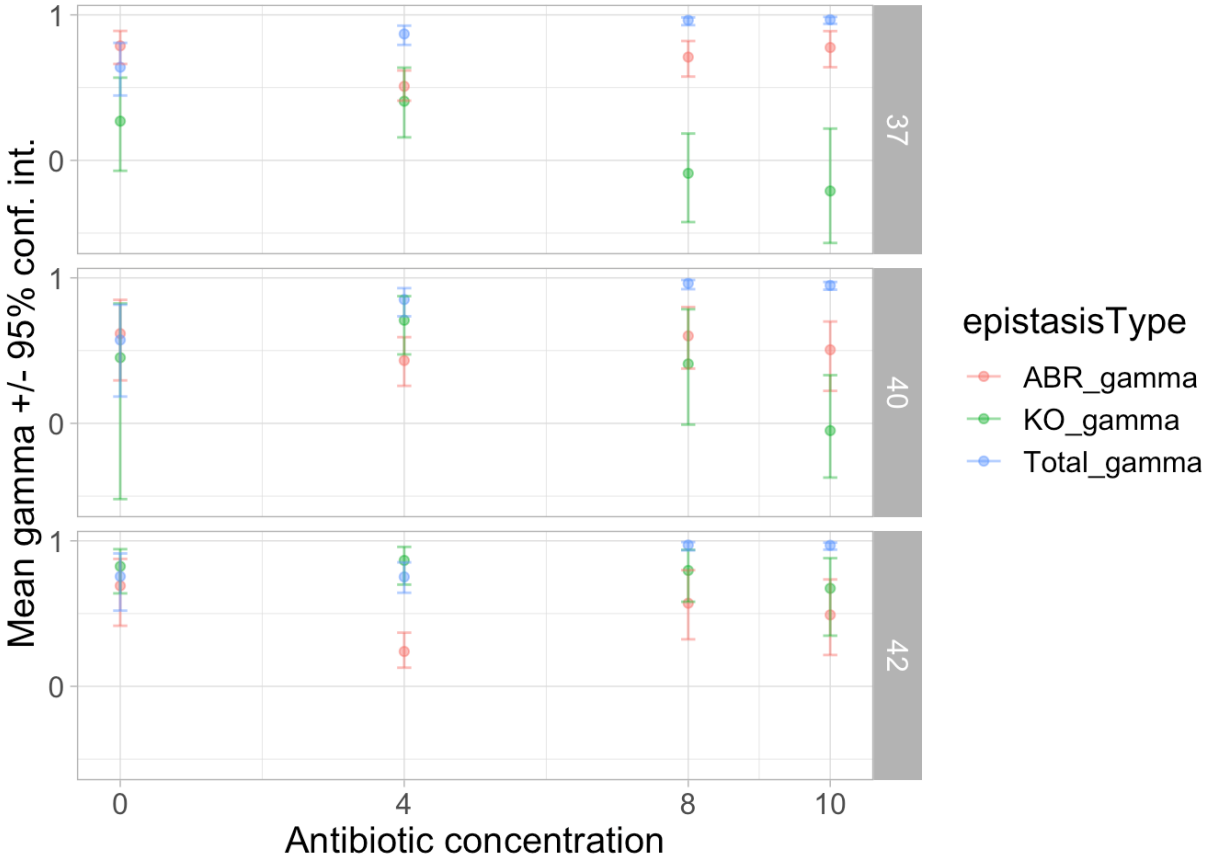

Figure S22: The amount of gamma epistasis is different for different gene classes and temperature environments. Points show the mean gamma epistasis for different gene classes as indicated by the colour (red for ABR mutations at *rpoB*, green for gene knock-out mutations, and blue for the total as already shown in figure 3a. The x-axis shows the rifampicin antibiotic concentration in $\mu g/mL$ and the rows show the three different temperature environments. The error bars show the 95% parametric bootstrap confidence interval. No regression lines are shown as the correlations are not significant at $\alpha = 0.01$.

8.5.3 Fraction of sign epistasis

Table S7: List of the genotypes that exhibited reciprocal sign epistasis in more than 5% of the 10 000 parametric bootstrap samples. The counts of observed reciprocal sign epistasis for all bootstrap samples is given for each of the three temperature environments. Only the environment without anitbiotic is shown because the other environments did not exhibit reciprocal sign epistasis in more than 5% of bootstrap samples.

rpoB mutation	**Knock-out mutation**	**Count at** $37°C$	**Count at** $40°C$	**Count at** $42°C$
I572S	ΔnuoC	3437	2514	2831
I572S	ΔmarR	2327	3538	2632
I572S	ΔyidK	1688	2331	2586
I572S	ΔybfG	698	2864	2242
S512F	ΔyidK	551	3236	1469
H526Y	ΔybfG	596	976	694
H526Y	ΔmarR	2480	(<500)	1227
S512F	ΔwaaP	2357	(<500)	(<500)
S512F	ΔmarR	(<500)	1831	1276
H526Y	ΔnuoC	(<500)	1473	(<500)
H526Y	ΔwaaP	(<500)	1381	(<500)
I572S	ΔwaaP	(<500)	744	(<500)
H526Y	ΔyidK	(<500)	565	(<500)
S512F	ΔnuoC	(<500)	(<500)	1268

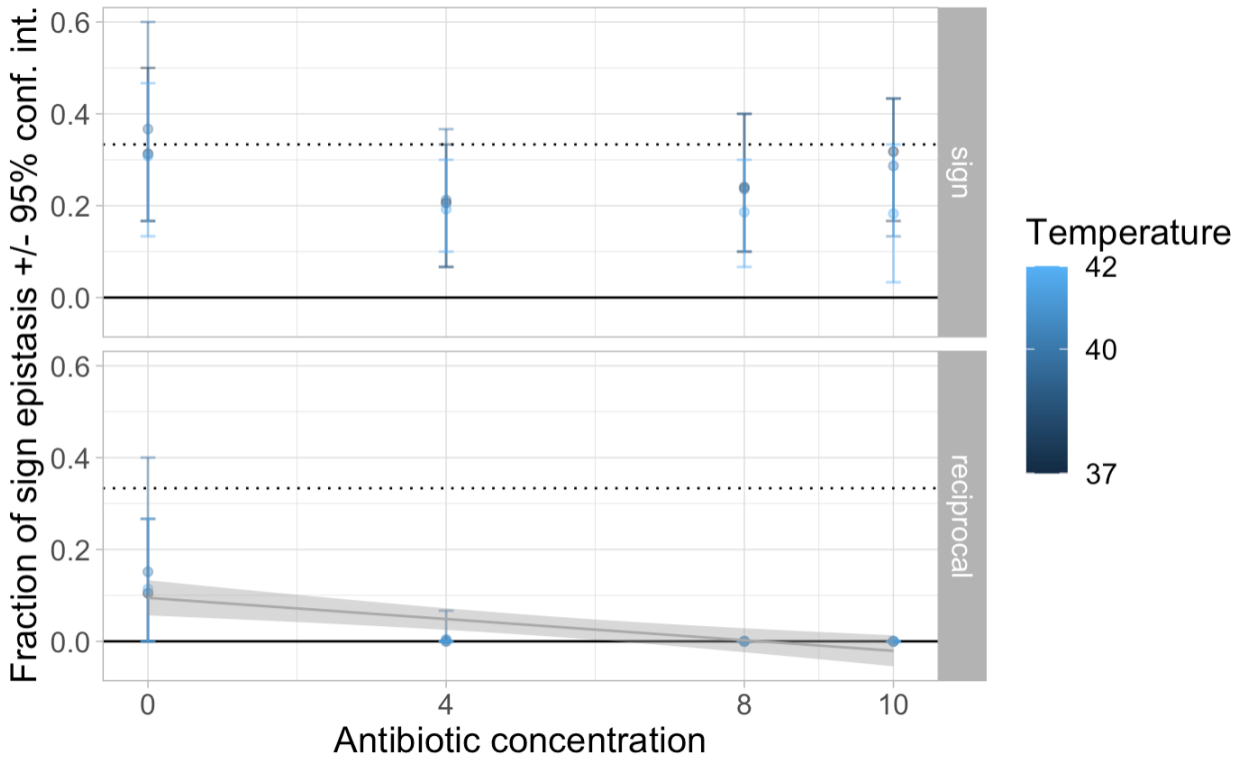

Figure S23: The fraction of simple and reciprocal sign epistasis for different environments. Reciprocal sign epistasis (bottom facet) is mostly observed in the absence of antibiotic while the fraction of simple sign epistasis (top facet) shows no apparent trend with different environments. The points show the mean fraction and the error bars show the 95% parametric bootstrap confidence interval. The x-axis shows the antibiotic concentration and the colour shows the temperature. The solid line at $y = 0$ highlights the fraction of simple and reciprocal sign epistasis expected in a purely additive landscape without any epistasis. The dotted line at $y = \frac{1}{3}$ highlights the fraction of simple and reciprocal sign epistasis expected in a completely epistatic house-of-cards landscape. There is no significant correlation between the antibiotic concentration and the fraction of simple sign epistasis ($F(1, 10) = 2.15$, $p = 0.17$). The grey trend-line shows the significant negative correlation of antibiotic concentration on the fraction of reciprocal sign epistasis ($F(1, 10) = 20.3$, $p < 0.005$, adjusted $R^2 = 0.637$) and the grey shaded region shows the 95% confidence interval of the mean for the least-squares estimated linear regression. Antibiotic concentration explains more of the variation in the fraction of reciprocal sign epistasis than environmental quality (figure S40).

8.5.4 Roughness-to-slope ratio

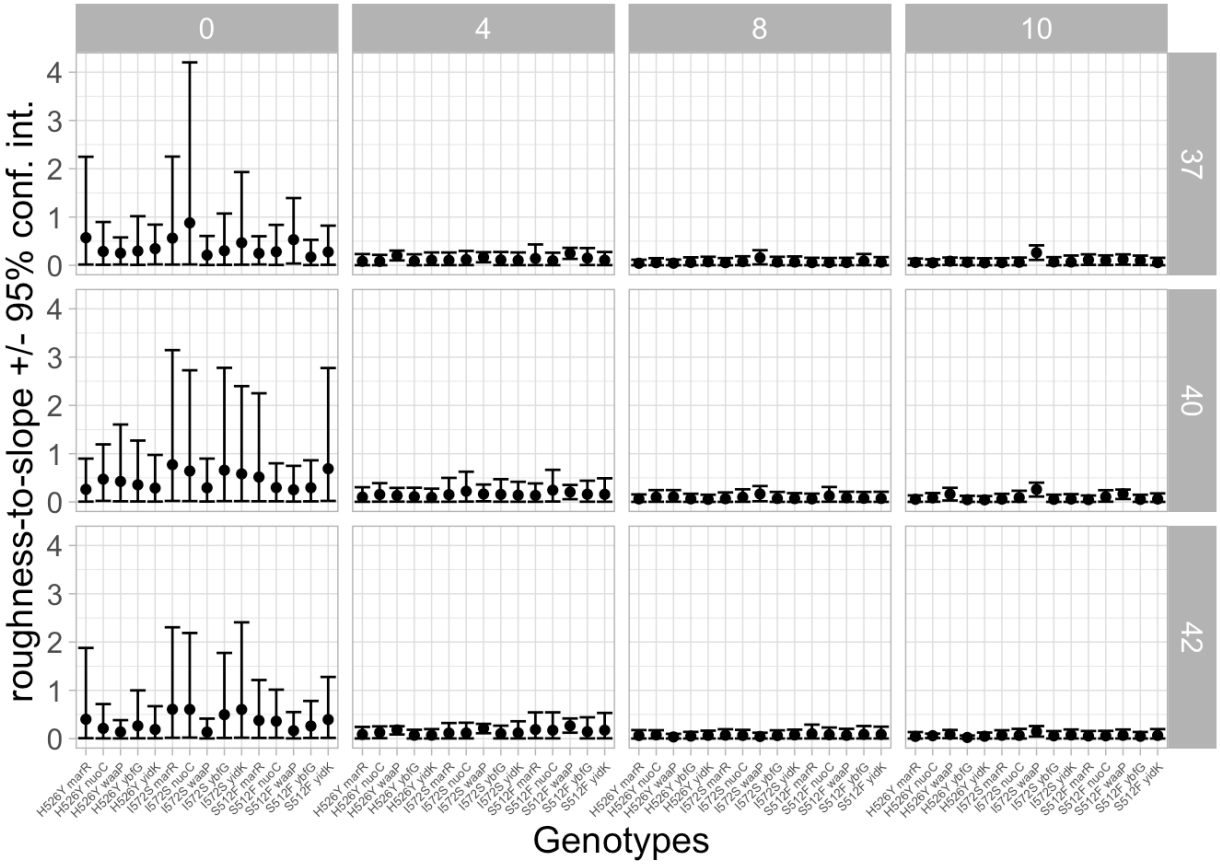

Figure S24: The roughness-to-slope ratio (y-axis) for each genotype (x-axis) in each environment. The dots show the mean roughness-to-slope ratios and the error bars show the 95% parametric bootstrap confidence interval. The columns show different antibiotic concentrations and the rows show different temperature environments.

8.5.5 Diminishing-returns epistasis

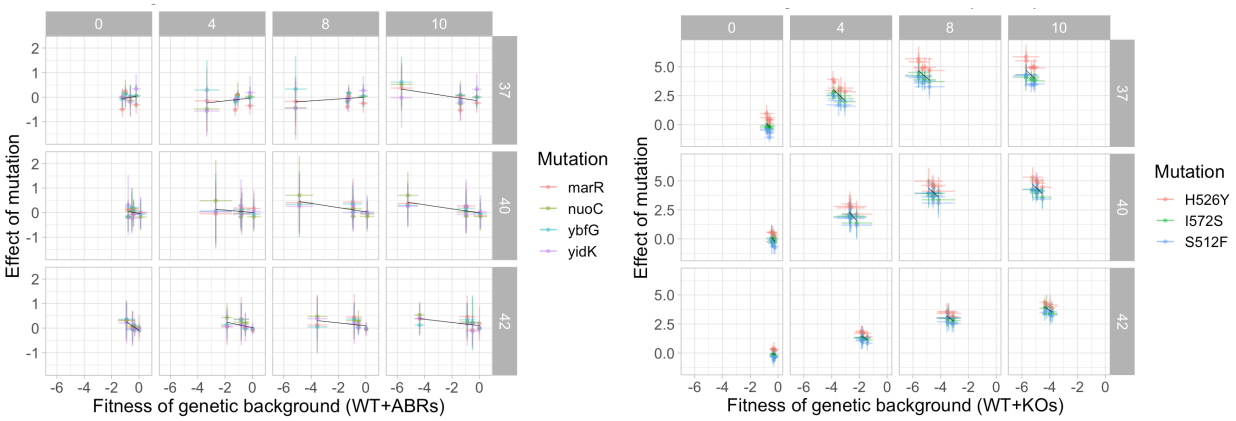

(a) knock-out mutations, excluding $\Delta waaP$

(b) ABR *rpoB* mutations, excluding $\Delta waaP$ background

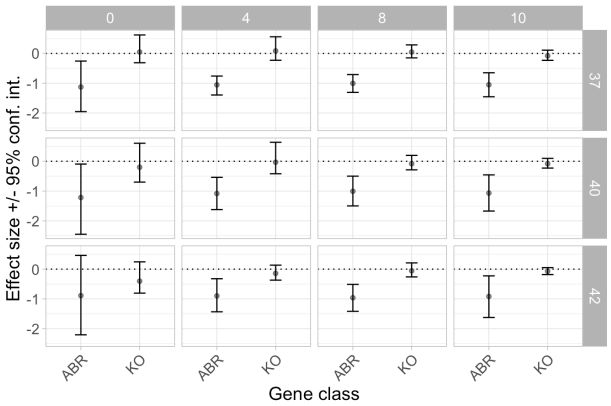

(c) Slopes of the diminishing-returns epistasis excluding $\Delta waaP$

Figure S25: **When the Δ*waaP* mutation and background are removed from the analysis, knock-outs continue to display no diminishing-returns epistasis and ABR *rpoB* mutations exhibit diminishing-returns epistasis in all but one of the environments.** The plots are in the same style as figure 4 except that the effect of the $\Delta waaP$ mutation and mutations on the $\Delta waaP$ background have been removed to confirm that $\Delta waaP$ is not responsible for the overall trend.

8.6 Multiple regression for competitive fitness

Table S8: Results of ANOVA show that the additive effects of *rpoB* and KO mutants as well as those of antibiotic concentration and temperature environments are all significant.

Source of Variation	**SS**	**df**	**MS**	**F statistic**	**p-value**
rpoB mutant	1245	3	415.0	533.7	$< 10^{-15}$
KO mutant	114.7	5	22.9	29.50	$< 10^{-15}$
Antibiotic concentration	216.6	3	72.2	92.83	$< 10^{-15}$
Temperature	66.7	2	33.3	42.86	$< 10^{-15}$
Residuals	763.6	982	0.8		

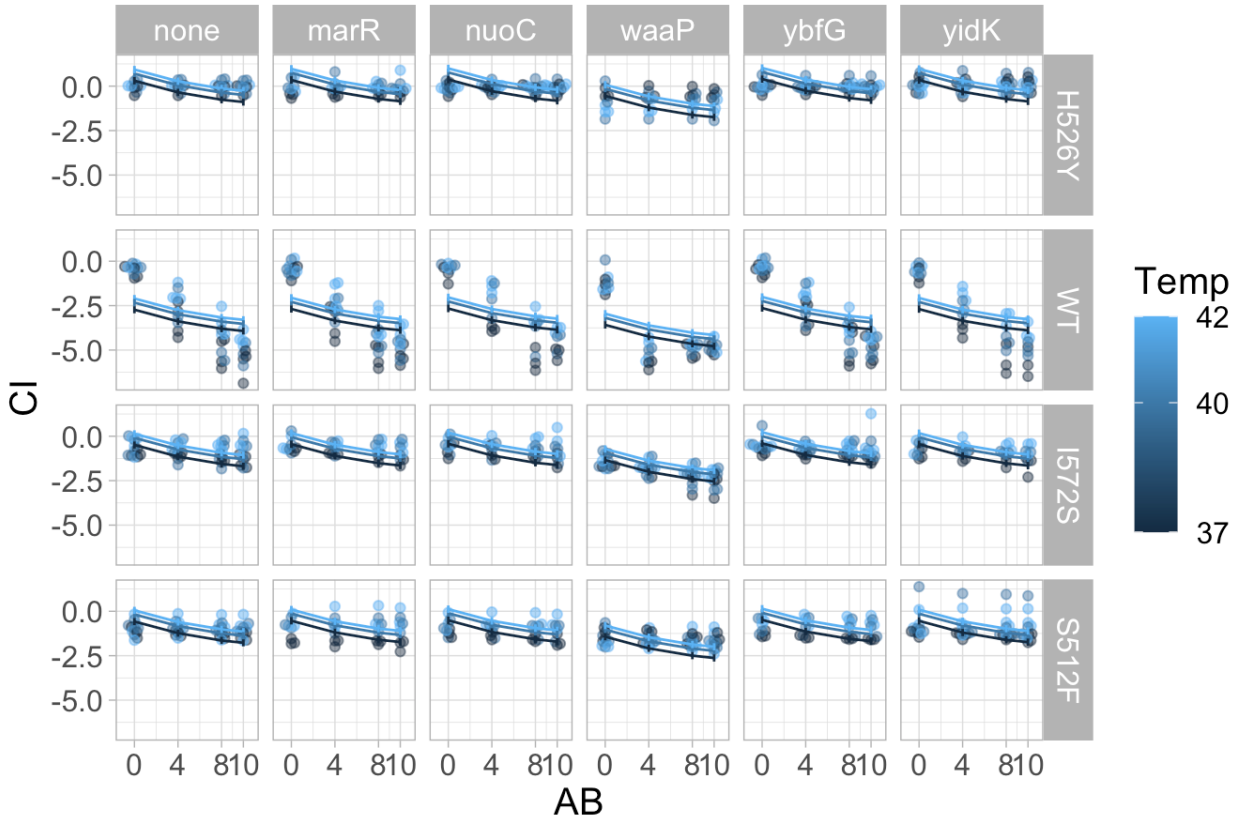

Figure S26: A linear regression with only additive effects explains almost 70% of the variation observed in the competition data. The x-axis shows the rifampicin antibiotic concentration (AB) in $\mu g/mL$ and the y-axis shows the $\hat{w}$ competitive index (CI). Points show the data and lines show the mean predictions with error-bars depicting the 95% confidence intervals for the means of the least-squares estimated linear regression. Therefore the space between the data points and the mean lines indicates the residuals of the model fitting. This plot shows us that much of the residual variation can be attributed to wild-type, antibiotic-susceptible genotypes (WT, second row) since this predictor has the biggest deviation between the data points and the model. This model was found to explain less of the variation than models with an interaction between *rpoB* genotypes and antibiotic environment.

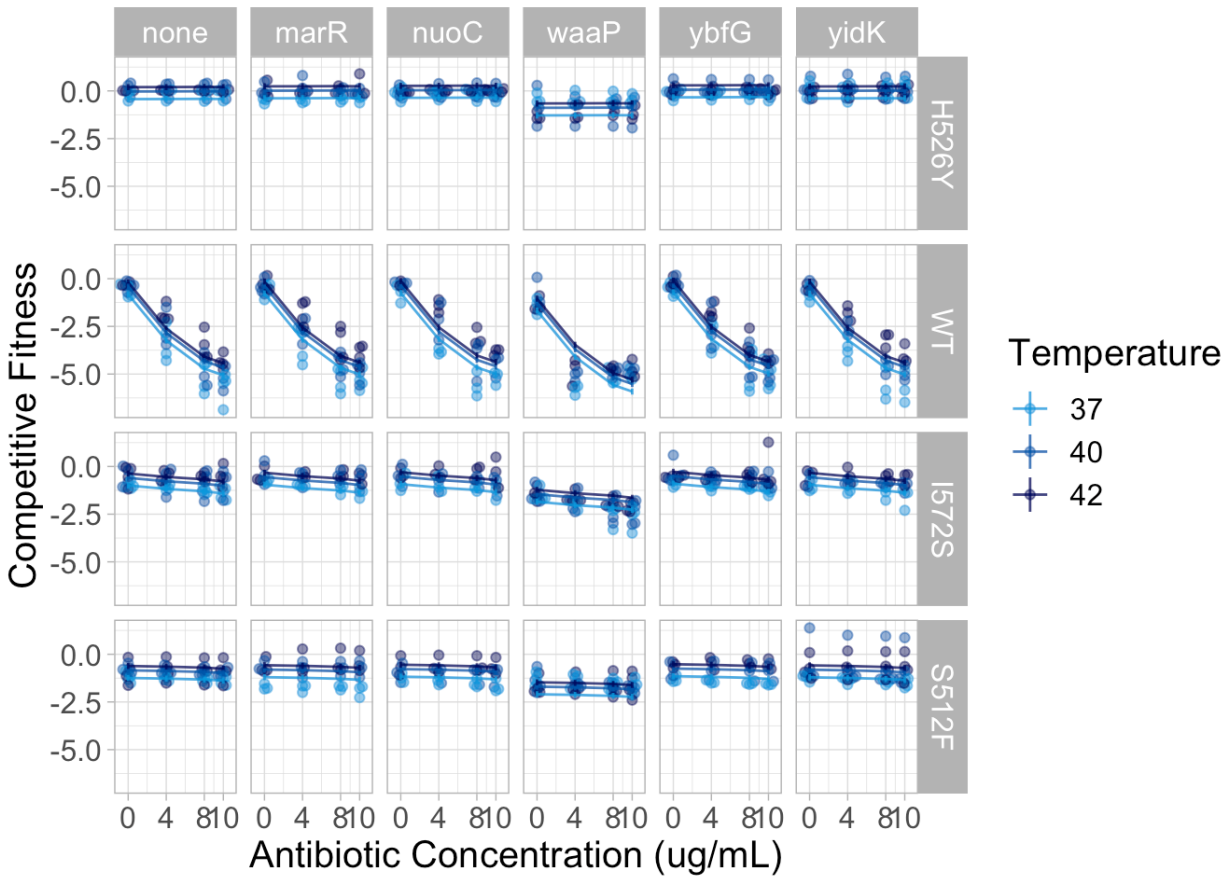

Figure S27: A linear regression with additive effects and $G_{rpoB} \times E_{\mathrm{AB}}$, an interaction between *rpoB* genotype and antibiotic environment, explains much of the variation observed in the competition data. The x-axis shows the rifampicin antibiotic concentration in $\mu g/mL$ and the y-axis shows the $\hat{w}$ competitive index. Points show the data and lines show the mean predictions with error-bars depicting the 95% confidence intervals for the means of the least-squares estimated linear regression. Therefore the space between the data points and the mean lines indicates the residuals of the model fitting. This plot shows that most of the systematic variation in the data is explained by this model.

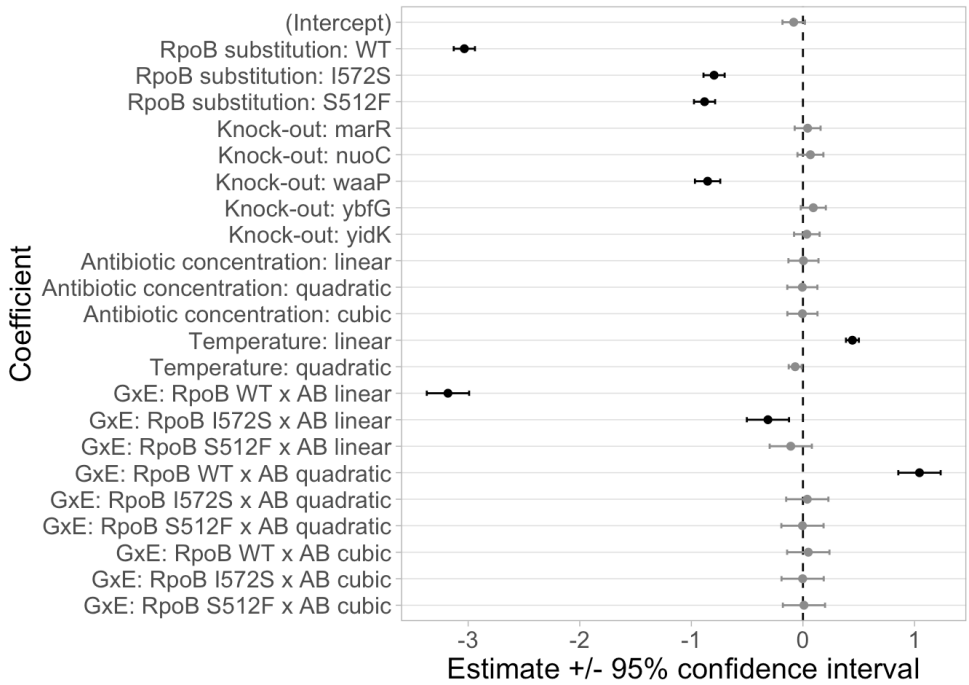

Figure S28: Estimated mean values for the coefficients in the regression model with additive effects and $G_{rpoB} \times E_{\mathrm{AB}}$, an interaction between *rpoB* genotype and antibiotic environment (error bars show 95% confidence intervals). The intercept is for *rpoB* with the H526Y substitution and without any knock-out mutation (i.e., the reference genotype for all competitions) as grown in the 37°C environment without any rifampicin antibiotic. Statistically significant coefficients ($\alpha = 0.05$) are shown in black and have confidence intervals that do not overlap with zero. Coefficients whose estimates are not statistically significant are shown in gray and have confidence intervals that overlap with zero (dashed vertical line).

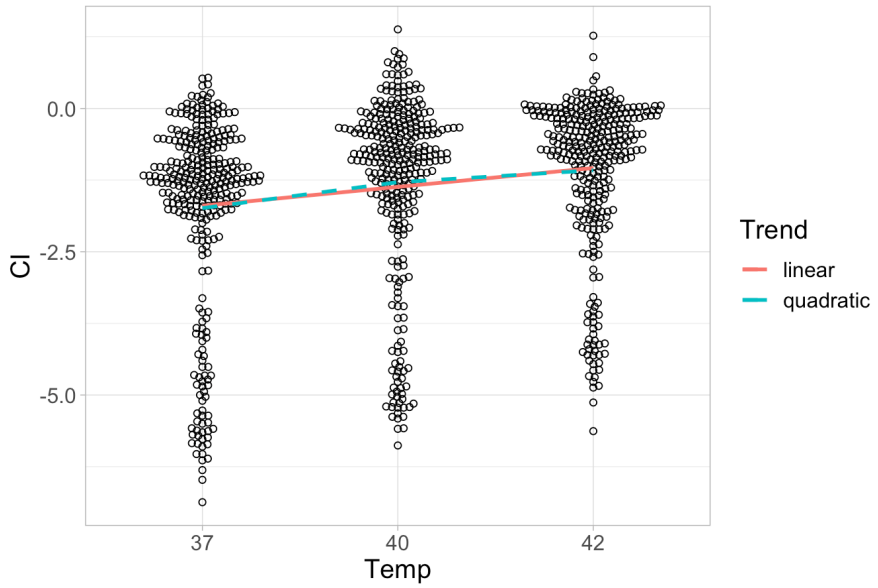

Figure S29: A beeswarm plot of the average effect of temperature (categorical x-axis) on estimated competitive index (quantitative y-axis) across all genotypes and antibiotic environments. Circles show individual estimates, but deviations along the x-axis away from the category labels are not quantitatively meaningful: it's merely to prevent overlapping of dense data points. The solid line shows the average linear (statistically significant) trend, and the dashed line shows the average quadratic (but **not** statistically significant) trend (see estimated coefficients in figures S28 and S31).

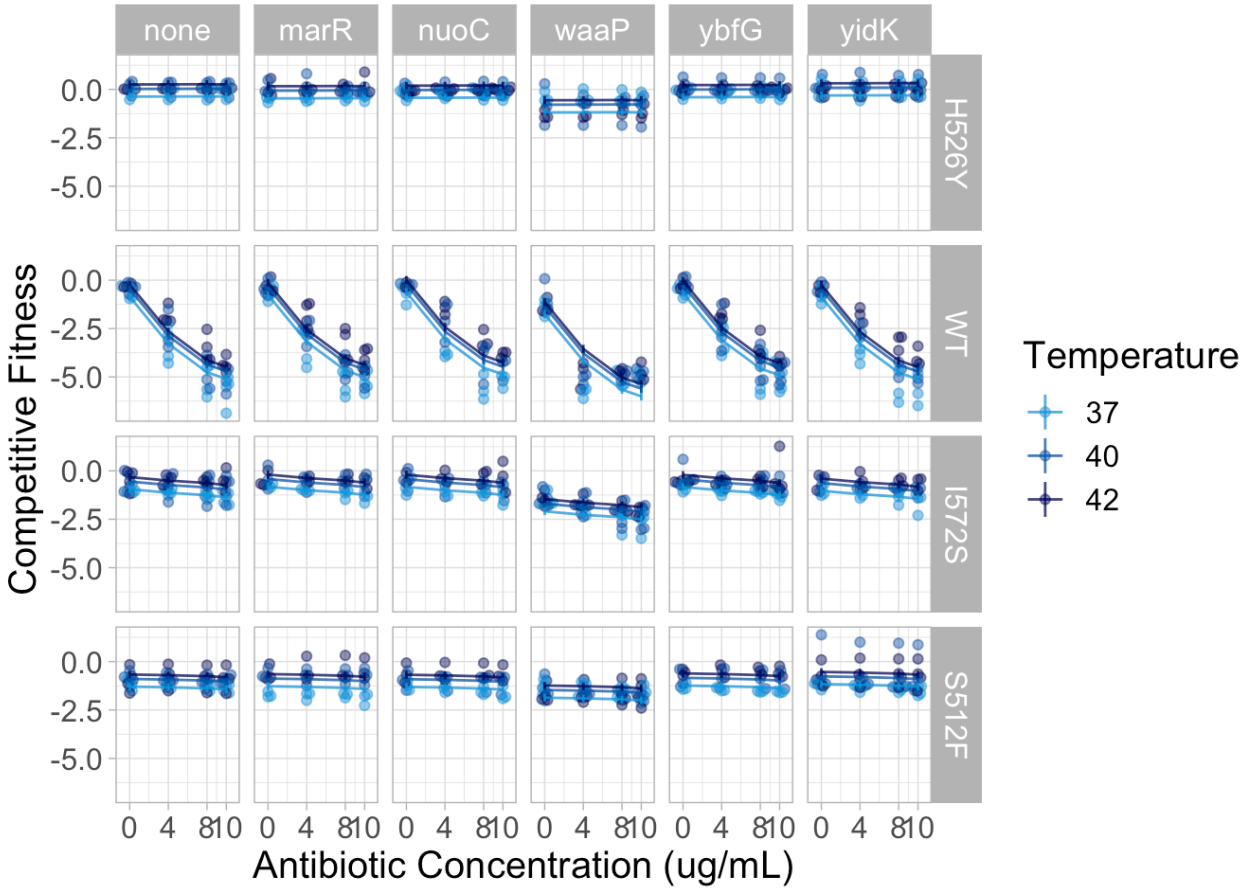

Figure S30: A linear regression with additive effects, an interaction between *rpoB* genotype and antibiotic environment ($G_{rpoB} \times E_{\mathrm{AB}}$), and a pairwise epistatic interaction between *rpoB* and knock-out genotypes ($G_{rpoB} \times G_{\mathrm{KO}}$) explains much of the variation observed in the competition data. The x-axis shows the rifampicin antibiotic concentration in $\mu g/mL$ and the y-axis shows the $\hat{w}$ competitive index. Points show the data and lines show the mean predictions with error-bars depicting the 95% confidence intervals for the means of the least-squares linear regression. Therefore the space between the data points and the mean lines indicates the residuals of the model fitting. This plot shows that most of the systematic variation in the data is explained by this model.

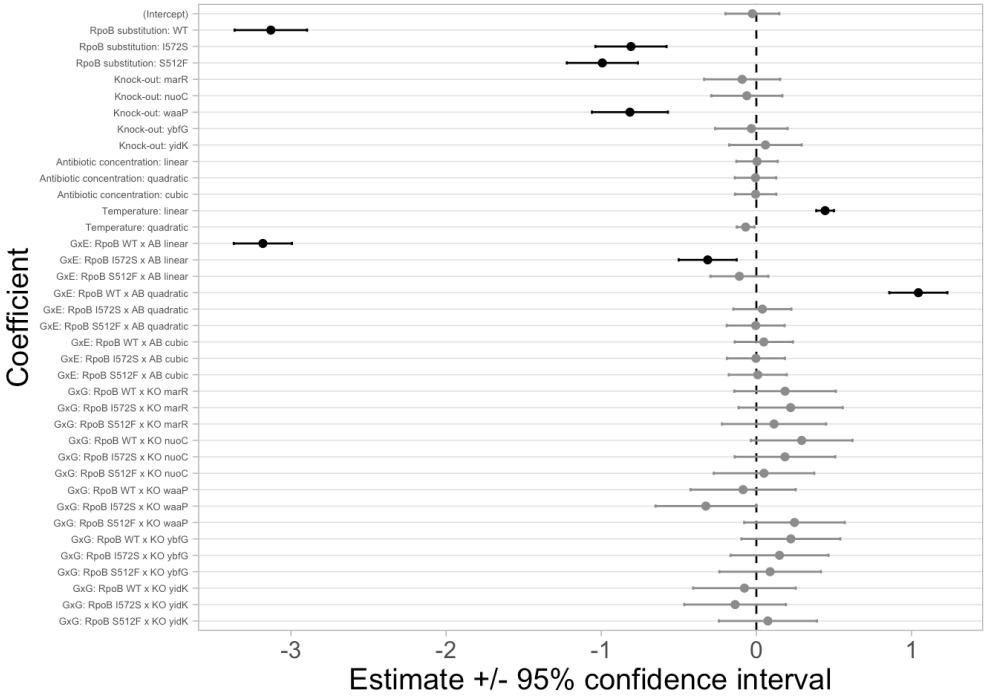

Figure S31: Estimated mean values for the coefficients in the regression model with additive effects and an interaction between *rpoB* genotype and antibiotic environment as well as epistasis between *rpoB* and knock-out genotypes (error bars show 95% confidence intervals). The intercept is for *rpoB* with the H526Y substitution and without any knock-out mutation (i.e., the reference genotype for all competitions) as grown in the 37°C environment without any rifampicin antibiotic. Statistically significant coefficients are shown in black and have confidence intervals that do not overlap with zero. Coefficients whose estimates are not statistically significant are shown in gray and have confidence intervals that overlap with zero (dashed vertical line). Notice that none of the coefficients associated with the epistatic interactions of *rpoB* and knock-out genotypes are significant. The interaction of *rpoB* I572S with the $\Delta waaP$ knock-out is barely significant ($p = 0.0492$).

8.7 Finlay-Wilkinson regression on overall environmental quality

8.7.1 Selecting the metric of environmental quality

Results of 3 metrics for environmental quality as part of Finlay-Wilkinson regression:

the mean growth of all competitor strains in each environment: This metric of environmental quality is the best since the environment explains more of that variation in the metric than the replicate block (table S9), it is able to distinguish environments from one another (figure S32), and it is able to distinguish specialist from generalist genotypes (figure S33).

the mean growth of the reference strain, H526Y, in each environment: This metric of environmental quality was not found to be good since more of the variation in the metric is explained by the replicate block than by the environment itself (figure S34 and table S10).

the mean total growth in the well (reference + competitor) in each environment: This metric of environmental quality is not as good as the mean growth of all competitor strains. The environment explains slightly less of the variation in the metric as the replicate block (table S11) and so environments are not well distinguished from one another (figure S35). As well, this metric does not correctly distinguish specialist from generalist genotypes (figure S36)

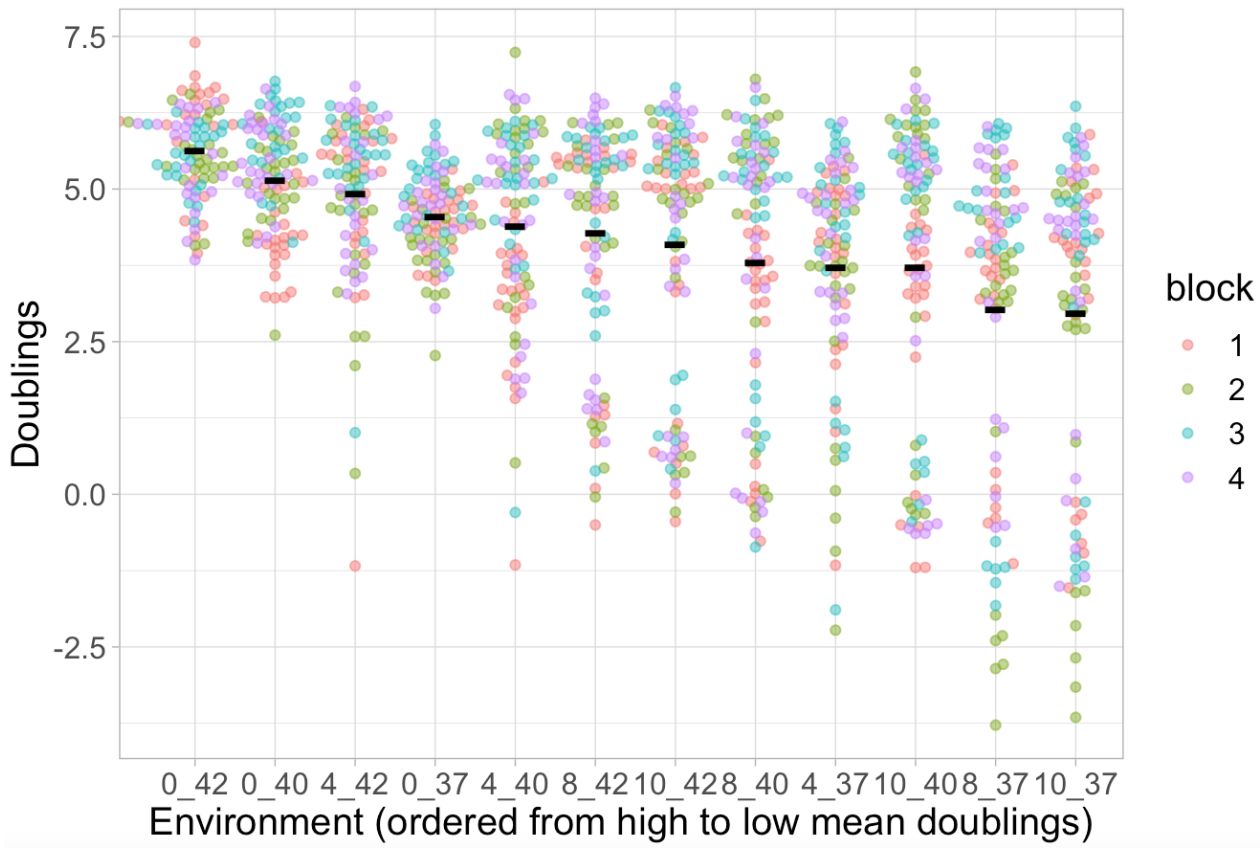

Figure S32: This plot shows that the environmental quality metric 'mean growth of all competitor strains in each environment' is able to distinguish between environments. The x-axis shows each environment in order from highest to lowest quality and the y-axis shows the total amount of growth estimated by the number of doublings observed between 0 and 20 hours (negative values suggest cell death). The black horizontal lines show the mean doublings across all replicates and genotypes: these values are used below as the metric of environmental quality. The coloured dots show the doublings of individual competitor genotypes and their replicates. Colours indicate the experimental replicate block and, ideally, should not show any trend. Both the environment and the replicate block explain a significant amount of the variation in the data (table S9). The genotypes that perform poorly in the low quality environments correspond to antibiotic susceptible *rpoB* wild-type genotypes as shown in figure S33.

Table S9: results of ANOVA for environmental quality metric: the mean growth of all competitor strains in each environment.

Source of Variation	**SS**	**df**	**MS**	**F statistic**	**p-value**
Environment	679	11	61.76	18.08	$< 10^{-15}$
Replicate block	105	3	34.91	10.22	$< 10^{-5}$
Residuals	3843	1125	3.42		

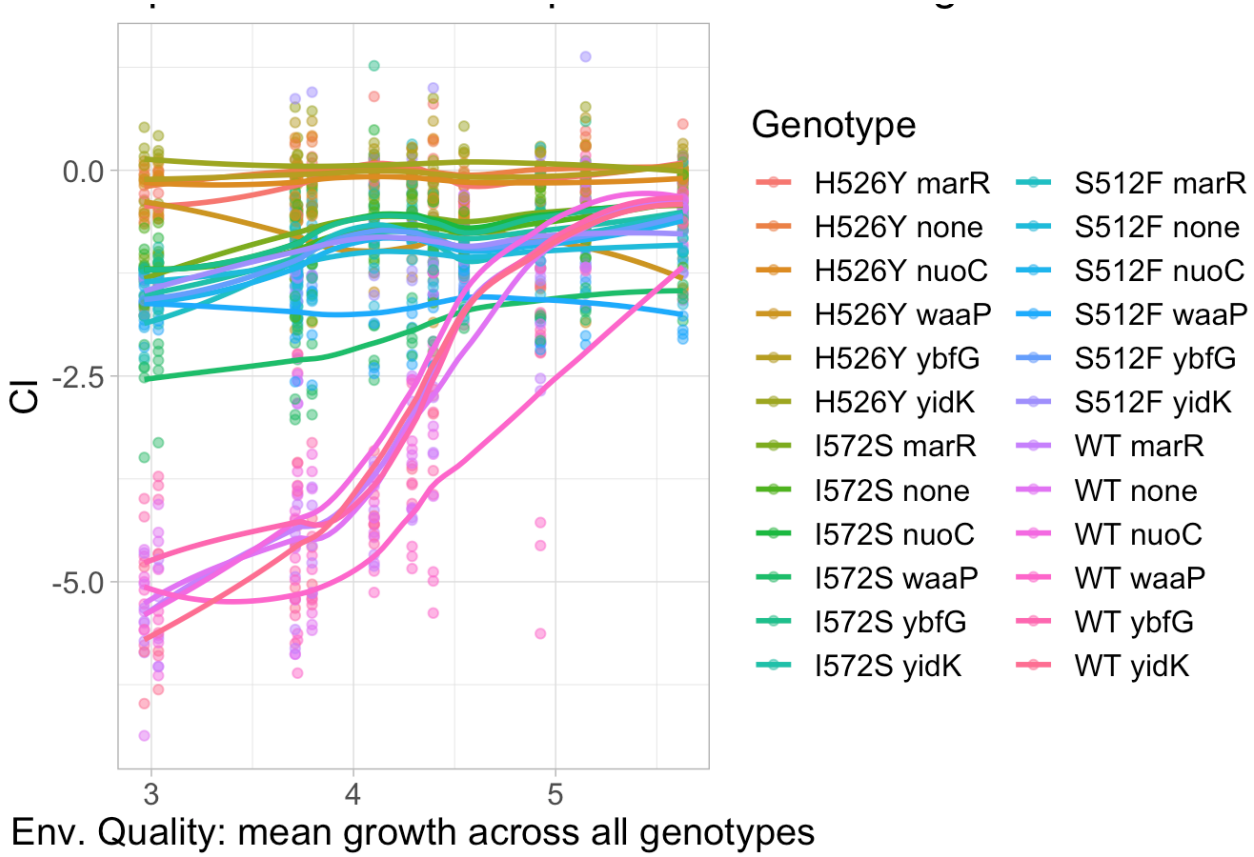

Figure S33: This plot shows that the environmental quality metric 'mean growth of all competitor strains in each environment' is able to distinguish specialist from generalist genotypes. The x-axis shows the 12 different abiotic environments as quantified by the environmental quality metric and ordered from lowest to highest quality; the y-axis shows the competitive index ($\hat{w}$) for each genotype, with values of individual replicates shown as dots ($n = 3{-}4$) and the mean value of each genotype shown as lines connected between environments. The colours indicate the genotype. All genotypes starting with "WT" are susceptible to rifampicin and therefore considered specialists to environments with no or low antibiotic concentrations. Conversely, all other genotypes are antibiotic resistant and can be considered generalists across all environments. Environments with higher antibiotic concentrations are grouped together as low quality and therefore susceptible genotypes perform poorly at lower values of the environmental quality metric (exhibiting a '/' or 'S' shape on the plot) and generalist genotypes perform about the same across all environments (exhibiting a straight line on the plot).

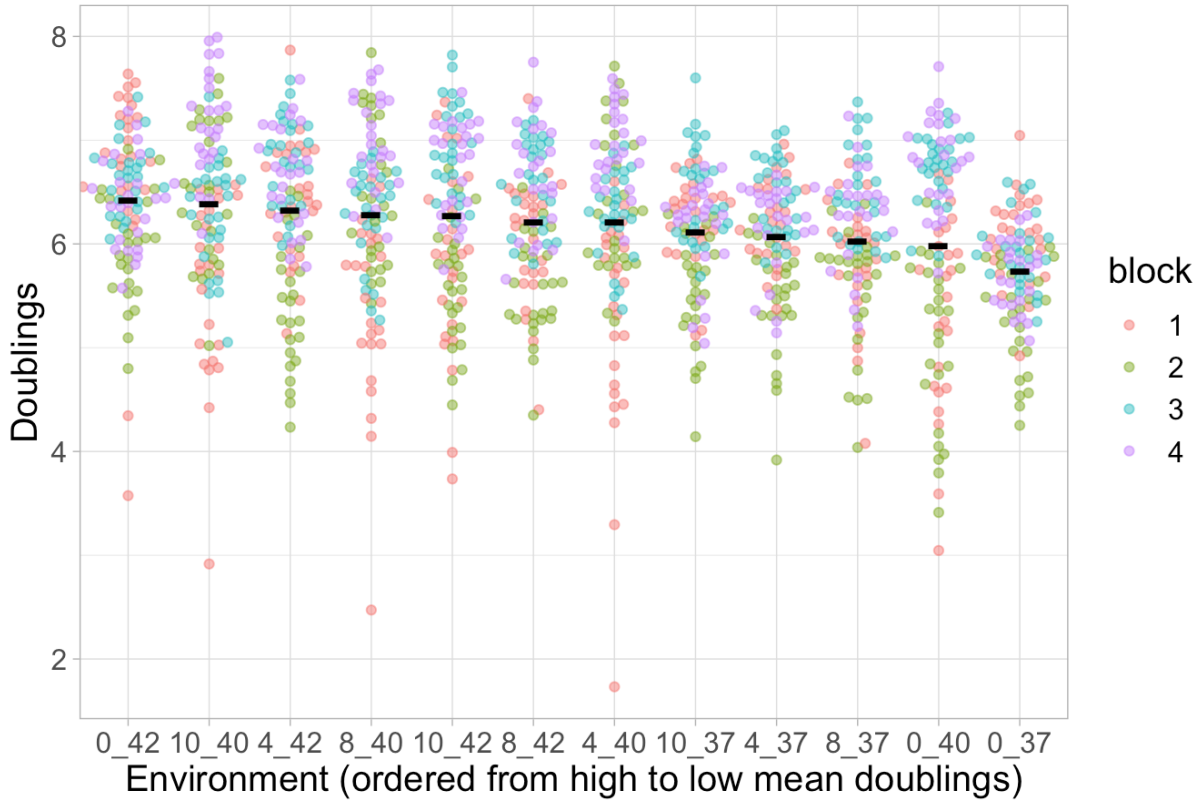

Figure S34: This plot shows that the environmental quality metric 'the mean growth of the reference strain, H526Y, in each environment' is not able to distinguish between environments. The data is plotted in the style of figure S32. However, unlike that figure, here there is a stronger effect of the replicate blocks as compared to environment (quantified in table S10).

Table S10: results of ANOVA for environmental quality metric: the mean growth of the reference strain, H526Y, in each environment.

Source of Variation	**SS**	**df**	**MS**	**F statistic**	**p-value**
Environment	40.6	11	3.69	8.01	$< 10^{-12}$
Replicate block	151.7	3	50.56	109.83	$< 10^{-15}$
Residuals	534.5	534.5	0.46		

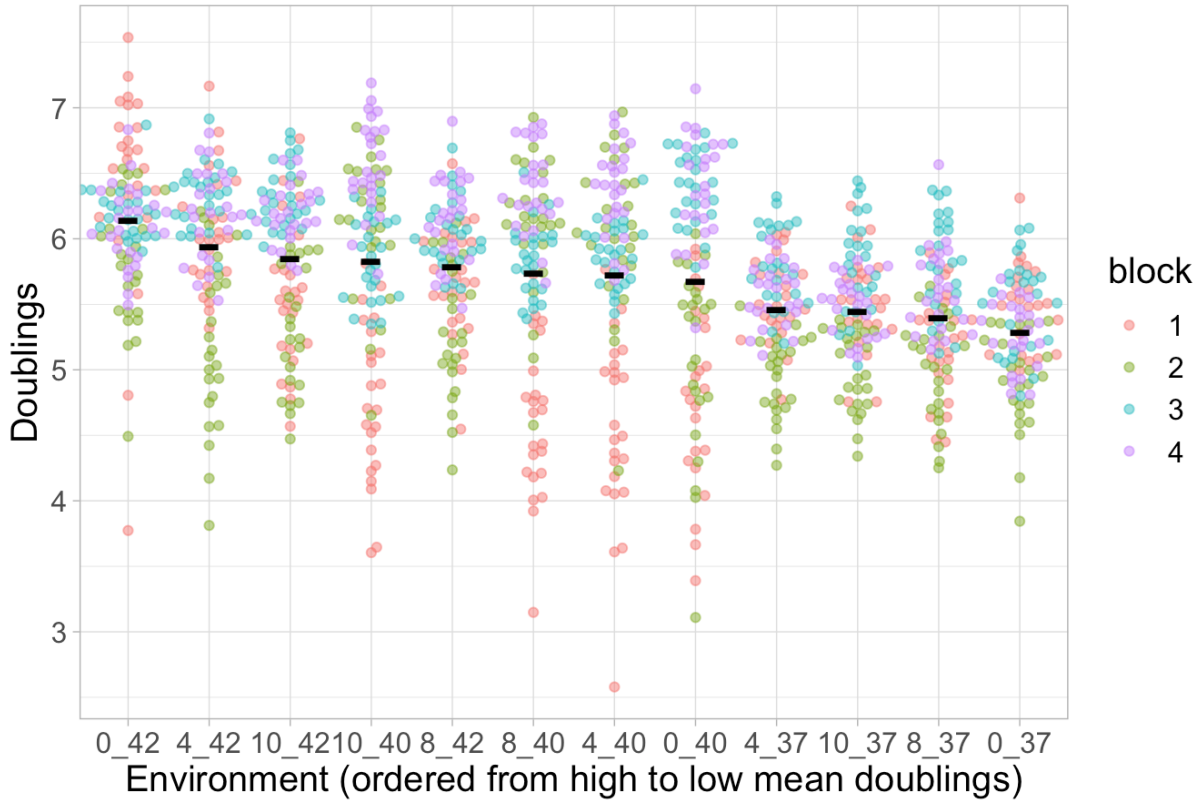

Figure S35: This plot shows that the environmental quality metric 'the mean total growth in the well (reference + competitor) in each environment' does not distinguish well between environments. The data is plotted in the style of figure S32. However, unlike that figure, here there is a stronger effect of the replicate blocks as compared to environment (quantified in table S11).

Table S11: results of ANOVA for environmental quality metric: the mean total growth in the well (reference + competitor) in each environment.

Source of Variation	**SS**	**df**	**MS**	**F statistic**	**p-value**
Environment	64.7	11	5.89	18.75	$< 10^{-15}$
Replicate block	113.6	3	37.88	120.66	$< 10^{-15}$
Residuals	353.2	1125	0.31		

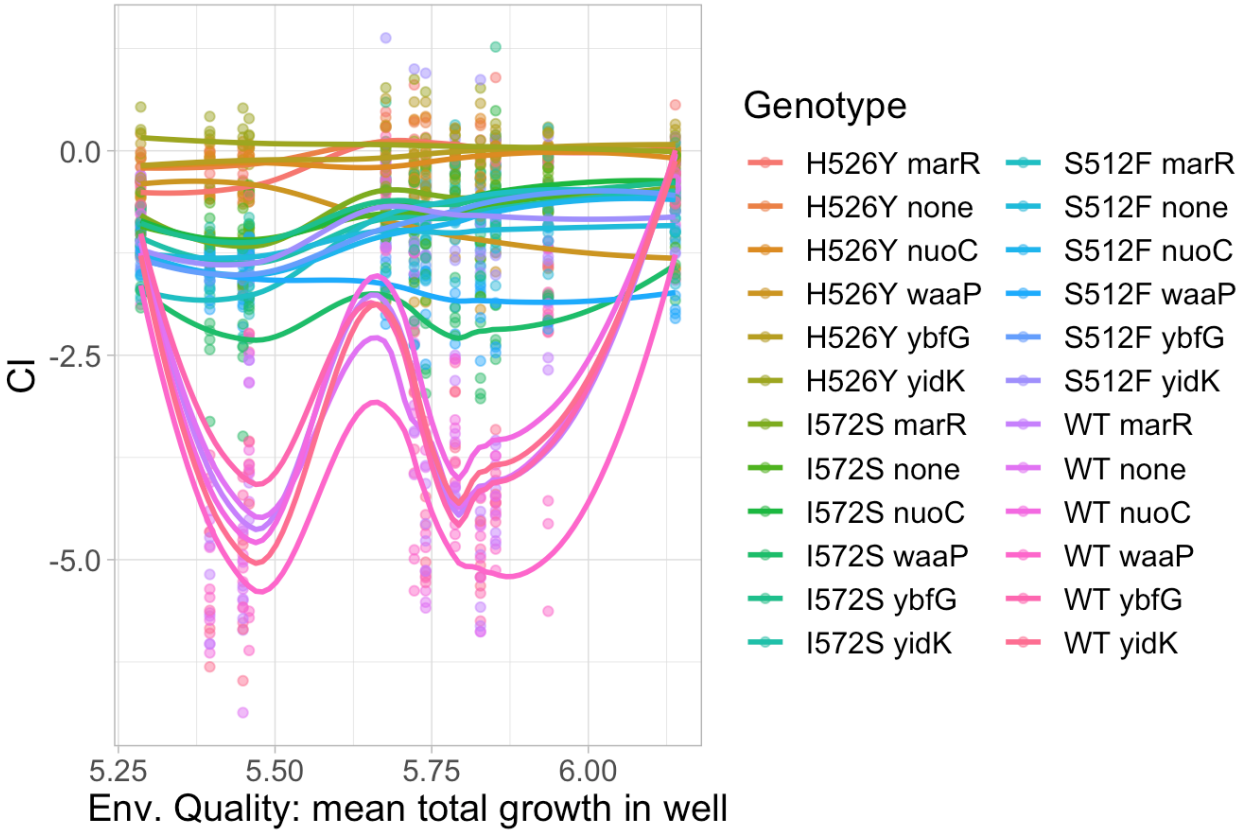

Figure S36: This plot shows that the environmental quality metric 'mean total growth in the well (reference + competitor) in each environment' is not able to distinguish specialist and generalist genotypes. The data is plotted in the style of figure S33. However, unlike that figure, here the antibiotic environments are not grouped together as low quality environments: that's why the specialist genotypes make a 'w' shape in the plot.

8.7.2 Finlay-Wilkinson environmental quality regression for GxG summary statistics

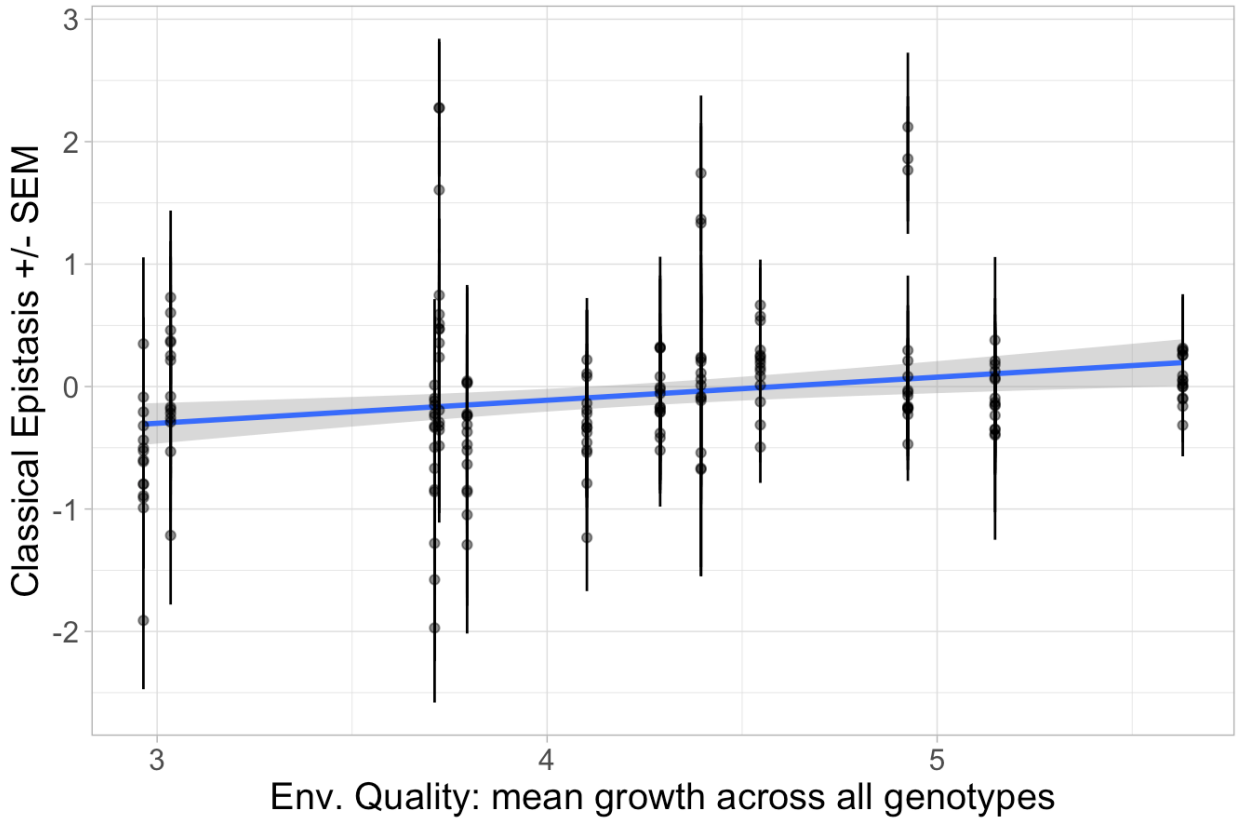

Figure S37: Plot of pairwise epistasis as a function of environmental quality across all genotypes and environments. The x-axis shows the environmental quality and the y-axis shows the mean pairwise epistasis for each of the 15 combinations of knock-outs and ABR *rpoB* mutations, with error bars for the standard error. The blue line shows the mean and the blue shaded region shows the 95% confidence interval of the least-squares estimated linear regression. The linear regression is significant ($F(1, 178) = 10.16$, $p < 0.005$) but does not explain much of the variation in the data (adjusted $R^2 = 0.0487$).

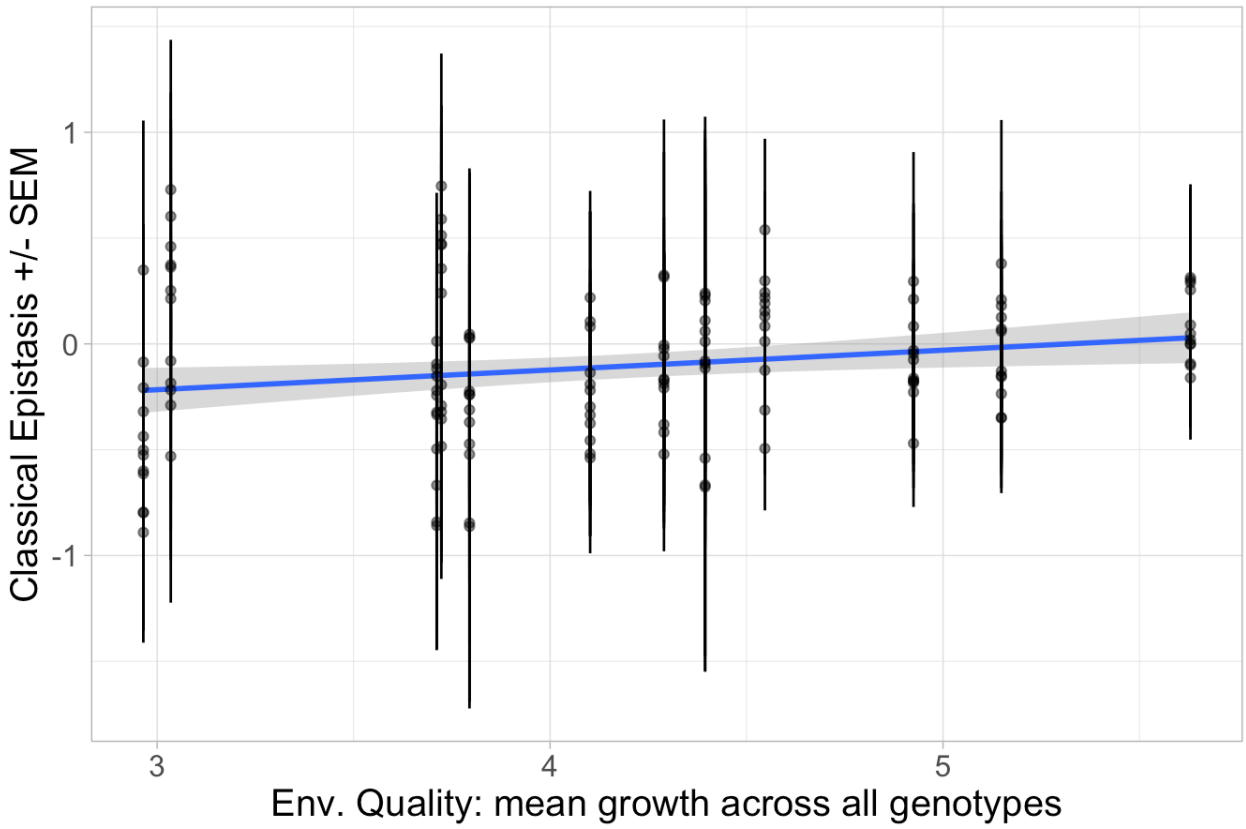

Figure S38: Plot of pairwise epistasis as a function of environmental quality for all gentoypes except the $\Delta waaP$ genotypes, as these have unusually high pairwise epistasis. This plot is similar to figure S37 except that only 12 points are shown (i.e., three $\Delta waaP$ genotypes were excluded) for each environment. The linear regression is marginally significant ($F(1, 142) = 6.357$, $p = 0.0128$) but it does not explain much of the variation in the data (adjusted $R^2 = 0.0361$).

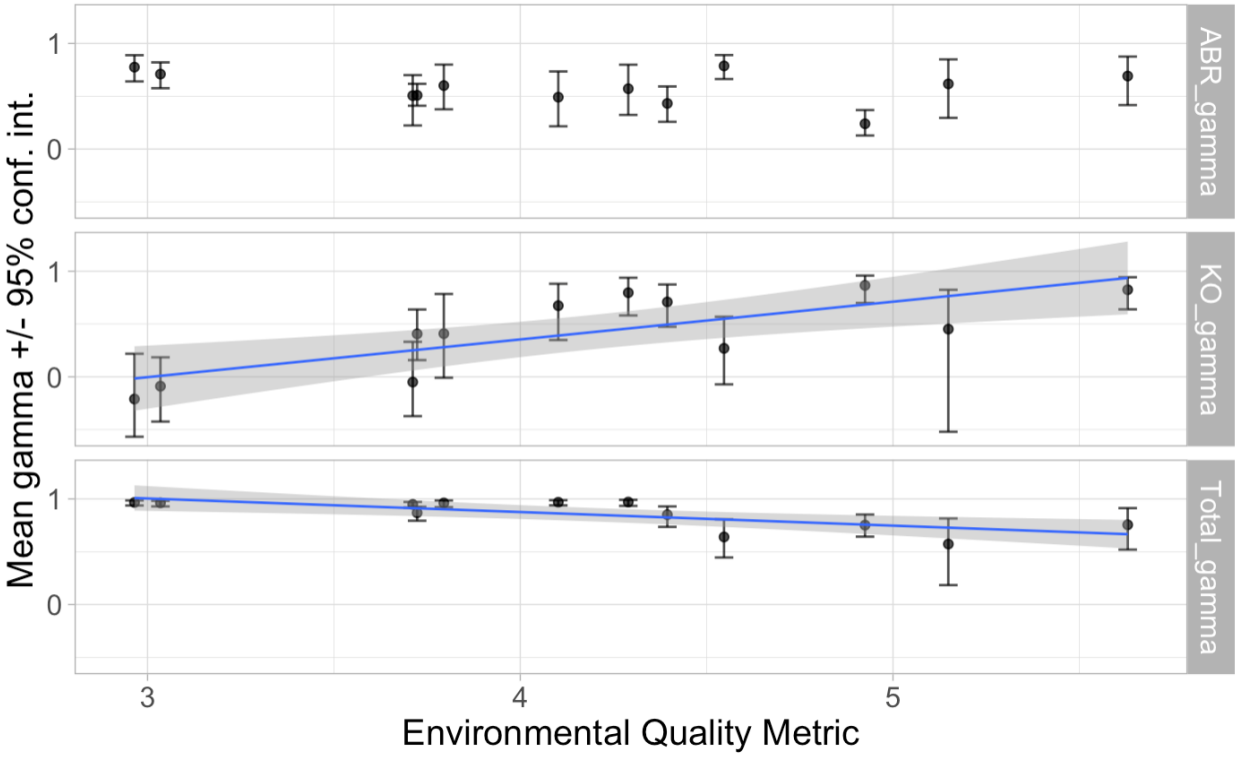

Figure S39: The mean gamma epistasis (y-axis) as a function of environmental quality (x-axis). The points show the mean gamma epistasis, with facets indicating the gene classes. The error bars show the 95% parametric bootstrap confidence intervals. If shown, the blue line indicates the mean of the significant, least-squares estimated linear regression and the grey shaded region shows its 95% confidence interval. Remember that gamma epistasis values near one indicate *low* G×G interactions and values near zero or negative one indicate *high* G×G interactions. **Top facet:** The gamma epistasis exhibited only by ABR *rpoB* mutations (ABR_gamma) is not correlated with either environmental quality ($F(1,10) = 0.614$, $p = 0.45$) nor antibiotic concentration alone ($F(1,10) = 0.0803$, $p = 0.78$; see figure S22). **Middle facet:** The gamma epistasis exhibited only by knock-out mutations (KO_gamma) is significantly correlated with environmental quality ($F(1,10) = 14.3$, $p < 0.005$) and explains more of the variation in the data (adjusted $R^2 = 0.547$) than when regressed against antibiotic concentration alone (adjusted $R^2 = 0.086$; the regression is not significant: $F(1,10) = 2.04$, $p = 0.184$, see figure S22). Note that this trend is opposite to that found for other measures: G×G is highest in the lowest quality environments and lowest in the highest quality environments. **Bottom facet:** For the total gamma epistasis, the regression on environmental quality is significant ($F(1,10) = 12.0$, $p < 0.01$) but explains about half the variation in the data (adjusted $R^2 = 0.5$) as compared to $\sim \frac{4}{5}$ of the variation in the data for the regression on antibiotic concentration alone (see main text and figure 3a).

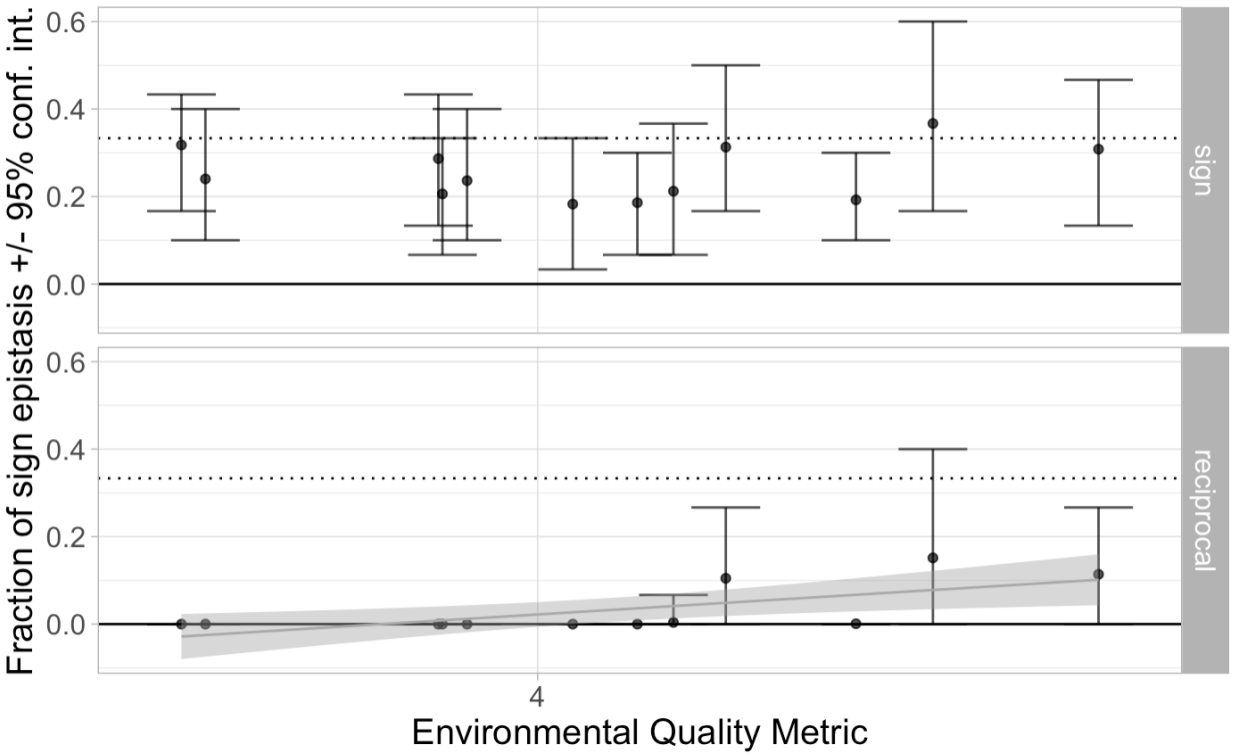

Figure S40: The mean fraction of simple sign (top facet) and reciprocal sign epistasis (bottom facet) as a function of environmental quality (x-axis) shows no specific trend that is an improvement over the effect of antibiotic concentration (figure S23). The points show the mean fraction and the error bars show the 95% parametric bootstrap confidence interval. There is no significant correlation between the environmental quality metric and the fraction of simple sign epistasis ($F(1, 10) = 0.375$, $p = 0.55$). For the reciprocal sign epistasis, the regression on environmental quality is marginally significant ($F(1, 10) = 9.30$, $p = 0.0122$, grey trend-line shows the mean and the shaded region shows the 95% confidence interval of the least-squares estimated linear regression). The regression of reciprocal sign epistasis explains less than half of the variation in the data (adjusted $R^2 = 0.430$) as compared to over 60% of the variation in the data for the regression on antibiotic concentration alone (see figures 3b & S23).

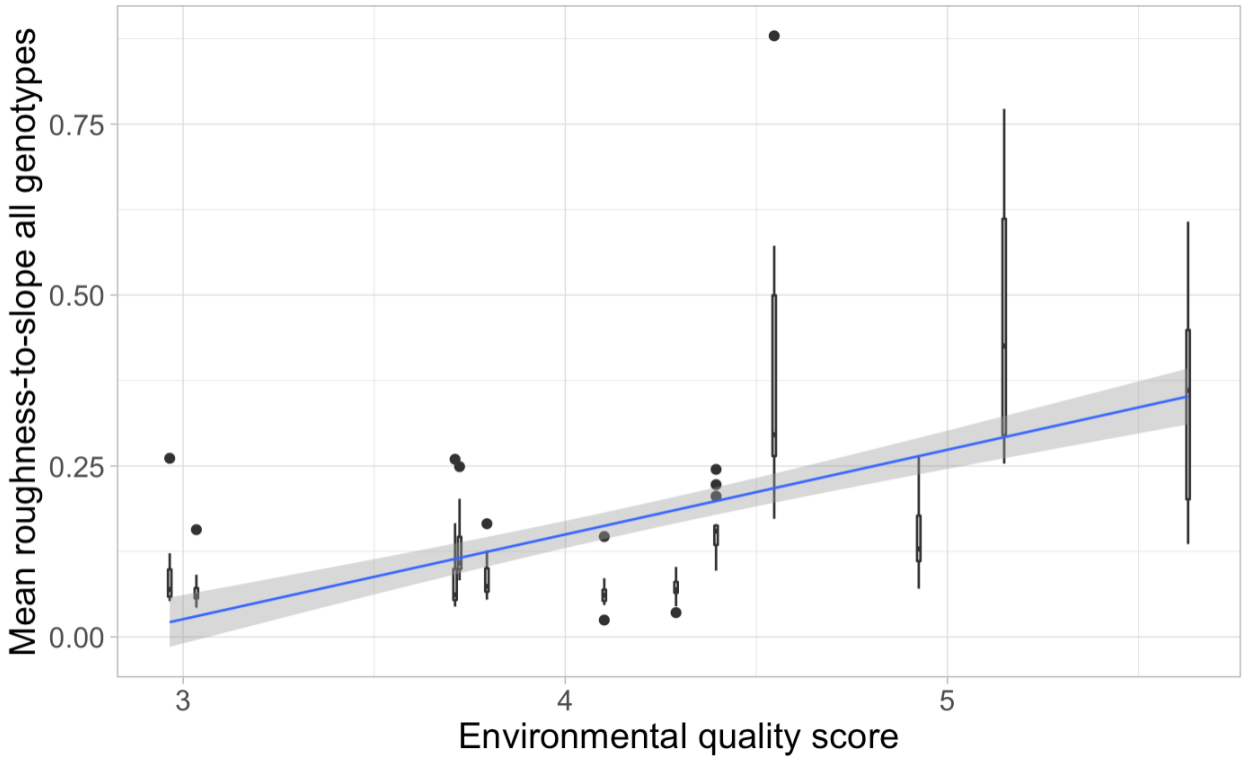

Figure S41: Boxplots of the roughness to slope ratio for all genes (y-axis) as a function of environmental quality (x-axis) shows a significant correlation ($F(1, 178) = 95.7$, $p < 10^{-15}$) but the amount of variation explained by the environmental quality score (adjusted $R^2 = 0.346$) is less than than explained by antibiotic concentration alone ($\sim 50\%$, see figure 3c).

9 Materials & Methods

9.1 Constructing and confirming the genotypes

9.1.1 Obtaining the ABR Mutations

RpoB H526Y and S512F mutants have strong resistance to rifampicin ($> 200\mu$g/mL) and were already available in the Gordo lab [78]. *RpoB* I572N happened to evolve *de novo* by screening for spontaneous mutations with intermediate rifampicin resistance (resistant at 20 $\mu g/mL$ but susceptible at 100 $\mu g/mL$) in rich media (Luria broth) batch culture and then using Sanger sequencing to confirm the SNP location on the *rpoB* locus.

9.1.2 Genetic engineering

P1*vir* phage transduction [79] with rifampicin selective plates was used to move each *rpoB* mutant onto two different fluorescently labeled backgrounds, one with Superfolder GFP and the other with mCherry, both with a chloramphenicol resistance cassette.

Knock-out single mutants were built onto the *rpoB* wild-type GFP-labeled and mCherry-labeled backgrounds by λ Red-mediated recombination using PCR products [80]. The homology primers listed in table S13 were used to PCR amplify the in-frame, single gene deletion mutants from the Keio collection samples, then these PCR products were used as templates for recombineering. P1 phage transduction with selection for the inserted kanamycin cassette was then used to clean-up any off-target mutations that may have been introduced by the λ Red recombinase. However, we did not counterselect to eliminate the kanamycin resistance cassette from knock-outs – meaning that all knock-outs have the gene-of-interest replaced with a kanamycin cassette.

Double-mutants were built by moving the knock-outs onto the *rpoB* mutant backgrounds, again using P1 phage transduction. All sample codes and their corresponding engineered mutations are listed in table S12.

All genotypes were phenotypically screened for their respective markers: resistance to chloramphenicol, susceptibility/resistance to rifampicin and kanamycin, and GFP or mCherry fluorescence. Fluorescence was screened using a BioTek H1 microplate reader with GFP (ex: 469 nm / em: 525 nm) and RFP (ex: 531 nm / em: 593 nm) filters.

Table S12: Sample names and their corresponding engineered mutations.

Sample	rpoB mutation	Knock-out	Fluorophore	Antibiotic resistance(s)
AHG015 (WT)	-	-	sfGFP	chloramphenicol
AHG056	-	ΔybfG	sfGFP	chloramphenicol, kanamyacin
AHG060	-	ΔmarR	sfGFP	chloramphenicol, kanamyacin
AHG064	-	ΔyidK	sfGFP	chloramphenicol, kanamyacin
AHG066	-	ΔnuoC	sfGFP	chloramphenicol, kanamyacin
AHG052	-	ΔwaaP	sfGFP	chloramphenicol, kanamyacin
AHG079 (Ref)	H526Y	-	mCherry	chloramphenicol, rifampicin
AHG080	H526Y	-	sfGFP	chloramphenicol, rifampicin
AHG090	H526Y	ΔybfG	sfGFP	chloramphenicol, rifampicin, kanamyacin
AHG092	H526Y	ΔmarR	sfGFP	chloramphenicol, rifampicin, kanamyacin
AHG094	H526Y	ΔyidK	sfGFP	chloramphenicol, rifampicin, kanamyacin
AHG096	H526Y	ΔnuoC	sfGFP	chloramphenicol, rifampicin, kanamyacin
AHG088	H526Y	ΔwaaP	sfGFP	chloramphenicol, rifampicin, kanamyacin
AHG082	S512F	-	sfGFP	chloramphenicol, rifampicin
AHG100	S512F	ΔybfG	sfGFP	chloramphenicol, rifampicin, kanamyacin
AHG102	S512F	ΔmarR	sfGFP	chloramphenicol, rifampicin, kanamyacin
AHG104	S512F	ΔyidK	sfGFP	chloramphenicol, rifampicin, kanamyacin

Continued on next page

Table S12 – continued from previous page

Sample	rpoB mutation	Knock-out	Fluorophore	Antibiotic resistance(s)
AHG106	S512F	ΔnuoC	sfGFP	chloramphenicol, rifampicin, kanamyacin
AHG098	S512F	ΔwaaP	sfGFP	chloramphenicol, rifampicin, kanamyacin
AHG068	I572S	-	sfGFP	chloramphenicol, rifampicin
AHG070	I572S	ΔybfG	sfGFP	chloramphenicol, rifampicin, kanamyacin
AHG072	I572S	ΔmarR	sfGFP	chloramphenicol, rifampicin, kanamyacin
AHG074	I572S	ΔyidK	sfGFP	chloramphenicol, rifampicin, kanamyacin
AHG076	I572S	ΔnuoC	sfGFP	chloramphenicol, rifampicin, kanamyacin
AHG078	I572S	ΔwaaP	sfGFP	chloramphenicol, rifampicin, kanamyacin

Table S13: The sequences of the homology primers used to PCR amplify the in-frame, single gene deletion mutants from the listed Keio collection samples, respectively. Product lengths are given for when the gene is present in MG1655 and for when the gene is knocked-out in the Keio sample. The names of the primers indicate their positions in the MG1655 reference genome (GenBank accession CP032667.1). PCR for the Datsenko-Wanner recombineering was done with New England Biolabs Phusion High-Fidelity DNA Polymerase (M0530) by following the manufacturer's guidelines with a 2.5 minute elongation at 67°C.

ΔmarR	
Primer name	Primer sequence
marR_2262520_For	AAGTAACAACTGGCTGCGTG
marR_2264206_Rev	CCACAAAATAACCGCCACCA
Product length in MG1655:	1687 bp
Product length in Keio JW5248:	2637 bp
ΔnuoC	
Primer name	Primer sequence
nuoC_1478699_For	GAGCGTATGAACCCGGAAAC
nuoC_1482106_Rev	GGCTCCATTTCATCGGCATT
Product length in MG1655:	3408 bp
Product length in Keio JW5375:	2933 bp
ΔpstA	
Primer name	Primer sequence
pstA_4613126_For	AATATCCCGATTGTTGGCGC
pstA_4615306_Rev	TCCTGCTTCAGTTCGGTGAT
Product length in MG1655:	2181 bp
Product length in Keio JW3704:	2618 bp
ΔsurA	
Primer name	Primer sequence
surA_3826005_For	CGTCTCTGCTGCAATCTGAC
surA_3828504_Rev	GGAATGCCAGCGTCGTTAA
Product length in MG1655:	2500 bp
Product length in Keio JW0052:	2560 bp
ΔwaaP	
Primer name	Primer sequence
waaP_76747_For	AATCGCCGATTTCCAGAAGC
waaP_78757_Rev	CGCCCTTTATCACGACCAAG
Product length in MG1655:	2011 bp
Product length in Keio JW3605:	2541 bp
ΔwcaE	
Primer name	Primer sequence
wcaE_1752899_For	AATTATCCTCACCGGTGGCA
wcaE_1755232_Rev	GAATTTCGGGTTGCAGGTGT
Product length in MG1655:	2334 bp
Product length in Keio JW2040:	2915 bp
ΔybfG	
Primer name	Primer sequence
ybfG_3164439_For	CAGAAGGTCGCTAATGTGCC
ybfG_3166129_Rev	TACCGCCACATTACTGCTGA
Product length in MG1655:	1691 bp
Product length in Keio JW5094:	2656 bp

Continued on next page

Table S13 – continued from previous page

ΔyhhS	
Primer name	Primer sequence
yhhS_271090_For	TAGCGCTGTGGTGAAGGTAA
yhhS_273647_Rev	ATGGCTGAACACTGGATGGA
Product length in MG1655:	2558 bp
Product length in Keio JW5945:	2635 bp
ΔyidK	
Primer name	Primer sequence
yidK_22529_For	TTTTCAATTTGCCGCCGTTG
yidK_25340_Rev	AACCAGTAATCAGCGTCCCA
Product length in MG1655:	2812 bp
Product length in Keio JW3655:	2424 bp
ΔyzgL	
Primer name	Primer sequence
yzgL_318532_For	GGTACCGCGCGTGAATATTT
yzgL_320142_Rev	CGTTCCTGACTGAATCGCTG
Product length in MG1655:	1611 bp
Product length in Keio JW3390:	2657 bp

9.1.3 Whole genome sequencing and analysis

Single colonies for each of the 25 competed genotypes were grown up in 10 mL of rich media (Luria broth) batch culture so that DNA could be extracted and purified using the standard phenol/chloroform method. All samples were sent for whole genome sequencing to the Next Generation Sequencing (NGS) Platform of UBern in Bern, Switzerland. Library preparation was done using the Illumina DNA Prep kit and sequencing was done by Illumina NovaSeq6000 flow cell, 2 x 150 bp run on two lanes.

Details about WGS analysis: The breseq pipeline (0.36.1), with bowtie2 (2.3.3) and R (4.1.1), was used to map reads to reference sequences in order to confirm the genetically engineered mutations-of-interest and discover any new, off-target mutations. The MG1655 reference sequence from GenBank (NC_000913.3) and the inserted GFP fluorescent construct sequence (given in supplementary methods) were used as reference sequences for the wild-type assigned GFP-labelled genotype (sample AHG015). Then, all subsequent single and double mutant genotypes were mapped against this wild-type genotype, so that any mutations common to all genotypes could be ignored in down-stream analysis. In addition to the wild-type reference, reads from single and double mutant genotypes also used the GenBank sequence for the pDK4 plasmid (AY048743.1) as an additional reference in order to identify knock-outs where target genes have been swapped with the kanamycin resistance cassette. Finally, for the mCherry-labelled reference genotype (sample AHG079), the inserted mCherry fluorescent construct sequence (given in supplementary methods) was used as a reference in order to identify the correct fluorescent tag on this genotype. An average read depth limit of 120x was set for breseq as recommended in the manual for efficient completion times: this means that up to a quarter of the read data was discarded per sample, regardless of the actual quality of that data (see tables S1-S2). The different *rpoB* substitutions that were engineered for all samples were readily detected by breseq's mutation prediction algorithm (table S3). The presence of engineered gene knock-outs was confirmed manually by looking for consistent results between three types of evidence: 1) high coverage of the kanamyacin coding sequence from the pKD4 plastmid (figure S6), 2) unassigned missing coverage evidence consistent with a knock-out of the target gene (figure S8), and 3) unassigned new junction evidence both upstream and downstream of the target gene (figure S11).

Sequence data for Superfolder GFP inserted construct (in GenBank format):

```
LOCUS       sfGFP                   2301 bp    DNA
DEFINITION  Template plasmid RB300, partial sequence.
ACCESSION   .
VERSION     .
SOURCE      Template plasmid RB300 made by Roberto Balbontin
  ORGANISM  Template plasmid RB300
            other sequences; artificial sequences; vectors.
REFERENCE   1  (bases 1 to 2301)
  AUTHORS   Balbontin, R.
FEATURES             Location/Qualifiers
     source          1..2301
                     /organism="synthetic construct"
                     /mol_type="other DNA"
     misc_feature    1..3
                     /note="yiaS"
     misc_feature    35..66
                     /note="ysaC"
     misc_feature    211..297
                     /note="PLTetO-1 promoter"
     misc_feature    298..324
                     /note="RBSpZA31-luc"
     CDS             325..1044
                     /note="Superfolder GFP fluorophore"
                     /codon_start=1
                     /transl_table=11
                     /product="sfGFP"
                     /protein_id="QBQ65835"
                     /translation="MASKGEELFTGVVPILVELDGDVNGHKFSVRGEGEGDATNGKLT
                     LKFICTTGKLPVPWPTLVTTLTYGVQCFSRYPDHMKQHDFFKSAMPEGYVQERTISFK
                     DDGTYKTRAEVKFEGDTLVNRIELKGIDFKEDGNILGHKLEYNFNSHNVYITADKQKN
                     GIKANFKIRHNVEDGSVQLADHYQQNTPIGDGPVLLPDNHYLSTQSVLSKDPNEKRDH
                     MVLLEFVTAAGITHGMDELYK-"
     misc_feature    1093..1138
                     /note="FRT site"
     CDS             1347..1985
                     /note="chloramphenicol resistance"
                     /codon_start=1
                     /transl_table=11
                     /product="type A chloramphenicol O-acetyltransferase"
                     /protein_id="WP_015420186 "
                     /translation="MEKKITGYTTVDISQWHRKEHFEAFQSVAQCTYNQTVQLDITAF
                     LKTVKKNKHKFYPAFIHILARLMNAHPELRMAMKDGELVIWDSVHPCYTVFHEQTETF
                     SSLWSEYHDDFRQFLHIYSQDVACYGENLAYFPKGFIENMFFVSANPWVSFTSFDLNV
                     ANMDNFFAPVFTMGKYYTQGDKVLMPLAIQVHHAVCDGFHVGRCLMNTTVLR"
     misc_feature    2023..2068
                     /note="FRT site"
     misc_feature    2120..2280
                     /note="ysaD"
     misc_feature    2299..2301
                     /note="yiaT"
ORIGIN
        1 taatccctca cgccggggct tcatcgcccc ggcactacga attgatatgt tccttgctgt
```

```
   61 aacgccgctt ccacgctgct ggcgttaaac cagtatgttt ctgaaaaatc tgccggaaat
  121 agccaacgtc attaaagata tcgacgtcta agaaaccatt attatcatga cattaaccta
  181 taaaaatagg cgtatcacga ggccctttcg tcttcacctc gagtccctat cagtgataga
  241 gattgacatc cctatcagtg atagagatac tgagcacatc agcaggacgc actgaccgaa
  301 ttcattaaag aggagaaagg taccatggct tctaaaggtg aagaactgtt caccggtgtt
  361 gttccgatcc tggttgaact ggatggtgat gttaacggcc acaaattctc tgttcgtggt
  421 gaaggtgaag gtgatgcaac caacggtaaa ctgaccctga aattcatctg cactaccggt
  481 aaactgccgg ttccatggcc gactctggtg actaccctga cctatggtgt tcagtgtttt
  541 tctcgttacc cggatcacat gaagcagcat gatttcttca aatctgcaat gccggaaggt
  601 tatgtacagg agcgcaccat ttctttcaaa gacgatggca cctacaaaac ccgtgcagag
  661 gttaaatttg aaggtgatac tctggtgaac cgtattgaac tgaaaggcat tgatttcaaa
  721 gaggacggca acatcctggg ccacaaactg gaatataact tcaactccca taacgtttac
  781 atcaccgcag acaaacagaa gaacggtatc aaagctaact tcaaaattcg ccataacgtt
  841 gaagacggta gcgtacagct ggcggaccac taccagcaga acactccgat cggtgatggt
  901 ccggttctgc tgccggataa ccactacctg tccacccagt ctgttctgtc caaagacccg
  961 aacgaaaagc gcgaccacat ggtgctgctg gagttcgtta ctgcagcagg tatcacgcac
 1021 ggcatggatg agctctacaa ataatgaatt cgagcattta aatctagagg catccatatg
 1081 aatatcctcc ttagttccta ttccgaagtt cctattctct agaaagtata ggaacttcgg
 1141 cgcgcctacc tgtgacggaa gatcacttcg cagaataaat aaatcctggt gtccctgttg
 1201 ataccgggaa gccctgggcc aacttttggc gaaaatgaga cgttgattgg cacgtaagag
 1261 gttccaactt tcaccataat gaaataagat cactaccggg cgtatttttt gagttgtcga
 1321 gattttcagg agctaaggaa gctaaaatgg agaaaaaaat cactggatat accaccgttg
 1381 atatatccca atggcatcgt aaagaacatt ttgaggcatt tcagtcagtt gctcaatgta
 1441 cctataacca gaccgttcag ctggatatta cggccttttt aaagaccgta aagaaaaata
 1501 agcacaagtt ttatccggcc tttattcaca ttcttgcccg cctgatgaat gctcatccgg
 1561 aattacgtat ggcaatgaaa gacggtgagc tggtgatatg ggatagtgtt cacccttgtt
 1621 acaccgtttt ccatgagcaa actgaaacgt tttcatcgct ctggagtgaa taccacgacg
 1681 atttccggca gtttctacac atatattcgc aagatgtggc gtgttacggt gaaaacctgg
 1741 cctatttccc taaagggttt attgagaata tgtttttcgt ctcagccaat ccctgggtga
 1801 gtttcaccag ttttgattta aacgtggcca atatggacaa cttcttcgcc cccgttttca
 1861 ccatgggcaa atattatacg caaggcgaca aggtgctgat gccgctggcg attcaggttc
 1921 atcatgccgt ttgtgatggc ttccatgtcg gcagatgctt aatgaataca acagtactgc
 1981 gatgagtggc agggcggggc gtaaggcgcg ccatttaaat gaagttccta ttccgaagtt
 2041 cctattctct agaaagtata ggaacttcga agcagctcca gcctacacta ttgcatggag
 2101 caggccgaca acgtcgagtc actgcataac ctgttgctgc ccgccgatgc gccatttacg
 2161 acatttgaag gcaagggatt gttcagccat aagatcctga ttcagacgcc aggttcccgg
 2221 tatgaacaga gcaatccaga gcaacaacct ttgtggcatt acgacggagc accagccgca
 2281 ccgacatcca ccggtgaatt a
//
```

Sequence data for mCherry inserted construct (in GenBank format):

```
LOCUS       mCherry                  2292 bp    DNA
DEFINITION  Template plasmid RB296, partial sequence.
ACCESSION   .
VERSION     .
SOURCE      Template plasmid RB296 made by Roberto Balbontin
  ORGANISM  Template plasmid RB296
            other sequences; artificial sequences; vectors.
REFERENCE   1  (bases 1 to 2292)
  AUTHORS   Balbontin, R.
FEATURES             Location/Qualifiers
     source          1..2292
                     /organism="synthetic construct"
                     /mol_type="other DNA"
     misc_feature    1..3
                     /note="yiaS"
     misc_feature    35..66
                     /note="ysaC"
     misc_feature    211..297
                     /note="PLTetO-1 promoter"
     misc_feature    298..324
                     /note="RBSpZA31-luc"
     CDS             325..1035
                     /note="mCherry fluorophore"
                     /codon_start=1
                     /transl_table=11
                     /product="mCherry"
                     /protein_id="AZQ25025.1"
                     /translation="MVSKGEEDNMAIIKEFMRFKVHMEGSVNGHEFEIEGEGEGRPYE
                     GTQTAKLKVTKGGPLPFAWDILSPQFMYGSKAYVKHPADIPDYLKLSFPEGFKWERVM
                     NFEDGGVVTVTQDSSLQDGEFIYKVKLRGTNFPSDGPVMQKKTMGWEASSERMYPEDG
                     ALKGEIKQRLKLKDGGHYDAEVKTTYKAKKPVQLPGAYNVNIKLDITSHNEDYTIVEQ
                     YERAEGRHSTGGMDELYK"
     misc_feature    1084..1129
                     /note="FRT site"
     CDS             1338..1976
                     /note="chloramphenicol resistance"
                     /codon_start=1
                     /transl_table=11
                     /product="type A chloramphenicol O-acetyltransferase"
                     /protein_id="WP_015420186 "
                     /translation="MEKKITGYTTVDISQWHRKEHFEAFQSVAQCTYNQTVQLDITAF
                     LKTVKKNKHKFYPAFIHILARLMNAHPELRMAMKDGELVIWDSVHPCYTVFHEQTETF
                     SSLWSEYHDDFRQFLHIYSQDVACYGENLAYFPKGFIENMFFVSANPWVSFTSFDLNV
                     ANMDNFFAPVFTMGKYYTQGDKVLMPLAIQVHHAVCDGFHVGRCLMNTTVLR"
     misc_feature    2014..2059
                     /note="FRT site"
     misc_feature    2111..2271
                     /note="ysaD"
     misc_feature    2290..2292
                     /note="yiaT"
ORIGIN
        1 taatccctca cgccggggct tcatcgcccc ggcactacga attgatatgt tccttgctgt
       61 aacgccgctt ccacgctgct ggcgttaaac cagtatgttt ctgaaaaatc tgccggaaat
```

```
 121 agccaacgtc attaaagata tcgacgtcta agaaaccatt attatcatga cattaaccta
 181 taaaaatagg cgtatcacga ggccctttcg tcttcacctc gagtccctat cagtgataga
 241 gattgacatc cctatcagtg atagagatac tgagcacatc agcaggacgc actgaccgaa
 301 ttcattaaag aggagaaagg taccatggtg agcaagggcg aggaggataa catggccatc
 361 atcaaggagt tcatgcgctt caaggtgcac atggagggct ccgtgaacgg ccacgagttc
 421 gagatcgagg gcgagggcga gggccgcccc tacgagggca cccagaccgc caagctgaag
 481 gtgaccaagg gtggcccccct gcccttcgcc tgggacatcc tgtcccctca gttcatgtac
 541 ggctccaagg cctacgtgaa gcaccccgcc gacatccccg actacttgaa gctgtccttc
 601 cccgagggct tcaagtggga gcgcgtgatg aacttcgagg acggcggcgt ggtgaccgtg
 661 acccaggact cctccctgca ggacggcgag ttcatctaca aggtgaagct gcgcggcacc
 721 aacttcccct ccgacggccc cgtaatgcag aagaagacca tgggctggga ggcctcctcc
 781 gagcggatgt accccgagga cggcgccctg aagggcgaga tcaagcagag gctgaagctg
 841 aaggacggcg gccactacga cgctgaggtc aagaccacct acaaggccaa gaagcccgtg
 901 cagctgcccg gcgcctacaa cgtcaacatc aagttggaca tcacctccca caacgaggac
 961 tacaccatcg tggaacagta cgaacgcgcc gagggccgcc actccaccgg cggcatggac
1021 gagctgtaca agtaatgaat tcgagcattt aaatctagag gcatccatat gaatatcctc
1081 cttagttcct attccgaagt tcctattctc tagaaagtat aggaacttcg gcgcgcctac
1141 ctgtgacgga agatcacttc gcagaataaa taaatcctgg tgtccctgtt gataccggga
1201 agccctgggc caacttttgg cgaaaatgag acgttgattg gcacgtaaga ggttccaact
1261 ttcaccataa tgaaataaga tcactaccgg gcgtattttt tgagttgtcg agattttcag
1321 gagctaagga agctaaaatg gagaaaaaaa tcactggata taccaccgtt gatatatccc
1381 aatggcatcg taaagaacat tttgaggcat ttcagtcagt tgctcaatgt acctataacc
1441 agaccgttca gctggatatt acggcctttt taaagaccgt aaagaaaaat aagcacaagt
1501 tttatccggc ctttattcac attcttgccc gcctgatgaa tgctcatccg gaattacgta
1561 tggcaatgaa agacggtgag ctggtgatat gggatagtgt tcacccttgt tacaccgttt
1621 tccatgagca aactgaaacg ttttcatcgc tctggagtga ataccacgac gatttccggc
1681 agtttctaca catatattcg caagatgtgg cgtgttacgg tgaaaacctg gcctatttcc
1741 ctaaagggtt tattgagaat atgtttttcg tctcagccaa tccctgggtg agtttcacca
1801 gttttgattt aaacgtggcc aatatggaca acttcttcgc cccgttttc accatgggca
1861 aatattatac gcaaggcgac aaggtgctga tgccgctggc gattcaggtt catcatgccg
1921 tttgtgatgg cttccatgtc ggcagatgct taatgaatac aacagtactg cgatgagtgg
1981 cagggcgggg cgtaaggcgc gccatttaaa tgaagttcct attccgaagt tcctattctc
2041 tagaaagtat aggaacttcg aagcagctcc agcctacact attgcatgga gcaggccgac
2101 aacgtcgagt cactgcataa cctgttgctg cccgccgatg cgccatttac gacatttgaa
2161 ggcaagggat tgttcagcca taagatcctg attcagacgc caggttcccg gtatgaacag
2221 agcaatccag agcaacaacc tttgtggcat tacgacggag caccagccgc accgacatcc
2281 accggtgaat ta
//
```

9.2 Estimating the competitive fitnesses

9.2.1 Cell growth protocol

The protocol is summarized in figure S42. Freezer stocks contain 15% glycerol and LB. Chloramphenicol antibiotic (CM) was used to prevent contamination but only with agar plates, not at any later steps. M9 liquid minimal media with 0.4% glucose was used for acclimitization and fitness measures. Glass inoculum tubes were used for acclimitization as these were found to provide superior culture aeration as compared to plastic well plates. Batch culture competitions were done in flat-bottom wells sealed with breathable film and incubated in a BioTek H1 microplate reader with continuous shaking in order to provide a homogeneous environment that minimized clumping.

Each 96-well plate contained 24 genotypes competing at each of the four rifampicin antibiotic concentrations. Media with different concentrations of rifampicin was aliquoted to the plate in randomly ordered blocks of two rows. As well, the locations of the samples on the plate was randomized to prevent bias from possible plate edge effects.

Only one plate was incubated at a time in the microplate reader. Therefore sample measures are grouped into four blocks, each with three temperature environments. The order of temperature environments was randomized to prevent any systematic bias that may arise due to the duration of time that cells were stored at 4°C.

All competitions began at a fixed inoculum size of 10^5 cells and equal (1:1) ratios of the competitor and reference genotypes. Flow cytometry was for three measures. First, it was used on the early stationary phase cultures to determine the precise dilution factor required for each sample in order to arrive at an inoculum size of 10^5 cells. Flow cytometry was also performed on the inocula after they were used for aliquoting to the 96-well plate: this way, the precise initial frequencies of competitor vs. reference are known, not assumed. Finally, flow cytometry was used to measure the final frequencies of competitor vs. reference after 20 hours of growth.

9.2.2 Flow cytometry protocol

Flow cytometry with fluorescent beads was used to determine the standardized relative cell counts. All Flow Cytometry experiments were performed on a BD LSR Fortessa SORP machine at the Flow Cytometry Facility of Instituto Gulbenkian de Ciência. Cell counts were extracted from flow cytometry data using `FlowJo` (10.7.1). Bacterial cells were separated from fluorescent beads and debris using side-scatter and forward-scatter gating, next doublets were excluded using side-scatter area and width, then, finally, GFP-only expressing cells were distinguished from mCherry-only expressing cells using rectangular subset gating. The raw flow cytometry data, `FlowJo` quantification files, and cell counts data are publicly available in a GitLab repository, https://gitlab.com/evoldynamics/epistasis-decreases-with-increasing-antibiotic-pressure.

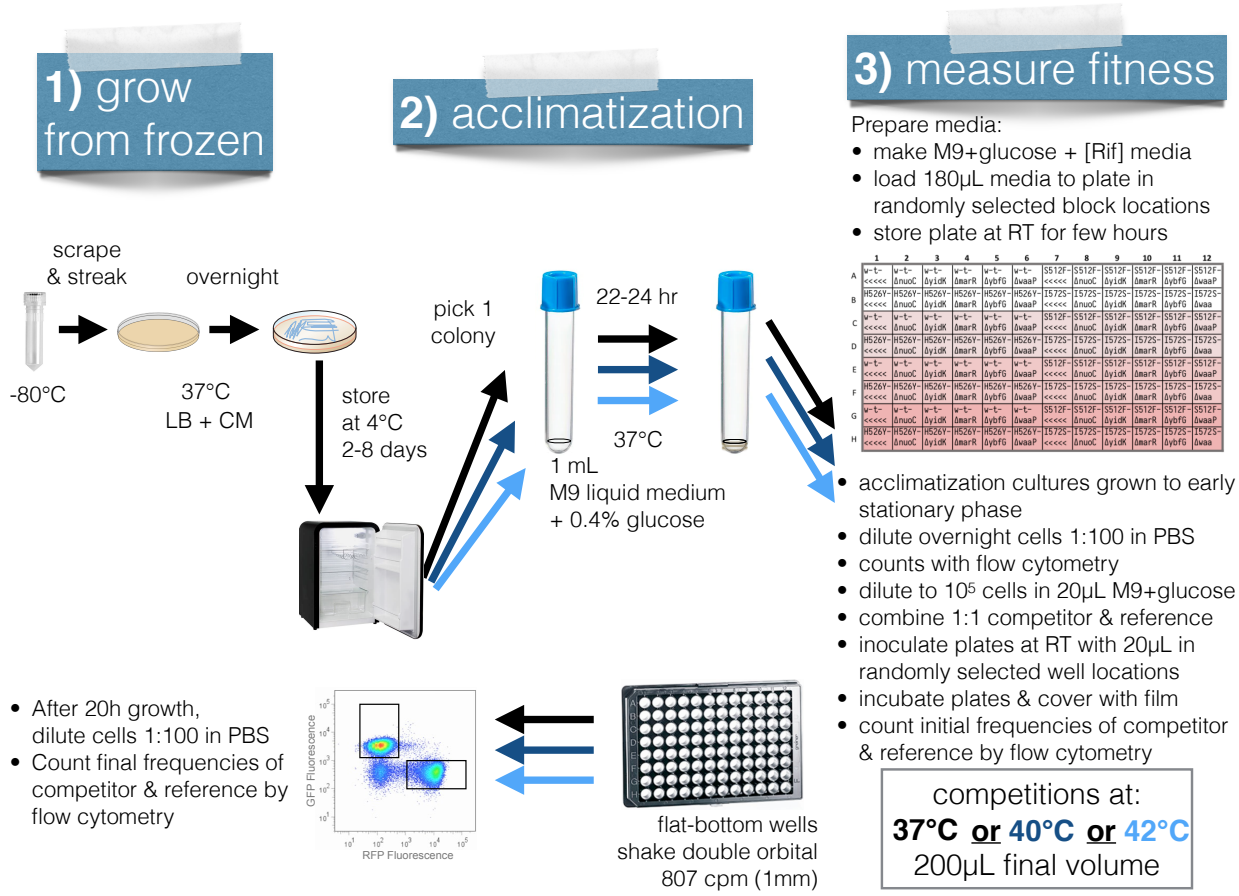

Figure S42: **Summary of the protocol used to estimate fitness in different antibiotic concentration and temperature environments. 1)** To ameliorate the possibility of *de novo* mutations, frozen glycerol stocks were bottle-necked to single colonies by streaking on agar plates. **2)** After streaking and growth on agar plates, all cells experienced the same temperature acclimitization of at least 40 hours and at most 8 days at 4°C followed by batch culture growth at 37°C for 22-24 hours. **3)** Batch culture competitions took place in 96-well plates with randomized positions of the four blocks of antibiotic concentrations and the 24 samples. Only one plate was incubated at a time, therefore triple arrows show steps in the protocol that had to be repeated for each temperature environment in order to sample a complete block of all samples in all environments. Regardless of the temperature environment where competition occurred, batch culture acclimitization always occurred at 37°C.

9.2.3 Estimating competitive index

We used `R` (4.1.1) as run using `RStudio` (2021.09.0+351) to calculate the competitive index using the equation indicated in the results. The GitLab repository for this manuscript, https://gitlab.com/evoldynamics/epistasis-decreases-with-increasing-antibiotic-pressure, contains the competitive index estimates and `R` code for calculating the competitive index from the cell counts data, `calculating_selection.Rmd`.

9.3 Analyses

Parametric bootstrapping (10 000 bootstrap replicates) was used to determine the 95% confidence intervals on all of the summary statistics of epistasis. For the diminishing-returns epistasis, linear regressions were run on each of the 10 000 bootstrap replicates (x = fitness of the background, y = fitness effect of the mutation) and the mean slope value was retained in order to determine the 95% confidence intervals across all linear regressions.

We fitted a linear model in `R` using the equation $\hat{w} \sim G_{rpoB} + G_{\mathrm{KO}} + E_{\mathrm{T}} + E_{\mathrm{AB}}$ and the `lm` command from the `stats` package (version 4.1.1). The genotypic effects of *rpoB* (G_{rpoB}) and knock-out (G_{KO}) mutations were treated as categorical variables (in `R`: unordered factors), while the environmental effects of temperature (E_{T}) and antibiotic concentration (E_{AB}) were treated as semi-quantitative variables (in `R`: ordered factors) using polynomial contrasts.

All analyses are publicly available on GitLab at https://gitlab.com/evoldynamics/epistasis-decreases-with-increasing-antibiotic-pressure. The epistasis calculations can be found in `estimating_epistasis.Rmd`, the linear model fitting can be found in `ANOVA_etal.Rmd`, and Finlay-Wilkinson regression can be found in `FinleyWilkinson.Rmd`.